Study on Ion-Exchanged Optical Waveguides Formed on Ferroelectric Crystals

強誘電体イオン交換光導波路に関する研究

平成7年11月

近藤　由紀子

①

Study on Ion−Exchanged Optical Waveguides Formed on Ferroelectric Crystals

強誘電体イオン交換光導波路に関する研究

by

Yukiko KONDO

近藤　由紀子

November, 1995

Study on Ion-Exchanged Optical Waveguides
Formed on Ferroelectric Crystals

Contents

To My Husband and Son

Preface

This thesis describes a part of the research work carried out at the Institute of Industrial Science, University of Tokyo, under the direction of Professor Fujii while the author was a research associate at the Department of Electronics Engineering, University of Tokyo, from 1986 to 1995.

Recently, the dielectric materials, such as lithium niobate, lithium tantalate, and potassium titanyl phosphate are of significant interest because these materials are promising for both the electro-optic and nonlinear-optic device application. Ion-exchanged waveguides formed on these materials are more efficient than the bulk crystal in the device application such as modulators, switches and second-harmonic generation devices because of their good light confinement. Moreover, the fabrication of the ion-exchanged waveguides is very easy.

In this thesis, the experimental studies on the optical properties of the ion-exchanged waveguide formed on the lithium niobate, lithium tantalate and potassium titanyl phosphate are described for the purpose of fundamental understanding and the future applications of these dielectric waveguides.

November 1995 Yukiko Kondo

Acknowledgment

This thesis describes the research work carried out at the Institute of Industrial Science, University of Tokyo, while the author was a research associate at the Department of Electronic Engineering, University of Tokyo, from 1986 to 1995.

The author would like to express her sincere gratitude to Professor Yoichi Fujii, Institute of Industrial Science, University of Tokyo, for continuous guidance and encouragement.

The author is grateful to Professor Tada, Professor Nakano and Mr. Murai, University of Tokyo, Prof. Li, Changchum Institute of Physics, Academia Sinica, China, and Prof. Wang, Zhejiang University for arranging the experimental environment, for fruitful discussions on the dielectric waveguides, and for their constant encouragement.

The author is grateful to Prof. Arakawa, Institute of Industrial Science, University of Tokyo, Prof. Hotate and Prof. Sakaki, Research Center for Advanced Science and Technology, University of Tokyo, and Prof. Takano, Institute of Space and Astronautical Science for their useful suggestions and advice.

The author wishes to express her special thanks to Prof. Taniuchi, Institute for materials research, Tohoku University, Prof. Minakata, Research Institute of Electronics, Shizuoka University, and Prof. Sasaki, Osaka University for their useful advice and for fruitful discussions.

The author also wishes to express her special gratitude to Mr. Onoe and Mr. Miyaguchi, Corporate Research and Development

Laboratory, Pioneer Electric Co., Ltd., Dr. Yuhara, Hitachi Cable, Ltd., and Prof. Hu, University of Electronic Science and Technology of China, Chengdu for their useful advice, for constant encouragement and for their great help.

The author is greatful to Dr. Yamamoto, Matsushita Electric Industrial Co., Ltd., Mr. Nakama, Nippon Sheet Glass Co., Ltd., and Mr. Nakamura and Mr. Tsuji, Ibiden Co., Ltd. for their fruitful discussions and for their great help.

The author is also grateful to Ms. Yamada and Dr. Yamamoto, Nippon Steel Corporation, Dr. Fujiwara, Toyota Technological Institute, Dr. Okada, Hoya Corporation, Dr. Li, the University of Electro-communications, Mr. Toyama and Mr. Togawa, Teijin Seiki Co., Ltd. and Dr. Kurimura, Waseda University for their useful discussions and suggestions.

The author would like to thank to the members of Fujii Laboratory, Mr. Ozaki, Mr. Levanon, Mr. Sotobayashi, Mr. Kato and Ms. Morimoto, and Mr. Nishioka in Arakawa Laboratory for their assistance and encouragement.

Finally, the author would like to express her sincere gratitude to her parents, her husband and son for their help and constant encouragement.

Abstract

The author has established the understanding of the optical and physical properties of the ion-exchanged waveguides formed on the dielectric materials such as $LiNbO_3$, $LiTaO_3$, and potassium titanyl phosphate. The author has addressed the following two points as the main purpose:

1)Exact estimation of the electrooptic constants
2)Quantitative estimation of the photorefractive effect

With respect to 1), the exact estimation of the electrooptic constants in the proton-exchanged layers formed on the lithium niobate crystals is investigated in detail.
With respect to 2), The photorefractive effect of the dielectric waveguides is quantitatively measured and compared. The influence of the photorefractive effect on the device application is also investigated.

Chapter I

Introduction

Abstract

The background of the study on the ion−exchanged optical waveguides is reviewed historically. The optical and physical properties of the dielectric bulk crystals and the optical devices formed on these crystals are reviewed. The purpose of the present study is presented.

1.1 Background of Study

In 1960, coherent light was obtained for the first time in the world by operating the ruby laser successfully. After that, various kinds of lasers, such as gas lasers, glass lasers, semiconductor lasers were invented in succession. In 1970 the double hetero structure which enables the CW operation of the semiconductor laser at the room temperature was proposed, and optical fiber with the loss low enough for the practical use (20dB/Km) was first fabricated by Corning Co., Ltd.. These two inventions have actually made the optical communication possible. After 1970, the optical communication has made a rapid progress. With the progress in the optical communication system, a variety of optical components and devices for optical modulation, optical switching, wavelength division multiplexing and coherent system techniques are required. Ti−indiffused waveguide formed on the $LiNbO_3$ crystal [1] − [30] has been extensively used for these devices [4] − [6] . However, other materials such as ion−exchanged waveguides formed on the $LiNbO_3$, [7] − [9] , $LiTaO_3$ [10] − [12] and potassium titanyl phosphate (KTP) [13] − [15] are found to be the promising alternative for this purpose.

On the other hand, these optical waveguides are also attractive for the optical measurement and optical signal processing applications. Various kinds of optical sensors such as voltage sensors [16] , temperature sensors [17] , and velocity sensors [18] using the Ti−indiffused optical waveguides have been proposed.

In optical sensor applications, He−Ne is often used as a light source. In this case, the index instability in the waveguide may be caused by the photorefractive effect (optical damage). Therefore, proton−exchanged waveguides with higher resistance to the optical damage than the Ti−indiffused waveguides [19] seem to be preferable.

Although above mentioned applications are based on the electrooptic effect, the applications based on the nonlinear−optic effect are also important. Among them, the second harmonic generation (SHG) device has recently attracted much attention.

There has been great demand for coherent blue light sources for optical data storage and laser printer applications. Many attempts have been made to obtain blue light, such as second−harmonic generation [20] − [22] , ZnSe laser diodes [23] , and the gallium nitride LED [24] . At present, the most promising method to obtain the coherent blue light source is second−harmonic generation because coherent light with very short wavelength (421nm) [22] can be obtained and the device of this type has the longest lifetime [25] .

The second harmonic generation was observed for the first time by Franken *et al.* in 1961 [26] . Nonlinear crystal is pumped by the infrared light and the light with the wavelength half as long as the original one is obtained. Since then, various types of the SHG devices were designed and fabricated.

$LiNbO_3$ crystal has been regarded as the most suitable material for the SHG devices. Waveguide type devices with much higher

conversion efficiency than that of the bulk devices have been fabricated on the $LiNbO_3$ crystal one after another. Many methods such as the Cerenkov radiation [35] and the quasi−phase matching [20] , [21] are proposed for the purpose of obtaining the high conversion efficiency. Only recently, however, the $LiTaO_3$ waveguides and potassium titanyl phosphate waveguides have attract considerable attention because second harmonic generation with extremely high conversion efficiency, using the quasi−phase matching has been reported for these materials [27] − [29] .

The optical and physical properties of dielectric crystals and the devices formed on these materials are reviewed in the following sections.

1.2 Optical and Physical Properties of Dielectric Crystals (Lithium Niobate, Lithium Tantalate and Potassium Titanyl Phosphate (KTP))

1.2.1 Crystal Structure and Curie Temperature

Both $LiNbO_3$ and $LiTaO_3$ belong to the $LiNbO_3$ family of compound. They belong to the trigonal system and acentric point group $3m$ (space group $R3c$).

In $LiNbO_3$ the oxygens are arranged in nearly hexagonal closed packed (HCP) planer sheets. The unit cell is rhombohedral (a=5.4944 Å , α=55° 52′) with two molecules per cell. The hexagonal cell (a_H=5.1483 Å , c_H=13.8631 Å , and c/a=2.693) has six molecules per cell [71] . In the (0 1 2) plane, the diamond

(parallelogram) shape surrounded by the four oxygen−octahedra appears, which results in the large electrooptic coefficient (Fig.1.1) [40] .

The crystal structure of the lithium tantalate is almost the same as that of the lithium niobate, and the lattice parameters are a_H=5.15428 Å and c_H=13.78351 Å (a=5.4740 Å , α=56° 10.5′) [72] .

Potassium titanyl phosphate (KTP) belongs to the family of compounds that have the formula unit $MTiOXO_4$, where M can be K, Rb, Tl, NH_4 or Cs (partial) and X can be P or As. KTP crystal is orthorhombic and belongs to the acentric point group $mm2$ (space group $Pna2_1$). The lattice constants are a=12.814 Å , b=6.404 Å , and c=10.616 Å , and each unit cell contains eight formula units. The structure is characterized by chains of TiO_6 octahedra, which are linked at two corners, and the chains are separated by PO_4 tetrahedra (Fig.1.2). There are two chains per unit cell, and the chain direction alternates between [0 1 1] and [0 −1 1] . Alternating long and short Ti−O bonds occur along these chains, which results in a net z−directed polarization and are the major contributor to KTP's large nonlinear−optic and electro−optic coefficients. The K ion sits in a high−coordination−number site and is weakly bonded to both the Ti octahedra and P tetra channels exists along the z−axis ([0 0 1] direction) whereby K can diffuse (through a vacancy mechanism) with a diffusion coefficient several order of magnitude greater than in the $x-y$ plane [13] .

Curie temperatures of the lithium niobate, lithium tantalate, and

KTP crystal are 1130, 600 ℃ and 936 ℃, respectively [13].

Lithium niobate crystal is the material suitable for the Ti−indiffusion method [1] − [4] because the Curie temperature of the lithium niobate crystal is very high. Although waveguides are formed also on the lithium tantalate crystal by the Ti−indiffusion process, the post poling process is needed in order to recover the reversed polarization caused by the Ti−indiffusion process. In the case of the lithium tantalate crystal, proton−exchanged method (see chapter Ⅱ), which is the fabrication process at the temperature much lower than the Curie temperature (200 ～ 260 ℃), is favorable.

Waveguides can be also formed on the KTP crystals by the ion−exchange method (see chapter Ⅱ) at the temperature lower than the Curie temperature (280 ℃ ～ 350 ℃).

1.2.2 Electrooptic Constant r_{33} and Nonlinear Coefficient d_{33}

Both Lithium niobate and lithium tantalate crystal are known as the attractive materials for electro−optical applications such as modulators and switches because of their large electrooptic constants. The KTP crystal is the relatively new material with the large electrooptic constant and is potentially attractive for various electrooptic applications such as modulators and Q switches.

The refractive index difference induced by the electric field is expressed as follows,

$$\Delta n=(1/2)n^3 rE, \qquad (1-1)$$

where n is the refractive index of the material, E is the applied field, and r is the electrooptic constant. The refractive index and the electrooptic constant of the lithium niobate, lithium tantalate, and the KTP bulk crystals are shown in Table 1.1. (T) and (S) indicate the electrooptic constants measured at low frequency and high frequency, respectively and all the values are measured at 633nm.

The figure of merit, $n^3 r/\varepsilon_{eff}$, which is related to the bandwidth/driving voltage ratio is important for the practical use. ε_{eff} is a geometric average dielectric constant $(\varepsilon_{11}\varepsilon_{33})^{1/2}$. The figure of merit is compared in Table 1.2 [13], [72].

The figure of merit of the KTP crystal is twice as large as those of the lithium niobate and lithium tantalate crystal. This property of KTP crystal should make it superior for the electrooptic modulator applications.

The intense electric field E which is present when the laser radiation propagates through the matter, gives rise to a number of effects owing to the polarization P induced by the field. P can be expressed as follows [73].

$$P=\varepsilon_0 [\chi^{(1)} E+\chi^{(2)} E^2+\chi^{(3)} E^3+\cdots]. \qquad (1-2)$$

The linear susceptibility $\chi^{(1)}$ is of such magnitude as to lead to observable effects at low optical intensity and is responsible for the refractive index and absorption of the material. The effects such as second harmonic generation, frequency mixing and parametric amplification result from second order susceptibility $\chi^{(2)}$. The

linear electro-optic coefficients r_{ijk} and nonlinear-optical (second harmonic) coefficients d_{ijk} are related to $\chi^{(2)}$ by

$$\chi^{(2)}_{ijk}(-\omega;\omega,0)=(n_{ii})^2\omega(n_{jj})^2 0 \cdot r_{ijk}(-\omega;\omega,0)/2,$$
$$\text{and } \chi^{(2)}_{ijk}(-2\omega;\omega,\omega)=2d_{ijk}(-2\omega;\omega,\omega). \quad (1-3)$$

The lithium niobate crystal has the high nonlinear-optical coefficient, and is regarded as one of the most efficient materials for the parametric device applications and the second harmonic generation (SHG) devices. Various kinds of SHG devices have been designed using the lithium niobate. Recently the waveguide-type devices with the extremely high conversion efficiency using the periodically domain-inverted structure is reported for both the lithium niobate and the lithium tantalate which has also high nonlinear-optical coefficient.

The KTP is widely used material for frequency-doubling Nd:YAG lasers and other Nd-doped laser systems emitting near 1.06μm. Periodically ion-exchanged KTP SHG devices with the conversion efficiency of 800%/Wcm^2 [29] and the Ta_2O_5/KTP waveguide SHG devices with the conversion efficiency of 1000%/Wcm^2 [74] are recently reported, and the latter is the SHG device with the highest conversion efficiency at present.

The nonlinear-optic coefficients of the lithium niobate, lithium tantalate, and the KTP bulk crystals are shown in Table 1.3.

The nonlinear-optical coefficients is the largest in lithium niobate crystal.

1.3 Optical Devices Using Dielectric Materials

1.3.1 Bulk Devices

Electrooptic devices are used for both optical communication and optical measurement such as voltage sensors.

Lithium niobate bulk crystal is used as the electrooptic modulator. There are two types of electrooptic bulk modulators, longitudinal-type and transverse-type modulators. For the voltage sensor application, the transverse-type lithium niobate modulator is usually used. The sensitivity increases as the distance between the electrode becomes smaller and length of the electrode becomes longer.

The lithium niobate and KTP crystals are often used for the second-harmonic generation devices. In the case of bulk devices, the phase-matching conditions may be adjusted by tilting or by controlling the temperature of the crystals. The conversion efficiency is very low in the bulk devices. KTP bulk crystals are also used for the electrooptic applications such as Q-switches.

1.3.2 Waveguide-type Devices

Waveguide-type devices are more effective than the bulk devices because of their good light confinement. The Ti-indiffused $LiNbO_3$ waveguides are mainly used as modulators and switches based on the electrooptic effect. Ti-indiffused $LiNbO_3$ waveguide is very advantageous for traveling-wave modulator because of the small frequency chirping, high modulation speed and low insertion loss. 33-GHz·cm broadband Ti-indiffused $LiNbO_3$ Mach-Zehnder modulator was reported by Seino *et al.* [30]. Matrix switch

arrays have been also fabricated using the Ti-indiffused waveguides [31] . TE/TM mode converter using the Ti-indiffused $LiNbO_3$ waveguide can be used as the excellent wavelength filter [32] . TE/TM mode converter combined with the TE/TM mode splitter with $\Delta\lambda$=6 Å at 1.5μm was reported [33] . The modulator formed on the Ti-indiffused waveguide is also used for optical sensor applications. The voltage sensor with high sensitivity was reported by Iwakura [16] . The velocity sensor using the Doppler effect was also reported by Toda *et al.* [18] .

The influence of the optical damage becomes very serious when the wavelength of the light source is very short. The proton-exchanged waveguides are suitable for the short wavelength device applications, especially the second harmonic device applications because they are resistant to optical damage. Many attempts have been made for obtaining high conversion efficiency of the second-harmonic generation (SHG) devices. SHG in waveguide with a Ti:$LiNbO_3$ strip guide resonator was reported by Regener *et al.* [34] . In this case, the conversion efficiency of SHG can be considerably improved by a resonant enhancement of the fundamental field inside a waveguide cavity. Taniuchi *et al.* demonstrated the narrow proton-exchanged strip waveguides with high conversion efficiency for SHG in the form of Cerenkov radiation [35] . The second harmonic generation with remarkably high conversion efficiency is reported for the quasi-phase matching SHG devices [27] - [29] . The devices of this kind are fabricated using the periodically domain-inverted structures with the ion-exchanged

waveguides formed on the $LiNbO_3$ [28] , $LiTaO_3$ [27] , and KTP [29] crystals. In these waveguides, the quantitative estimation of the photorefractive effect is important because the conversion efficiency is limited by this effect.

The proton-exchanged waveguides are also used for the electrooptical devices. Dawar [36] reported the acousto-optic diffraction interaction in proton-exchanged waveguides with diffraction efficiency as high as 72% for the electrical input power of 540 mW at 425 MHz by controlling the time of proton-exchange and by annealing the waveguide. Miyawaki *et al.* [37] fabricated the $LiNbO_3$ acousto-optic waveguides deflector which is efficient and also damage resistant with controlling the refractive index and the depth of the proton-exchanged $LiNbO_3$ by the amount of lithium benzoate and by annealing. Wong *et al.* [38] fabricated an efficient proton-exchanged waveguide phase modulator making use of the largest electro-optic constant r_{33}. Chen *et al.* [39] fabricated an electro-optic cutoff modulator with low drive voltage by controlling the proton-exchange time and the annealing time. In such electrooptical devices, the degradation of the electrooptic constant [40] by the proton-exchange method is the most serious problem, and exact estimation of the electrooptic constant is necessary.

1.4 Purpose of Study

There has been a great demand for the electro-optic devices for both the optical communication and sensor applications, and the

nonlinear-optical devices such as the second-harmonic generation devices.

As reviewed in the former section, many kinds of devices with high ability has been proposed and fabricated, and most of them are waveguide-type devices.

The properties of these devices are highly dependent on the waveguide fabrication process. The optical and physical properties of the waveguides, however, have not yet been investigated enough. In order to find the waveguide fabrication techniques and the optimum fabrication conditions suitable for each devices, the exact estimation of the optical and physical properties of the waveguides becomes necessary.

The purpose of this study is to investigate the optical and physical properties of the ion-exchanged waveguides formed on the $LiNbO_3$, $LiTaO_3$ and KTP crystals, and to find the materials most suitable for each devices.

The main subject of our study is focused on the following two points.

(1)Exact estimation of the electrooptic constants:

In the case of the electrooptic devices, exact estimation of the electrooptic constants is the most important. The exact estimation of the electrooptic constant of the waveguiding layer is investigated for the first time, and the relation between the electrooptic constant and crystal structure is discussed.

(2)Quantitative estimation of the photorefractive effect:

The conversion efficiency of the second-harmonic generation is

actually limited by the photorefractive effect. The photorefractive effect of the dielectric waveguide is quantitatively measured and compared for the first time. The influence of the photorefractive effect on the device application is also investigated.

1.5 Summary of Study

In chapter Ⅱ , the fabrication methods of the ion-exchanged optical waveguides are reviewed and the refractive index profiles are measured by the prism coupler method. The lattice constants in the waveguides are also determined by the x-ray rocking curve analysis using the double crystal method. The lattice constants in the proton-exchanged $LiTaO_3$ waveguides formed on the domain-inverted structure are investigated for the first time.

In chapter Ⅲ , the electrooptic effects of the proton-exchanged waveguides fabricated on the *z*-cut and *y*-cut $LiNbO_3$ crystals are investigated. The electrooptic constants of the proton-exchanged $LiNbO_3$ waveguiding layers are measured considering the field distribution of the light propagating in the substrates. The effect of annealing the proton-exchanged layer is also investigated.

In chapter Ⅳ , the photorefractive sensitivities of the ion-exchanged waveguides formed on the $LiNbO_3$ and KTP crystals are quantitatively measured by the photorefractive grating method. The photorefractive sensitivities of the Ti-indiffused $LiNbO_3$ waveguides and $LiNbO_3$ thin-film waveguide formed by the liquid-phase epitaxy are also measured and the results are compared.

In chapter V , the influence of the photorefractive effect on device application is investigated and discussed. The optical damage resistance of the proton−exchanged $LiNbO_3$ and $LiTaO_3$ waveguides, and ion−exchanged KTP waveguides are investigated in detail and are compared from the view point of the device application. The effect of the periodically domain−inverted structure for the second harmonic generation on the photorefractive sensitivity is investigated. The temperature dependence on the photorefractive effect of the the proton−exchanged $LiTaO_3$ waveguide is also investigated.

As a result, the effect of annealing the proton−exchanged layer is slightly different between the $LiNbO_3$ and $LiTaO_3$ waveguides. The annealed proton−exchanged $LiTaO_3$ waveguide is proven to be the most attractive material for the second−harmonic generation device application because of its high resistance to the photorefractive effect. The annealed proton−exchanged $LiNbO_3$ is attractive for the electro−optic device application because of its large electrooptic constant recovered by the annealing process. Ion−exchanged KTP waveguide is potentially attractive for both SHG device application and electrooptic device application which is used at the relatively short wavelength because of its large electrooptic constant as well as its high resistance to the photorefractive effect.

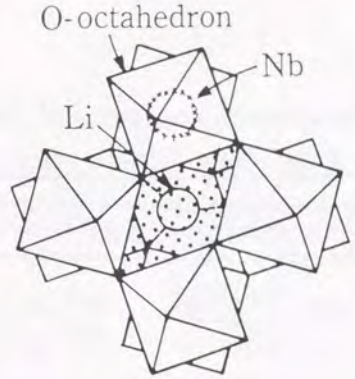

(0 1 2) plane

Fig. 1.1. Diamond shape appears in (0 1 2) plane [50] .

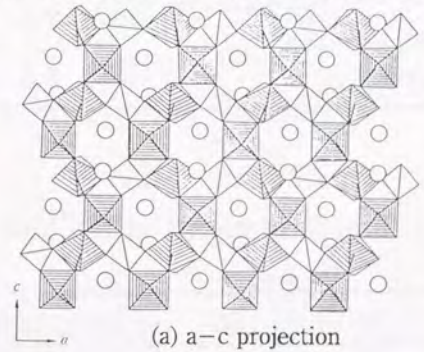

Fig. 1.2. KTP crystal structure [13] :
Shaded elements are the Ti octahedra, open elements are the P tetrahedra, and open circles are the K.
The short Ti−O bonds are shown as bold lines

Table 1.1. Electrooptic constants of the bulk crystals

Crystal	Refractive index		Electrooptic constant				
	no	ne		r33	r13	r22	r42
$LiNbO_3$	2.286	2.200	(T)	32.2	10	6.8	
			(S)	30.8	8.6	3.4	28
$LiTaO_3$	2.175	2.180	(S)	30.3	7	1	20
				r33	r13	r23	r42	r51
KTP	nx=1.764		(T)	36.3	9.5	15.7	9.3	7.3
	ny=1.773							
	nz=1.864		(S)	35.0	8.8	13.8	8.8	6.9

Table 1.2. Figure of merits of the bulk crystals

Crystal	r(pm/V)	εff	Figure of merit ($n^3r/\varepsilon eff$)
$LiNbO_3$	r33: 30.8	36	9.2
	r13: 8.6	36	2.9
$LiTaO_3$	r33: 30.3	42	7.5
	r13: 7	42	1.7
KTP	r33: 35	13	17.3
	r13: 14	13	5.9

Table 1.3. Nonlinear−optical coefficients of the bulk crystals

Crystal	Nonlinear−optical coefficient (pm/V)
$LiNbO_3$	$d_{22}=4.0$
	$d_{31}=6.5$
	$d_{33}=34.4$
$LiTaO_3$	$d_{22}=2.8$
	$d_{31}=1.7$
	$d_{33}=26$
KTP	$d_{31}=6.5$
	$d_{32}=5.0$
	$d_{33}=13.7$
	$d_{24}=7.6$
	$d_{15}=6.1$

Chapter II

Formation of Optical Waveguides and Lattice Constants of Ion-exchanged Waveguides

Abstract

The refractive index profiles of the proton-exchanged $LiNbO_3$ and the Rb ion-exchanged KTP waveguides are determined using the prism coupler method. The step-index profile of the proton-exchanged layer is gradually changed into the Gaussian profile. The refractive index profile of the ion-exchanged layer is approximate erfc function. After annealing this layer, the refractive index profile is also changed into the Gaussian profile.

The lattice constant changes of the ion-exchanged planer waveguides are investigated. The lattice constant is increased by the Rb ion-exchange process as well as in the proton-exchange process. The increased lattice constant is considerably reduced by the annealing process.

The lattice constants in the proton-exchanged waveguide layers formed on the $LiTaO_3$ substrate with and without the domain-inverted structure are compared. The increase in lattice constant caused by the proton-exchange process ($\Delta c/c$) is 0.53 %. The values $\Delta c/c$ measured in the annealed proton-exchanged waveguides with domain-inverted slab structure, with the periodically domain-inverted structure, and without the domain-inverted structure are 0.19 %, 0.21 % and 0.23 %, respectively.

2.1 Introduction

The waveguide type devices are more effective than bulk devices because their light confinement is very good.

In this chapter, the fabrication methods for the waveguides formed on the $LiNbO_3$, $LiTaO_3$, and KTP waveguides are reviewed and the refractive index profiles of these waveguides are measured. The lattice constant change caused by the fabrication process of the waveguide is also investigated. The lattice constants are determined by the X-ray rocking curve analysis using the double crystal methods.

In 2.2, the fabrication methods of the ion-exchanged waveguides formed on the dielectric materials for the electrooptical and nonlinear optical use are explained.

In 2.3, the experimental results of the measurements of the refractive index profiles are shown. It is very important to control the refractive index profile of the waveguide properly in designing the optical devices with low insertion and transmission loss. The effect of ion-exchange source and the post annealing process on the refractive index profiles of the ion-exchanged waveguides is investigated in order to obtain the refractive index profiles suitable for each purpose.

In 2.4, the experimental results of the measurement of the lattice constants in the ion-exchanged planer waveguides are shown. The optical properties of the materials, such as electrooptic constants and nonlinear-optical coefficients are determined by their structure. For instance, the electro-optic constant and second order nonlinear-optical coefficient are zero in a material with the

centrosymmetric structure. The crystal structure is changed by the formation of the waveguide. The properties of the original crystal may be largely changed in the waveguiding layer if this structural change is very large. In this chapter, the lattice constant change due to the fabrication process is investigated.

The relation between the structural change and the optical properties of the waveguide will be discussed in the following chapters.

In 2.5, the lattice constant change in proton-exchanged waveguide formed on the periodically domain-inverted $LiTaO_3$ crystal is investigated. This structure is designed for the quasi-phase matching SHG device application [41] , [21] , [22] . In this section, the structural change of the $LiTaO_3$ crystal caused by the domain-inversion process is experimentally studied in detail for the first time.

2.2 Fabrication Methods

The optical waveguides are easily fabricated at low temperature by the ion-exchange process. The refractive index profiles of the ion-exchanged waveguides can be properly controlled by the annealing process. Therefore, the ion-exchange methods are very attractive for the fabrication of optical devices. The fabrication methods of the ion-exchanged waveguides are explained in this section.

2.2.1 Ion-exchange process for the waveguide formation

The ion-exchange process can be described by the following equation [8] .

$$\partial C/\partial t = Da\ \partial/\partial x\ [\ 1/(1-\alpha C)\cdot \partial C/\partial x\ ]\ , \quad (2-1)$$

where C is the concentration of indiffused ions to the total concentration of ions, $\alpha=1-Da/Db$, Da is the indiffusion coefficient for indiffused ions, and Db is the outdiffusion coefficient for outdiffused ions.

The diffusion depth of the waveguide is defined as the depth which gives the refractive index of $ns+(1/e)\Delta n$ (ns is the refractive index of the substrate and Δn is the increase in the surface refractive index), and can be obtained by the effective index measurement. The diffusion depth of the waveguide (d) is related to the exchange time (t) as follows [8] .

$$d=2(t\cdot D(T))^{1/2}, \quad (2-2)$$

where $D(T)$ is the diffusion coefficient and can be expressed as follows.

$$D(T)=D0\exp(-Q/RT), \quad (2-3)$$

where $D0$ is a constant for the ion-exchange process, R the universal gas constant, T the absolute melt temperature, and Q is the activation energy for the exchange process.

It is reported that the annealing process after the ion-exchange process can also be described by the diffusion equation (2-1).

2.2.2 Proton-Exchange Method

The proton-exchanged waveguides can be formed in $LiNbO_3$ or $LiTaO_3$ crystals by using the benzoic acid or the pyrophosphoric acid as a proton-exchange source. The substrates are first heated in a furnace up to the temperature of 200 ℃ ~ 250 ℃ [7] , [12] , [43] , [44] . Then the crystals are dipped into the melt acid. The protons from pyrophosphoric (or benzoic) acid diffuse into the crystal, while the lithium ions diffuse out of the crystal into the acid. The layer of $Li_{1-x}H_xNbO_3$ ($Li_{1-x}H_xTaO_3$) of higher refractive index is formed by this proton-exchange process (Fig. 2.1).

In the case of proton-exchange process, Da is the indiffusion coefficient for protons, and Db is the outdiffusion coefficient for Li ions. It is reported that the rate of protons diffusing in is very much smaller than that of the lithium ions diffusing out ($\alpha \fallingdotseq 1$) [8] . This result indicates that the solution of the Eq.(2-1) is a step function. The parameters $D(T)$, $D0$ and Q reported for the proton-exchanged waveguide lithium niobate (PE-LN) and lithium tantalate (PE-LT) waveguides are shown in Table 2.1 [75] .

The diffusion depth d can be expressed as $d=1.01\times10^{5}(t)^{1/2}\exp(-5.72\times10^{3}/T)(\mu m)$, and $d=1.73\times10^{4}(t)^{1/2}\exp(-5.19\times10^{3}/T)(\mu m)$ for the proton-exchanged waveguides formed on the $LiNbO_3$ and $LiTaO_3$ crystal, respectively.

In order to recover the electrooptic constants (or the nonlinear optic constants), the proton-exchanged layer is sometimes annealed at

300 ~ 400 ℃ [45] , [46] . Index instability of the proton-exchanged layer can be reduced by the annealing process.

2.2.3 Ion-Exchange Method

The optical waveguides are also fabricated on KTP crystals by the ion-exchange method [13] - [15] . Both the KTP crystal placed in a stainless holder, and the $RbNO_3/Ba(NO_3)_2$ molten salt are heated up to 300 ~ 350 ℃ (Fig. 2.2). The Rb^+ ions are diffused into the substrate. Ba^{2+} ions are added to the salt for the purpose of controlling the diffusion rate of the Rb^+ ions and reducing the melting point of the salt [47] . K^+ ions are replaced by the Rb^+ ions and the layer with higher refractive index is formed by this ion-exchange process.

In the Rb ion-exchange process, the indiffusion coefficient D_a of the Rb ions is almost the same as the outdiffusion coefficient D_b of the K^+ ions ($\alpha=0$), and the diffusion equation (2-1) can be rewritten as,

$$\partial C/\partial t = D_a \partial^2 C/\partial x^2, \qquad (2-4)$$

where C is the concentration of indiffused Rb ions to the total concentration of ions. The solution of equation (2-4) is a complementary error-function, and the refractive index profile of the waveguiding layer can be expressed using the complementary error-function [13] .

$$n(z) = n_s + \Delta n \, \mathrm{erfc}(z/d),$$

where n_s is the refractive index of the KTP substrate, Δn is the refractive index change at the surface ($z=0$), and d is the depth of the waveguide.

It is reported that the diffusion coefficients $D(T)$ of Rb^+ ions in $RbNO_3/Ba(NO_3)_2$ (80/20) molten salts at 350 ℃ are 2.0 μm^2/min for the TM mode and 2.5μm^2/min for the TE mode [76] .

2.3 Refractive Index Profiles of Optical Waveguides

2.3.1 Methods for Measurement of Refractive-Index Profiles

The equivalent index N is measured by the prism coupler method (Fig. 2.3) using Eq. (2-5).

$$N = n_p \sin(\alpha + \sin^{-1}(\sin\theta/n_p)) \qquad (2-5)$$

where θ is the incident angle of the laser beam, n_p (=2.584) is the refractive index of the rutile prism, and α is the angle of the rutile prism. The refractive index profile and the diffusion depth of the waveguide are calculated by the WKB approximation [77] for the wave equation or the dispersion curve obtained from the eigen value equation.

2.3.2 Refractive Index Profiles of Proton-Exchanged and Annealed Proton-Exchanged Waveguide

The proton-exchanged layer has the step index profile and only

the extraordinary surface refractive index ne is increased by the proton-exchange (Δn_e=0.12 ~ 0.145 for $LiNbO_3$ and 0.015 for $LiTaO_3$).

The thickness of the waveguide is obtained from the equivalent index N using the dispersion curve. The dispersion curve for the proton-exchanged $LiNbO_3$ is shown in Fig. 2.4 and the relation between the thickness of the guiding layer and the proton-exchange time is shown in Fig. 2.5.

The refractive index profiles of the proton-exchanged layers formed on the three types of z-cut $LiNbO_3$ substrates: non-doped, Ti-indiffused and MgO-doped, are shown in Fig. 2.6, Fig. 2.7 and Fig. 2.8, respectively. The proton-exchanged layers of 0.5μm are formed on the nondoped $LiNbO_3$, the Ti-indiffused $LiNbO_3$, and the MgO-doped $LiNbO_3$ crystals by the proton-exchange process at 230 ℃ for 12min, 15min and 23min respectively.

The refractive index profile of the proton-exchanged layer is gradually changed into the Gaussian profile by the annealing process. In all cases, the surface refractive index decreases according as the annealing time increases. The decrease in the surface refractive index is the largest in non-doped $LiNbO_3$ and the smallest in the MgO-doped $LiNbO_3$. Judging from this result, the diffusion of the protons into the substrate due to the annealing process seems to be disturbed by the impurities such as MgO ions.

The increase in the surface refractive index caused by the annealing process which is reported for the proton-exchanged $LiTaO_3$ waveguide [12] , [44] , [48] is not observed in the proton-exchanged $LiNbO_3$ waveguides.

2.3.3 Refractive Index Profile of the Rb-Ion Exchanged Waveguides

The refractive index profile of the Rb-ion exchanged waveguide is first reported by Bierlein *et al.* [14] . In their experiment, the post-annealing process at 300 ℃ ~ 350 ℃ for 30 min to 2 hours did not significantly change the surface refractive index change and the diffusion depth of the planer waveguide formed on the z-cut KTP crystal by the ion-exchange process in the pure rubidium nitrate melt.

Shi *et al.* reported [49] however, that the refractive index profile of the ion-exchanged layer was actually changed by the annealing process. Pure rubidium nitrate melt was also used as the ion-exchange source in their experiment.

In our experiment, the effect of annealing on the ion-exchanged KTP waveguides is investigated. The $RbNO_3/Ba(NO_3)_2$ molten salt is used as the ion-exchange source because the diffusion rate of the rubidium ions is controlled by adding the barium ions to the pure rubidium nitrate melt.

The refractive index profiles of the Rb-ion exchanged waveguides are shown in Fig. 2.9 and Fig. 2.10.

The KTP substrate is first dipped into the molten mixture of 97% molar rubidium nitrate and 3% barium nitrate for at 320 ℃ for 45min, after that the sample is annealed at 325 ℃ for 50min (Fig. 2.9). In the case of the sample shown in Fig. 2.10, the substrate is dipped into the molten salt with 15% molar $Ba(NO_3)_2$ at 320 ℃ for 10min,

followed by the annealing process at 325 for 80min.

The refractive index profile of the ion−exchanged layer without annealing process is approximate erfc function, and the surface refractive index is considerably reduced by the annealing process in both samples. In the case of sample shown in Fig. 2.9, the refractive index profile is changed into almost Gaussian profile by the annealing. Therefore, the ions as large as rubidium ions at the surface can be diffused deep into the substrate by the annealing process at 325 ℃ .

The results obtained by our experiment are in good agreement with the results obtained by Shi *et al.* As a result, it is proven that annealing process is effective for controlling the refractive index profile in the Rb ion−exchanged KTP waveguide as well as in the proton−exchanged $LiNbO_3$ and $LiTaO_3$ waveguides.

2.4 Measurement of Lattice Constants of Ion−Exchanged Planer waveguides

2.4.1 Principle of Measurement

The X−ray rocking curve analysis using the double crystal method [40] , [50] shown in Fig. 2.11 is employed to determine the lattice constants of the optical waveguides formed on the *z*−cut $LiNbO_3$, *z*−cut $LiTaO_3$ and *z*−cut KTP crystals. The samples are placed on a rotating table and the angle of the sample is adjusted so that the $K\alpha_1$ beam can be diffracted by the $(0,0,l)$ plane of the crystal (l=12 for the $LiNbO_3$, $LiTaO_3$ and l=8 for KTP waveguides). The lattice constant c is obtained in terms of the Bragg angle of the X−ray diffraction as follows.

$$c = \lambda l /(2\sin\theta_B), \qquad (2-6)$$

where λ (=1.5406 Å) is the wavelength of the $K\alpha_1$ beam of the X−ray, θ_B is the Bragg angle of the X−ray diffraction.

The lattice constant c is calculated by the measured Bragg angle of the X−ray diffraction, and the strain $\Delta c/c$ along the c−axis is obtained.

2.4.2 Lattice Constants of Proton−Exchanged Slab Waveguides and Rb Ion−Exchanged Slab Waveguides

The lattice constants of the proton−exchanged $LiNbO_3$ waveguides and proton−exchanged $LiTaO_3$ waveguides determined by x−ray rocking curve methods are reported by Minakata *et. al* [40] , [50] and Li *et al.* [44] , respectively. The satellite peak, separated from the substrate peak is observed in each case, and this peak corresponds to the proton−exchanged layer. In the case of the proton−exchanged layer without annealing process, the satellite peak is completely separated from the substrate peak (see Fig. 2.13 in section 2.5), which corresponds to the fact that this proton−exchanged layer has a step−like refractive index profile. The lattice constants of the $LiNbO_3$ and $LiTaO_3$ substrates are 13.863 Å and 13.784 Å , respectively. The increase in lattice constant caused by the proton−exchange process ($\Delta c/c$) is 0.46% in the case of $LiNbO_3$, while

in the case of $LiTaO_3$ it is 0.53 %.

The satellite peak becomes closer to the substrate peak after the annealing process, and the substrate peak and the satellite peak smoothly connected with each other at the bottom (Fig. 2. 13). This profile corresponds to fact that the annealed proton−exchanged layer has the graded index profile. The lattice constant of the annealed proton−exchanged layer decreases with the annealing process (Table 2.2).

The example of the x−ray rocking curves for the Rb ion−exchanged waveguides measured by our experiment is shown in Fig. 2.12. The peak which corresponds to the ion−exchanged layer is not so clear as in the case of the proton−exchanged waveguides, and connected with the the substrate peak. The maximum lattice constant change ($\Delta c/c$) is shown in Table 2.2.

The lattice constant is increased by the ion−exchange process. The maximum lattice constant change decreases as the $Ba(NO_3)_2/RbNO_3$ ratio increases. The lattice constant change is considerably reduced by the annealing process, and is hardly recognized in sample KTP4A. The strain caused by the ion−exchange process seems to be recovered by the annealing process.

2.5 Lattice Constants of Proton−Exchanged Waveguides Formed on Domain−Inverted $LiTaO_3$

2.5.1 Preparation of Samples

The z−cut $LiTaO_3$ substrate is kept in the pyrophosphoric acid at 260 ℃ for 30 min, and the proton−exchanged layer is formed. Then, the proton−exchanged layer is annealed at 525 ℃ for 2 min and the domain−inverted slab structure, which is 4 μm thick, is formed.

The periodically domain−inverted structure is formed with the process mentioned above by adding a tantalum mask which is 5 μm wide and 10.8 μm in period.

Several slab waveguides are formed on $LiTaO_3$ substrates (0.5 μm thick) with the proton−exchange process in pyrophosphoric acid at 260 ℃ for 30min. After the proton−exchange process, some of the waveguides are annealed at 340 ℃ for 30 min. The thickness of the annealed proton−exchanged waveguide is about 2 μm.

These are formed on a simple as−polished substrate, a substrate with a domain−inverted slab structure, and a substrate with a periodically domain−inverted structure. The fabrication conditions of the samples are shown in Table 2.3.

2.5.2 Results of the Experiment

The lattice constants of the samples are measured by the X−ray rocking curve analysis using the double crystal method. The X−ray rocking curves of the samples LT1 ～ LT7 are shown in Figs. 2.13 and 2.14. The rate of the lattice constant change ($\Delta c/c$) caused by the fabrication process is calculated from these curves. The results are shown in Table 2.3, where PE stands for the proton−exchanged

waveguide without annealing process, and APE stands for the annealed proton-exchanged waveguide.

The lattice constants of the $LiTaO_3$ substrates without and with the domain-inverted slab structure (LT11, LT13) and with the periodically domain-inverted structure (LT15) are compared, and are found to be the same, 13.784 Å .

A tiny peak appears on the right side of the substrate peak, in the substrate with domain-inverted slab structure (LT13) and in each sample of the proton-exchanged and the annealed proton-exchanged waveguide formed in the slab domain-inverted structure (Fig. 13(b)).

The lattice constants of the proton-exchanged waveguides formed on the substrates with and without the domain-inverted structure (LT1, LT3, and LT5) are compared from the rocking curve data shown in Fig. 13. The satellite peak in the rocking curve means the existence of the proton-exchanged layer with larger lattice constant than that of the substrate [40] , [44] , [50] . The increase in lattice constant caused by the proton-exchange process ($\Delta c/c$) is 0.53 %. This is almost the same in samples LT1, LT3, and LT5, as shown in Table 2.3.

The height of the satellite peak corresponds to the waveguiding layer thickness [10] . The satellite peak of the proton-exchanged layer formed in the domain-inverted structure (LT3) is higher than that in the substrate without domain-inverted structure (LT1). This shows that a thicker waveguide may be formed in the domain-inverted substrate than in the noninverted substrate. This is because the protons induced by the

domain-inversion process will also contribute to the waveguide formation.

The peak profiles of the annealed proton-exchanged waveguides are also shown in Fig. 2.13. The satellite peak becomes high and moves closer to the substrate peak after the annealing process. The values $\Delta c/c$ measured in the waveguides with domain-inverted slab structure (LT4), with the periodically domain-inverted structure (LT6), and without the domain-inverted structure (LT2) are 0.19 %, 0.21 % and 0.23 %, respectively, as listed in Table 2.3. This result suggests that protons diffuse deep into the substrate, and the lattice constant of the annealed proton-exchanged layer decreases with the annealing process. This result is in good agreement with the result obtained by Li *et al.* [44] . This can be explained as follows: the structure of the $LiTaO_3$ (trigonal system, 3m) changes to the perovskite structure (cubic system, m3m) by the proton exchange, as in the case of $LiNbO_3$. [40] , [50] . This structure has a larger lattice constant than the original. The perovskite structure of the proton-exchanged layer changes back to the original structure, as the protons are diffused into the substrate by the annealing process.

It seems that protons are diffused more rapidly into the substrate by the annealing process in the substrate with the domain-inverted structure than in the substrate without the domain-inverted structure.

In the domain inversion process, the lithium ions should be replaced by the protons and then the protons should be diffused deep into the substrate by the rapid annealing process. Consequently, many lithium vacant sites will appear and the protons introduced in the

waveguiding layer in the proton−exchange process may be diffused rapidly by the annealing process.

A domain−inverted slab structure which is twice as thick as the domain−inverted structure in sample LT3 is formed. The domain−inversion process is the same as the above−mentioned process except for the annealing temperature, which is 550 ℃ . On this domain−inverted slab structure (8μm thick), the proton−exchanged layer without annealing process is formed (LT7).

If the tiny peak were due to the lattice constant change of the domain−inverted structure, this peak would become more prominent as the domain−inverted structure became thicker. However, the tiny peak on the right side of the substrate peak cannot be observed at all in the sample with the thick domain−inverted slab structure as shown in Fig.14. Therefore it may be concluded that no lattice constant change is caused by this domain−inversion process.

2.6 Conclusion

In this chapter, the refractive index profiles of the ion−exchanged waveguides and the lattice constant changes due to the fabrication process are investigated.

The refractive index profiles of the ion−exchanged planer waveguides are determined using the prism coupler method. The refractive index profiles of the proton−exchanged layers formed on the three types of *z*−cut $LiNbO_3$ substrates: non−doped, Ti−indiffused and MgO−doped, are measured. In all cases, the surface refractive

index decreases according as the annealing time increases, and the refractive index profile of the proton−exchanged layer is gradually changed into the Gaussian profile. The diffusion of the protons into the substrate by the annealing process seems to be disturbed by the impurity such as MgO−doped ions.

The increase in the surface refractive index caused by the annealing process, which might be caused by the movement of the protons between interstitial and substitutional sites, is reported for the proton−exchanged $LiTaO_3$ waveguide [44] . This phenomenon is not observed in the proton−exchanged $LiNbO_3$ waveguides formed on the non−doped, Ti−indiffused, and MgO−doped substrates.

The refractive index profile of the Rb ion−exchanged layer without annealing process is approximate erfc function. After annealing the waveguide, the surface refractive index is considerably reduced, and the refractive index profile is changed into an Gaussian profile. It is confirmed by our experiment that annealing process is effective for controlling the refractive index profile in the Rb ion−exchanged KTP waveguide as well as in the proton−exchanged $LiNbO_3$ and $LiTaO_3$ waveguides.

The lattice constant changes of the ion−exchanged planer waveguides are investigated in detail. The lattice constant is increased by the Rb ion−exchange process as well as by the proton−exchange process. The lattice constant change is considerably reduced by the annealing process both in the case of the proton−exchanged waveguide and Rb−ion exchanged waveguide. The strain caused by the ion−exchange process seems to be

recovered by the annealing process.

The structural change of the $LiTaO_3$ crystal caused by the domain−inversion process and its influence on the waveguide formation are experimentally studied for the first time.

The lattice constants of the $LiTaO_3$ substrates without and with the domain−inverted slab structure and with the periodically domain−inverted structure are the same, 13.784 Å . The increase in lattice constant caused by the proton−exchange process ($\Delta c/c$) is 0.53 %. The values $\Delta c/c$ measured in the annealed proton −exchanged waveguides with domain−inverted slab structure, with the periodically domain−inverted structure, and without the domain−inverted structure are 0.19 %, 0.21 % and 0.23 %, respectively.

From our experimental results, it is very likely that protons will diffuse more rapidly into the substrate by the annealing process (at 340 ℃) in the domain−inverted structure than in the substrate without the domain−inverted structure. This may be because in the domain−inversion process, many lithium vacant sites will appear due to the annealing process at the high temperature (525 ℃).

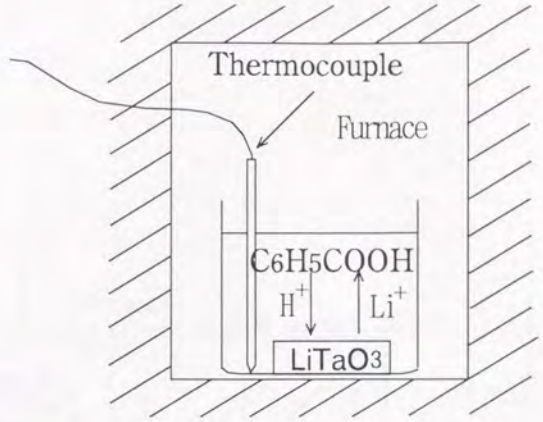

Fig. 2.1. Proton−exchange Method

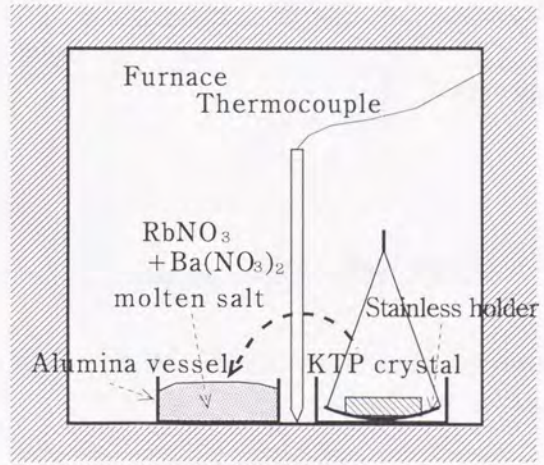

Fig. 2.2. Ion−exchange method

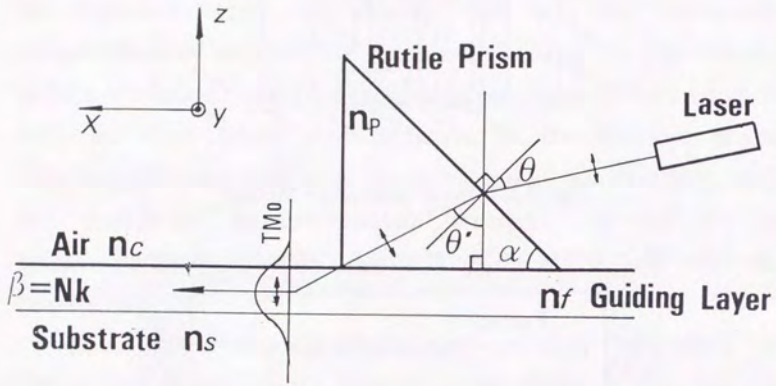

Fig. 2.3. Prism−coupler method.

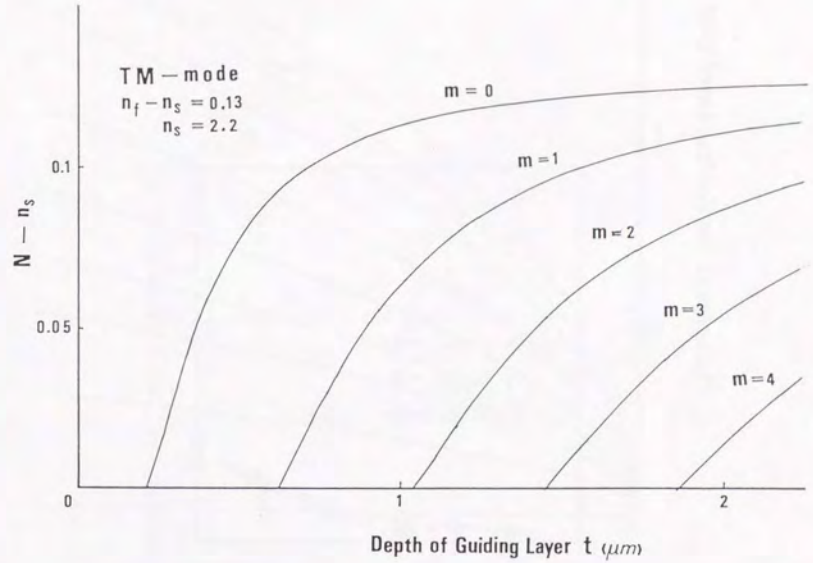

Fig. 2.4. Dispersion curves for proton−exchanged $LiNbO_3$ waveguide.

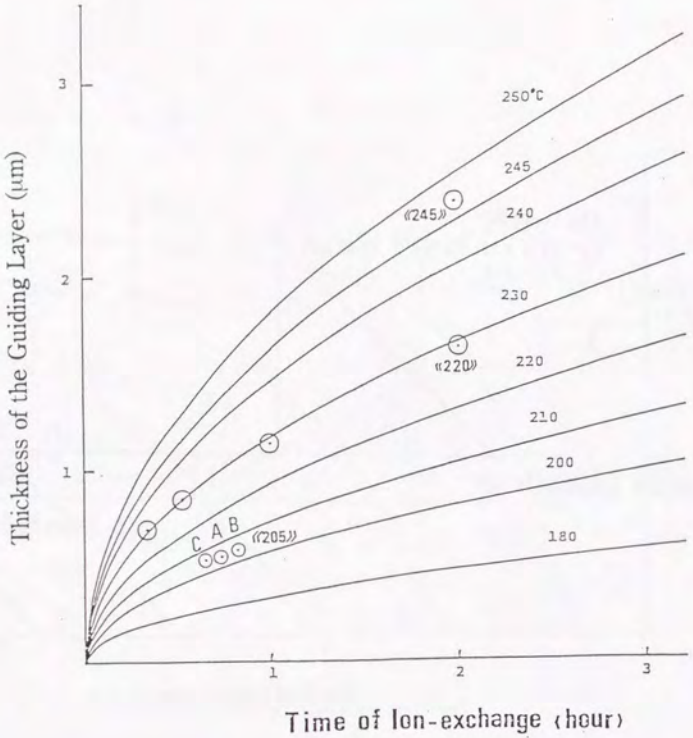

Fig. 2.5. Relation between the thickness of the proton-exchanged layer and exchange time.

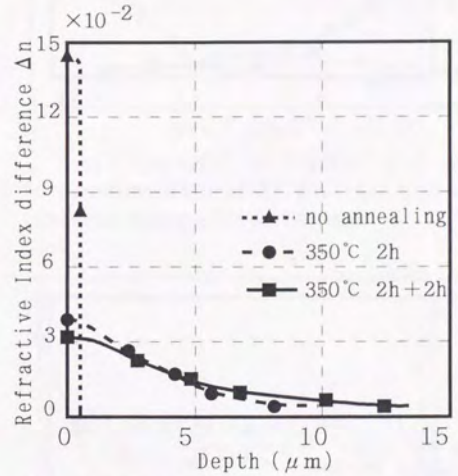

Fig. 2.6. Refractive index profile of the PE layer formed on the nondopeded LN crystal

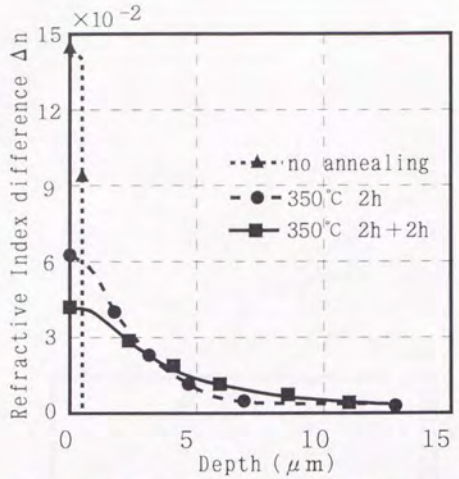

Fig. 2.7. Refractive index profile of the PE layer formed on the Ti-indiffused LN crystal

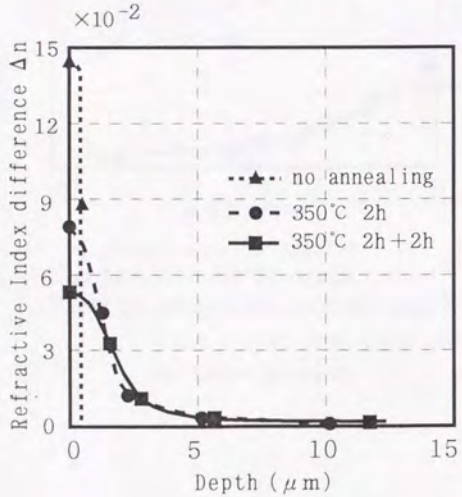

Fig. 2.8. Refractive index profile of the PE layer formed on the MgO-doped LN crystal

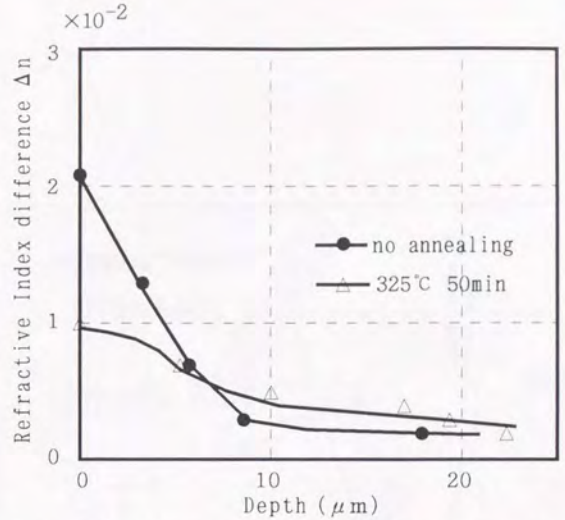

Fig. 2.9. Refractive index profile of the ion-exchanged layer formed on the KTP crystal

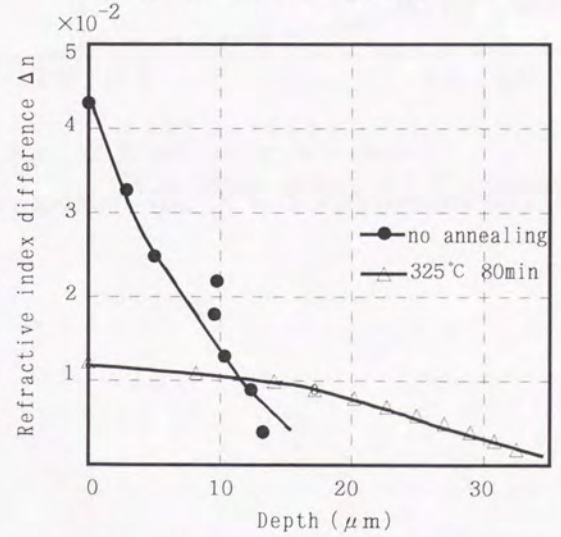

Fig. 2.10. Refractive index profile of the ion-exchanged layer formed on the KTP crystal
(Δn is the refractive index difference between the ion-exchanged layer and the substrate)

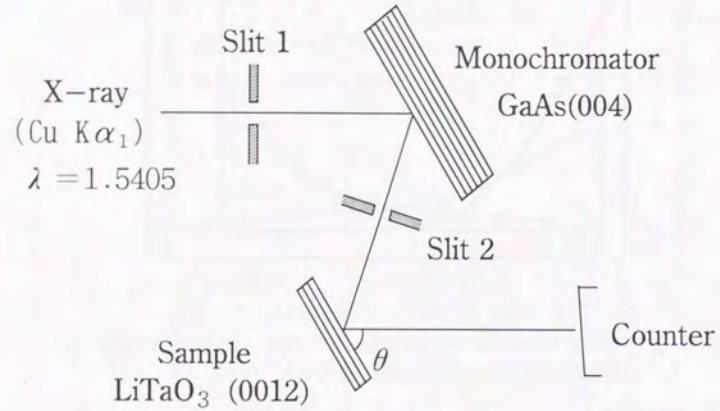

Fig. 2.11. The measurement of X−ray rocking curves

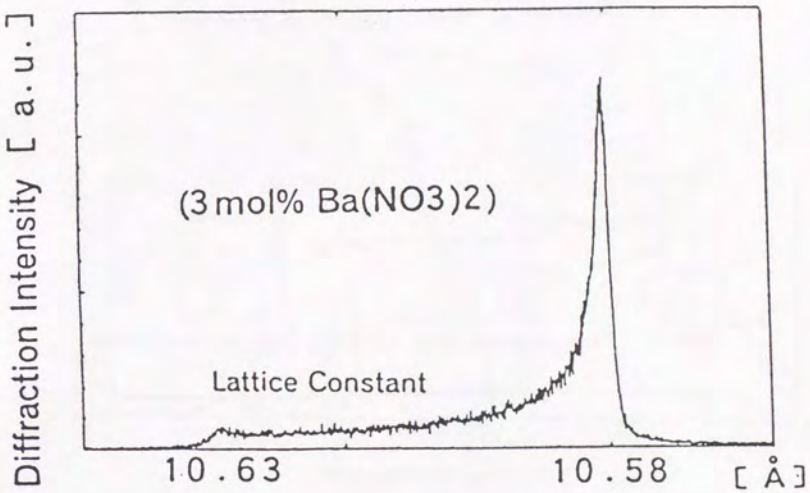

Fig. 2.12. X−ray rocking curve analysis
of the Rb ion−exchanged KTP waveguide.

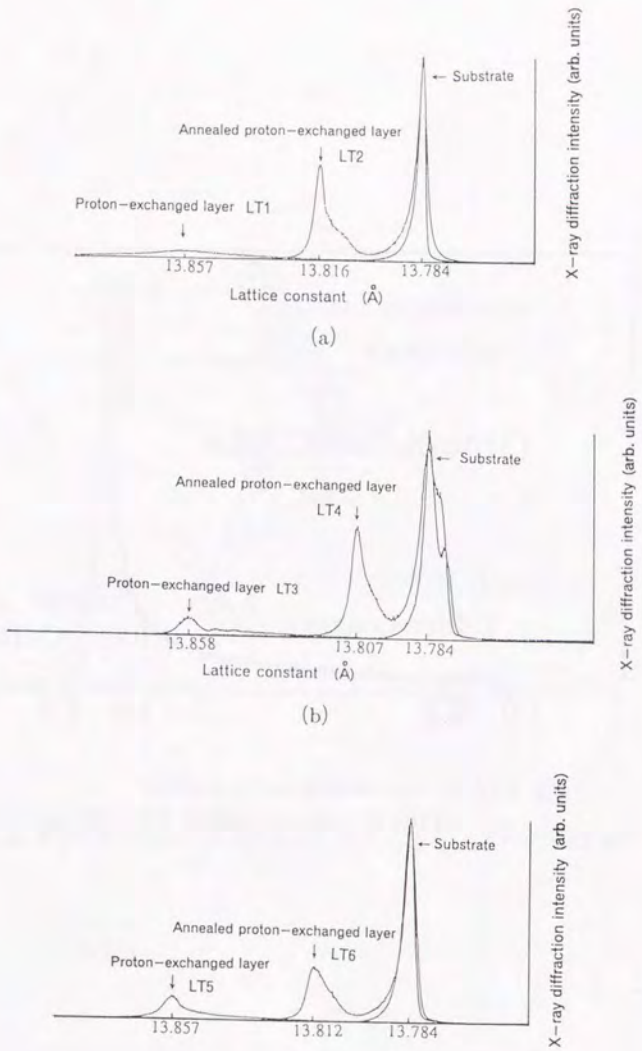

Fig. 2.13. (a) X-ray rocking curves for proton-exchanged waveguides formed in the $LiTaO_3$ substrate (LT1, LT2) (b) X-ray rocking curves for proton-exchanged waveguides formed in the domain-inverted slab structure (4 μm thick) on the $LiTaO_3$ substrate (LT3, LT4). (c) X-ray rocking curves for proton-exchanged layer formed in the periodically domain-inverted structure on the $LiTaO_3$ substrate (LT5, LT6).

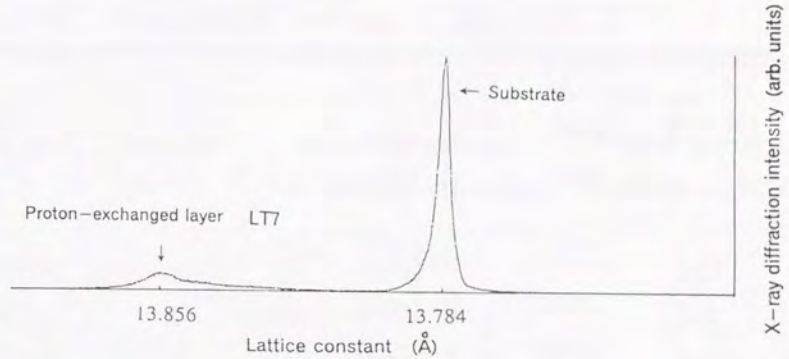

Fig. 2.14. X-ray rocking curve for proton-exchanged layer formed in the thick domain-inverted slab structure (8 μm thick) on the $LiTaO_3$ substrate.

Table 2.1. Diffusion coefficient and activation energy of the ion-exchange process

	T(℃)	D(T) ($\mu m^2/h$)	Q (kJ/mol)	Do ($\mu m^2/h$)
	170	0.012		
PE-LN	200	0.069	95	2.5×10^9
	220	0.309		
	260	0.282		
PE-LT	300	0.862	86	7.5×10^7
	330	2.339		

Table 2.2. The lattice constants of the ion-exchanged waveguides

Sample	$Ba(NO_3)_2$ (mol%)	fabricationcondition ion-exchange	annealing	lattice constant change (Δ c/c%)
KTP1	3	320 ℃ 45min		0.36
KTP2	3	340 ℃ 45min		0.42
KTP3	7	340 ℃ 45min		0.34
KTP4	15	320 ℃ 10min		0.25
KTP1A	3	320 ℃ 45min	325 ℃ 80min	0.06
KTP4A	15	320 ℃ 10min	325 ℃ 80min	/

Table 2.3. Measured lattice constants in the proton-exchanged $LiTaO_3$ waveguides.

Sample	Waveguide	Substrate structure	Lattice constant [Å]	Δ c/c [%]
LT1	PE	$LiTaO_3$	13.857	0.53
LT2	APE	$LiTaO_3$	13.816	0.23
LT3	PE	Domain-inverted slab structure (4μm thick)	13.858	0.53
LT4	APE	Domain-inverted slab structure (4μm thick)	13.807	0.19
LT5	PE	Periodically domain-inverted structure	13.857	0.53
LT6	APE	Periodically domain-inverted structure	13.812	0.21
LT7	PE	Domain-inverted slab structure (8μm thick)	13.856	0.52
LT11		$LiTaO_3$	13.784	
LT13		Domain-inverted slab structure (4μm thick)	13.784	
LT15		Periodically domain-inverted structure	13.784	

Chapter Ⅲ

Exact Estimation of Electrooptic Constants in Optical Waveguides

Abstract

Electro-optic constants of single-mode proton-exchanged slab waveguiding layers fabricated on *z*-cut $LiNbO_3$ crystals are estimated, taking into account the field distribution of the propagating TM_0 mode.

The effect of annealing on the electrooptic constants r_{33} in the proton-exchanged optical waveguides on three types of $LiNbO_3$ crystals: undoped, titanium-indiffused and MgO-doped, is investigated. The exact estimation shows that the deterioration of electrooptic constant is recovered by annealing; the best in undoped, then titanium-indiffused and the worst, MgO-doped.

The electrooptic constants r_{22} in the PETi waveguides formed on the *y*-cut $LiNbO_3$ crystals are also measured for the purpose of designing the polarization independent switches.

3.1 Introduction

The lithium niobate, lithium tantalate, and KTP waveguides are the attractive materials for the electrooptic devices. The degradation of the electrooptic effect in the proton-exchanged layer is reported for the lithium niobate and lithium tantalate waveguides [50] , [51] . Higuchi *et al.* reported that no degradation of the electrooptic effect is observed in the KTP waveguides [47] .

Yuhara *et al.* reported that r_{33} decreases to 2.2pm/V after the proton-exchange, which is 1/14 of the original value of the lithium tantalate and that its recovery is observed after the post annealing process [78] .

The degradation of the electrooptic constant r_{33} in the lithium niobate is also reported in several papers. Becker [51] fabricated interferometric modulators by Ti-indiffusion method and proton-exchange method and compared them. He has reported that the half wave-voltage in the proton-exchanged modulator was 2.7 times larger than that in Ti-diffused one. And he also reported that electro-optic effect increases as the wavelength increases and the mode confinement of the proton-exchanged $LiNbO_3$ becomes less sufficient, from the experimental results of measurement of the half-wave voltage in Ti-diffused guides and proton-exchanged ones. And from this measurement Becker suggested that there may not be any electro-optic in proton-exchanged $LiNbO_3$.

Minakata *et al.* [40] , [50] have reported the experimental results of electro-optic constant in proton-exchanged ridge waveguides using the phase modulation technique. The electro-optic constant measured by them was 3.3×10^{-12} m/V, which is significantly small comparing with the values in the unexchanged crystal. This value is obtained, however, without considering the field distribution of the propagating mode in the substrate .

Since the field penetration into the substrate can not be neglected especially for the fundamental mode, the measured values of the electro-optic constants are seriously affected by this effect. This assumption agrees with Beckers report [51] . The degradation of the electro-optic effects can be explained by the deformation from the original diamond structure of $LiNbO_3$ to the Perovskite structure due to the strain induced from the indiffused protons [40] , [50] . It can be assumed that the proton-exchanged layer may be changed into a material with a different electro-optic constant.

In 3.2 and 3.3, we report experimental method and its results of the electro-optic constants in proton-exchanged slab waveguides fabricated on z-cut $LiNbO_3$ crystal, considering the influence of the field distribution in the substrate. By this measuring system, the electro-optic constants of the proton-exchanged layer r'_{33}, r'_{32} are measured.

On the other hand, there have been several papers trying to improve the deterioration of the electrooptic constant after proton exchange process [52] - [53] . In 3.4, the effect of annealing is compared on three types of $LiNbO_3$ crystals, undoped, titanium-indiffused (250- Å -thick titanium film is diffused at about 1000 ℃ for 8 hours in wet O_2) and MgO-doped (5mol%) from the

experimental values of the electrooptic constant r_{33}.

In 3.5, the electrooptic effects in the Ti-indiffused waveguide and in the the proton-exchanged Ti-indiffused (PETi) waveguides formed on the *y*-cut $LiNbO_3$ crystals are investigated. The PETi process has been found to be a powerful tool in the fabrication of low-loss polarization independent waveguide due to its unique and simple passive tuning capability combined with the ability to equalize TE and TM mode propagation characteristics [55] . The next step is to fabricate active structures using the same techniques in order to fabricate simple easily controllable polarization independent switches.

Although waveguide loss is minimal using the PETi process, there is the fear that the electro-optic effects will be degraded, making the smaller E-O coefficient r_{22} unusable. Therefore the electrooptic constants r_{22} in the PETi waveguides and the normal Ti waveguide are exactly measured and compared.

3.2 Measurement of Electrooptic Effect

3.2.1 Principle of Measurement

The electrooptic constants are measured using the Mach-Zehnder interferometer. The laser beam is modulated by applying the voltage to the crystal.

The voltage across the crystal V_S is given as follows (Fig. 3.1).

$$V_S = \frac{V_0}{1+\varepsilon_s(d-d_S)/(\varepsilon_0 d_S)} , \qquad (3-1)$$

where V_0 is the voltage between the electrodes, ε_0 is the dielectric constant of the air, and ε_s is the dielectric constant of the crystal. Assuming that the dielectric constant ε_s of the guiding layer is the same as the dielectric constant of the substrate, it is 32 at the frequency of 50 Hz. d is the distance between the electrodes and d_s is the thickness of the crystal.

The electric field E_{spont} which may be independent of the applied voltage to the crystal is induced by the spontaneous polarization P_{spont}. If $E_{spont.}$ is large, the modulation degree changes according to the distance of the electrodes when the same voltage is applied to the crystal. So the half wave-voltage $V_{s\lambda/2}$ should be dependent of the distance between the electrodes, if $P_{spont.}$ is large and cannot be neglected. The electro-optic constants are measured by changing the distance between the electrodes to check the influence of the spontaneous polarization of the $LiNbO_3$ crystal.

When the voltage is applied to the $LiNbO_3$ crystal, the propagating constants β changes into β' $(=\beta+\Delta\beta)$. The phase difference $\Delta\phi$ should be

$$\Delta\phi=\Delta\beta l , \qquad (3-2)$$

where l is the length of the crystal.

The index ellipsoid of the crystal using the principal axes is given by the following equation.

$$x^2/(nx)^2 + y^2/(ny)^2 + z^2/(nz)^2 = 1. \qquad (3-3)$$

When the voltage is applied to the crystal, the axes, x,y,z can be no longer the principle axis. In this case, the index ellipsoid is expressed as,

$$B_{11}x^2+B_{22}y^2+B_{33}z^2+2B_{23}yz+2B_{31}zx+2B_{12}xy=1, \qquad (3-4)$$

where each coefficients are given in terms of the electrooptic coefficients and the applied electric field E_e as follows.

$$\begin{bmatrix} B_{11}-\dfrac{1}{nx^2} \\ B_{22}-\dfrac{1}{ny^2} \\ B_{33}-\dfrac{1}{nz^2} \\ B_{23} \\ B_{31} \\ B_{12} \end{bmatrix} = \begin{bmatrix} r_{11} & r_{12} & r_{13} \\ r_{21} & r_{22} & r_{23} \\ r_{31} & r_{32} & r_{33} \\ r_{41} & r_{42} & r_{43} \\ r_{51} & r_{52} & r_{53} \\ r_{61} & r_{62} & r_{63} \end{bmatrix} \begin{bmatrix} E^e x \\ E^e y \\ E^e z \end{bmatrix}.$$

Considering the symmetry of the crystal, the above tensor of electrooptic coefficients is written as follows.

$$\begin{bmatrix} 0 & -r_{22} & r_{13} \\ 0 & r_{22} & r_{13} \\ 0 & 0 & r_{33} \\ 0 & r_{51} & 0 \\ r_{51} & 0 & 0 \\ -r_{22} & 0 & 0 \end{bmatrix}$$

The index ellipsoid cut at $x=0$ can be assumed when the voltage is applied in the z direction and the light propagates in the x direction. eq. (3−4) is rewritten as,

$$(1/n_o^2+r_{13}E^e z)y^2+(1/n_e^2+r_{33}E^e z)z^2=1. \qquad (3-5)$$

The refractive index change caused by the Pockels' effect is small and the following approximation can be made.

$$|\, r_{13}n_o^2 E^e z \,| \ll 1, \quad |\, r_{33}n_e^2 E^e z \,| \ll 1. \qquad (3-6)$$

Therefore, the eq. (3−6) is written under this approximation as,

$$\frac{y^2}{n_o^2(1-\frac{1}{2}r_{13}n_o^2E^e z)^2}+\frac{z^2}{n_e^2(1-\frac{1}{2}r_{33}n_e^2E^e z)^2}=1\ . \qquad (3-7)$$

In this case, the ordinary refractive index n_y and extraordinary index n_z is expressed as,

$$n_y = n_o - \Delta n_o, \quad \Delta n_o = (1/2) r_{13} n_o^3 E_z, \tag{3-8}$$

$$n_z = n_e - \Delta n_e, \quad \Delta n_e = (1/2) r_{33} n_e^3 E_z \tag{3-9}$$

The index in the guiding layer changes by this Pockels' effect, and the index in the substrate changes as well. The difference of the refractive index Δn_f (guiding layer) and Δn_s (substrate) are given by the following equations.

$$\Delta n_f = -(1/2) n_f^3 r'_{33} E, \tag{3-10}$$

$$\Delta n_s = -(1/2) n_s^3 r_{33} E, \tag{3-11}$$

where r'_{33} and r_{33} are the electro-optic constants of the guiding layer and the substrate respectively, and E is the applied field.

The difference between the propagating constant before and after the voltage is applied ($\Delta\beta$) can be calculated from the eigen equation, but the difference of the refractive index is so small that the value of $\Delta\beta$ is easily corrected by the variational method considering the effect of the field distribution of the light propagating in the substrate. In the coordinates shown in Fig. 3.1, the light propagates in the x direction, the voltage is applied to the z direction and the transverse electric field of the TM_0 mode is E_z.

When the electric field is applied to the crystal, the transverse electric field of TM_0 mode (E_z) slightly changes into E'_z. So the following equations can be obtained from the Maxwell's equations.

$$\frac{\partial^2 E_z(z)}{\partial z^2} + (n^2 k_0^2 - \beta^2) E_z(z) = 0, \tag{3-12}$$

$$\frac{\partial^2 E'_z(z)}{\partial z^2} + (n'^2 k_0^2 - \beta'^2) E'_z(z) = 0. \tag{3-13}$$

From eqs. (3-12) and (3-13), the following equation is obtained.

$$E'_z(z)\frac{\partial^2 E_z(z)}{\partial z^2} - E_z(z)\frac{\partial^2 E'_z(z)}{\partial z^2} + ((n^2 - n'^2)k_0^2 - (\beta^2 - \beta'^2)) E_z(z) E'_z(z) = 0 \tag{3-14}$$

where n, n' are the refractive index before and after the voltage is applied to the crystal respectively, and k_0 is the propagating constant in the air.

By integrating the eq. (3-14) along the z axis,

$$(\beta^2 - \beta'^2) \int_{-\infty}^{\infty} E_z(z) E'_z(z) dz = k_0^2 \int_{-\infty}^{\infty} (n^2 - n'^2) E_z(z) E'_z(z) dz, \tag{3-15}$$

can be obtained. As both $\Delta\beta (= \beta - \beta')$ and $\Delta n (= n - n')$ are very small, we can estimate $\Delta\beta$ as follows from eq. (3-15)

$$\Delta\beta = \frac{k0^2}{\beta} \frac{\int_{-\infty}^{\infty} n\,\Delta n Ez(z)E'z(z)dz}{\int_{-\infty}^{\infty} Ez(z)E'z(z)dz}$$

$$= \frac{k0^2}{\beta} \frac{\left[n_C \Delta n_C \int_0^{\infty} Ez^2(z)dz + n_f \Delta n_f \int_{-t}^{0} Ez^2(z)dz + n_S \Delta n_S \int_{-\infty}^{-t} Ez^2(z)dz \right]}{\int_{-\infty}^{\infty} Ez^2(z)dz} \qquad (3-16)$$

where Δn_C, Δn_f, Δn_S are the difference of the refractive index of the air, guiding layer, and the substrate, respectively.

The relation between equivalent index N and the propagation constants β is

$$\beta = Nk_0. \qquad (3-17)$$

From the Eqs. (3−2), (3−10), (3−11), (3−16), (3−17), the electro−optic constant of the guiding layer r'_{33} can be calculated.

$$r'_{33} = \left(\frac{\lambda N d_S}{2.828 V_{S\lambda/2} l} - n_S^4 r_{33} \frac{p_S}{p} \right) / (n_f^4 p_f / p) \quad , \qquad (3-18)$$

where

$$p = \int_{-\infty}^{\infty} Ez^2(z)dz, \quad p_f = \int_{-t}^{0} Ez^2(z)dz, \quad p_S = \int_{-\infty}^{t} Ez^2(z)dz, \qquad (3-19)$$

and λ is the measuring wavelength, t is the depth of the waveguides.

So r'_{33} is obtained from Eq. (3−18) from the measured values of $V_{S\lambda/2}$ experimentally. By using a similar procedure, we can measure r'_{32} with applying the voltage to the y direction.

3.2.2 Configuration of Experiments

The experimental set up by Mach−Zehnder interferometer is shown in Fig. 3. 2. A He−Ne laser (633 nm, 7 mW) is used as a light source. The laser light is split into two beams, one for the reference and the other for the guided beam through a half mirror 1. The a.c. voltage of 50 Hz is applied to the waveguide by a pair of electrodes with air gap on the crystal.

The reference beam and the guided beam interfere with each other by the half mirror 2 and interference pattern is observed by a photodetector and an oscilloscope to measure the value of $V_{S\lambda/2}$ (Fig. 3.3).

In this experiment, the half−wave voltage at which the modulation degree reaches the maximum, is calculated through the values of modulation degree as a function of the corrected voltage to the crystal (Fig. 3.3). The electrooptic constant r_{33} is calculated from the obtained half−wave voltage.

3.3 Electrooptic Constants in Proton-Exchanged Layer with Step-Index Profile

3.3.1 Fabrication of The Waveguides

Two kinds of the proton-exchanged waveguides in z-cut $LiNbO_3$ crystals by pyrophosphoric acid and benzoic acid are prepared. The proton-exchange temperature ranges from 200 ~ 230 ℃ and the proton-exchange time ranges from 12 ~ 76min. After the proton-exchange process, some of the samples are annealed (200 ℃, 2h) in order to control the index instabilities.

3.3.2 Measurement of Electrooptic Constant

The Mach-Zehnder interferometer explained in the former section, is used for the experiment. He-Ne laser (633nm, 7mW) is used as a light source. The laser beam is focused by a microscopic objective (x100) into an end of the waveguide, and the a.c. voltage is applied. The output beam is reformed by the cylindrical lense.

3.3.3. Experimental Results

By this measuring system, the electro-optic constants of the proton-exchanged layer r'_{33}, r'_{32} are measured.

The measured half-wave voltage is shown in Table 3.3. As the measured half-wave voltage $V_{s\lambda/2}$ seems to be independent of the distance between the electrodes (Table 3.3), the influence of the

spontaneous polarization of the $LiNbO_3$ is negligible. Measured r'_{33} are shown in Table 3.1. The electro-optic constants r'_{33} in the waveguides are reduced to about 1/20 of r_{33} in the bulk crystal (Table 3.2). The influence of annealing the crystal seems to be negligible. The electro-optic constants without the correction of the field distribution of the propagating mode can be estimated by the assumption that the light is completely confined to the guiding layer. So it can be obtained from Eq. (3-18) by neglecting the second term, and assuming that p_f is almost the same as p. The uncorrected value is about 1/10 of the electro-optic constants in the bulk crystal (Table 3.1). These values are a little larger but almost agree with the results of Minakata *et al.* [40], [50]. The electro-optic constant r'_{32} is about 0.59×10^{-12} m/V.

The electro-optic constants r_{33}, r_{13}, and r_{22} in the MgO-doped bulk crystal (1.34 weight percent) and non-doped bulk crystal are also measured and compared. These results give almost the same value (Table 3.2).

3.4 Effect of Annealing on Electrooptic Constants of Proton-Exchanged Waveguides

3.4.1 Fabrication of the waveguides

Proton-exchanged waveguides are formed on the three types of substrates, undoped, titanium-indiffused (250- Å -thick titanium film was diffused at about 1000 ℃ for 8 hours in wet O_2), and MgO-doped (5mol%) z-cut $LiNbO_3$ substrates. All the $LiNbO_3$

substrates are first heated in a furnace up to 230 degrees centigrade and dipped into the pyrophosphoric acid kept at the same temperature as the substrate. The optical waveguiding layers of thickness of 0.5 μm are formed on the nondoped, titanium−indiffused, and MgO−doped substrates after 12 min, 15min, and 23min respectively. After this proton exchange process, each of the waveguide is annealed at 350 degrees centigrade changing the annealing time. The fabrication conditions of the waveguides are shown in Table 3.4.

3.4.2 Measurement of the electrooptic constant

The electrooptic constants are measured by the Mach−Zehnder interferometer (see section 3.2). In this experiment, the laser beam is coupled into and out the waveguide by a couple of rutile prisms and the TM_0 mode is excited (Fig. 3.4).

The value obtained is an equivalent value for the guided wave. This value includes both the effect in the guiding layer and the substrate. This equivalent value is calculated without considering the field distribution of the light propagating in the substrate. At present work, this equivalent value is measured. This is because the crystal is annealed after the proton exchange process and because the index profile becomes smooth.

Generally the field distribution should be considered in order to obtain the electrooptic constant r_{33} of the material in the guiding layer itself. The electrooptic constant r_{33} of the material in the guiding layer is called as the pure electrooptic constant r_{33}.

In the proton−exchanged waveguide, the guiding layer has a step index profile and the material in this guiding layer is regarded as a different material from the substrate. In this case, the pure electrooptic constant r_{33} is calculated as shown in section 3.2.1. The pure electrooptic constant r_{33} is also calculated for the crystal with the step profile as shown in Table 3.4 (Δn is the refractive index difference between the substrate and the waveguide).

3.4.3 Experimental Result

The values of electrooptic constants r_{33} in three types of proton exchanged $LiNbO_3$ optical waveguides for the different annealing time are shown in Table 3.4. The value of electrooptic constant r_{33} for the undoped $LiNbO_3$ crystal before annealing is 3.4×10^{-12} m/V. After two hours plus another two hours of annealing, it increased to the value of 23.6×10^{-12} m/V. Similarly the values of electrooptic constant r_{33} for the Ti−indiffused $LiNbO_3$ crystal and the MgO−doped $LiNbO_3$ crystal after the annealing are also increased. This is shown in Fig. 3.5. When the annealing time exceeds two hours plus another one hour, the increase of the values of electrooptic constant r_{33} becomes very slow. Thus the annealing shows less effect on the refractive index change. Due to the annealing, the exchanged region in the crystal is diffused deeper and the concentration of hydrogen reduces at the surface [52] , [53] . When the annealing time exceeds more than two hours plus one hour, the concentration of hydrogen reaches the minimum value and thus the annealing becomes

less effective.

Since the undoped crystal has the maximum value of hydrogen concentration, the recovering due to the annealing is most effective. The value of electrooptic constant r_{33} increased by the annealing is the minimum for the MgO−doped crystal, because it contains large amount of impurities during doping process.

3.4.4 Discussion

From the results of the experiment, the values of electrooptic constant r_{33} decrease significantly after the proton exchange process and these values increase again to 70% of the original after the annealing.

This result proves to be supported by the explanation of Minakata *et al.* [40] . They wrote that the $LiNbO_3$ crystal has the diamond structure (trigonal system, 3m) which has large electrooptic effect. This structure changes to Perovskite structure (cubic system, m3m) induced by the strain due to the concentration of the lithium ions inside the crystal after the proton exchange process. When the crystal is annealed, the protons diffuse deep into the substrate and the hydrogen concentration at the surface is reduced. This effect causes the structural change from the cubic m3m to the trigonal system, 3m again. So the value of electrooptic constant r_{33} increases. It should be considered that the impurity such as the Mg ions may hinder the structural change. Because the value of r_{33} increased again after the annealing is the smallest for the MgO−doped crystal.

3.5 Electrooptic Constants of y−cut PETi Waveguides for Polarization−Independent Switch

3.5.1 Fabrication of the waveguides

The proton−exchange process (PE) in $LiNbO_3$ produce a large increase in the extraordinary refractive index n_e (0.12 at 633nm [7]) and a significant decrease in the ordinary refractive index no (−0.04 at 633nm [7]). Therefore, it is possible to simply and effectively reduce the refractive index of the surface region in a *z*−propagating Ti− indiffused $LiNbO_3$ waveguide by making use of the negative change in refractive index [55] . The refractive index profile of the proton−exchanged layer without annealing process is a step. Assuming that n_o is modified in a manner similar to that of n_e during the annealing process, it is possible to modify the properties of a Ti−indiffused waveguide by modifying the surface region (Fig. 3.6).

Ti−indiffused waveguide and PETi waveguides are fabricated on *y*−cut $LiNbO_3$ crystal under the conditions shown in Table 3.5.

250− Å −thick titanium metal film is evaporated on to the surface of the *y*−cut $LiNbO_3$ crystal. Ti−indiffused waveguide is formed by diffusing the titanium film at 1000 ℃ for 8h in a wet oxygen atmosphere.

PETi waveguides are formed in two steps. Firstly, Ti−indiffused waveguides are formed by diffusing the titanium film (800 Å) into the crystal at 1000 ℃ for 10h. The second step, the proton−exchange process is carried out on the Ti−diffused samples by inserting them

into pure molten benzoic acid in a stainless beaker placed in a temperature-controlled oil bath at 210 ℃ . The exchange time is 4 ~ 8min. After the proton-exchange process, some of the waveguides are annealed at 350 ℃ for 80min ~ 2h.

3.5.2 Measurement of the electrooptic constant r_{22}

The half-wave voltage is measured by the same measuring system as that in 3.3.2, and electrooptic constant r22 is calculated from the following equation.

$$r_{22}=\frac{\lambda N d_s}{2.828 n_f^4 V_s \lambda/2 l} \quad . \qquad (3-20)$$

3.5.3 Experimental results

The measured electrooptic constants r_{22} are shown in Table 3.5. The electrooptic constants r_{22} are almost the same in both Ti-indiffused waveguide and PETi waveguides with and without the annealing process.

Although the electrooptic constant r_{22} is verified to be slightly dependent upon exchange time, all the waveguides measured are verified to have almost identical coefficients after annealing.

3.6 Conclusion

The electro-optic constant r'_{33} of the proton-exchanged $LiNbO_3$ is measured with the correction considering the field distribution of

the propagating mode. The electro-optic constants of $LiNbO_3$ proton-exchanged by benzoic acid and pyrophosphoric acid obtained by our experiment are 1.52×10^{-12} m/V and 1.45×10^{-12} m/V, respectively. The electro-optic constant of the guides proton exchanged by benzoic acid was half of the value obtained by Minakata *et al.* [40] , [50] . This difference may be explained by considering the influence of the field distribution of the propagating light in the substrate. The degradation of the electro-optic constants looks like to be larger for the waveguides with a larger index-difference.

In our experiment, the electro-optic constant r'_{33} in the proton-exchanged $LiNbO_3$ is very small compared with the value in the bulk crystal. And we can support the explanation by Minakata *et al.* [40] that the cause of this degradation should be the deformation of the diamond structure of $LiNbO_3$ (trigonal system, 3m) into a Perovskite structure (cubic system, m3m) with electro-optic constant is zero. The reason why the electro-optic constant r'_{32} is not zero can be explained by the local fluctuation of the structure. The influence of annealing at 200 ℃ for two hours is almost negligible because the depth of the guiding layer is not changed by annealing, under this annealing condition.

The effect of annealing on the electrooptic constant r_{33} for z-cut single mode optical waveguides in three types of proton exchanged $LiNbO_3$ crystals is also investigated in detail.

After the annealing process, the values of electrooptic constant r_{33} increase in all the waveguides. Among three crystals the undoped

one gives the most advantageous result and the MgO−doped crystal has the least effect. The MgO−doped $LiNbO_3$ crystal is rather insensitive to the increase of the value of r_{33} by the annealing method .

From the result of the experiment the annealing method gives advantages for optical waveguides to be used as integrated optical devices such as modulators and switches.

The polarization independent switches can be designed using the annealed PETi waveguide formed on the *y*−cut $LiNbO_3$ substrate [55] . In this case, the electrooptic effect depends on r_{22} in the waveguide. The electrooptic constants r_{22} is measured for the case of Ti−indiffused waveguide, and for the case of proton−exchanged waveguides with and without annealing process formed on the Ti indiffused *y*−cut substrate.

The electrooptic constant r_{22} at low frequencies is verified to be slightly dependent upon exchange time. However, after annealing, all the waveguides measured are verified to have almost identical coefficients. There is no detrimental effect to r_{22} after annealing. Moreover, the waveguide characteristics such as coupling loss and polarization independence can be controlled by the fabrication condition [55] . Therefore, it is possible that the simple polarization independent switches are fabricated using this PETi process on the *y*−cut $LiNbO_3$ crystal.

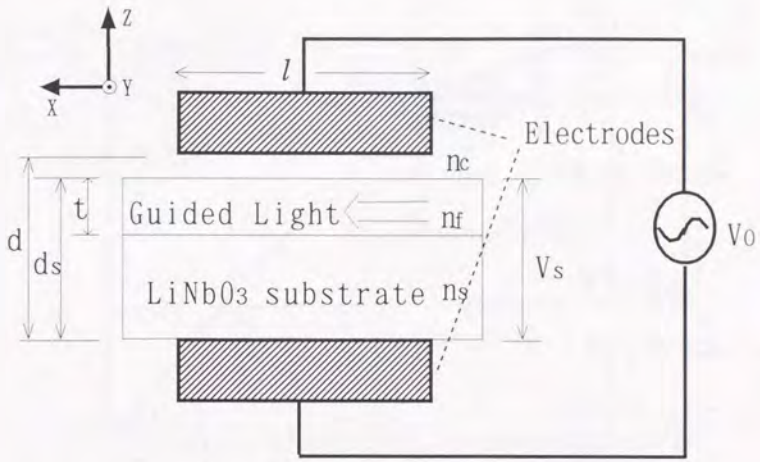

Fig. 3.1. Measurement of electro-optic effect

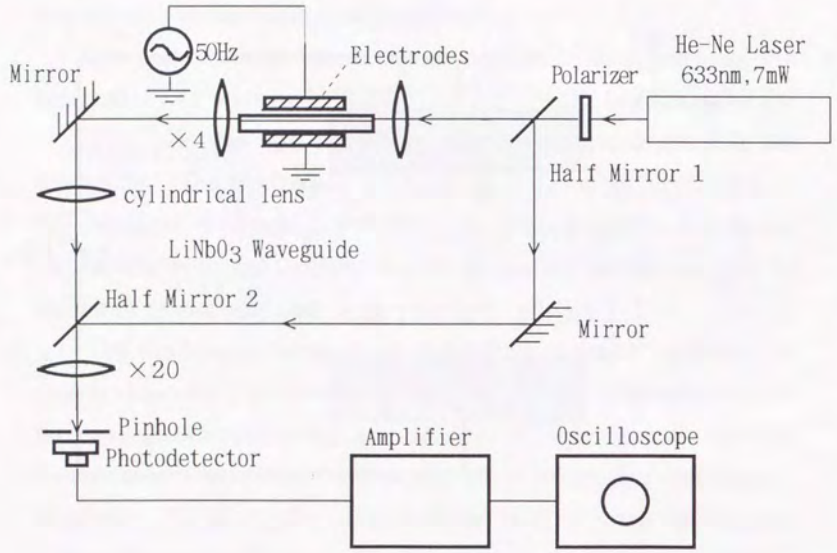

Fig. 3.2. Mach-Zehnder interferometer

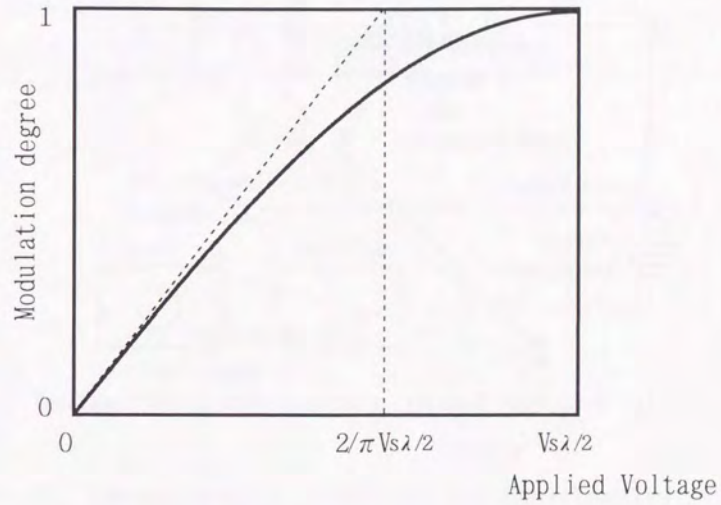

Fig. 3.3. Modulation degree and half-wave voltage

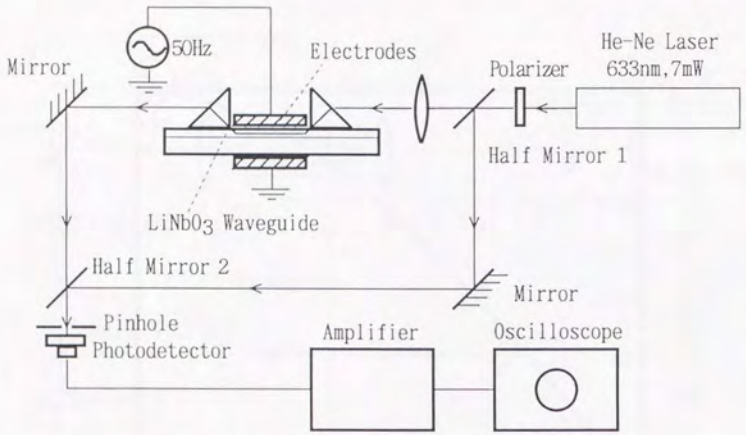

Fig. 3.4. Mach-Zehnder interferometer (prism coupling)

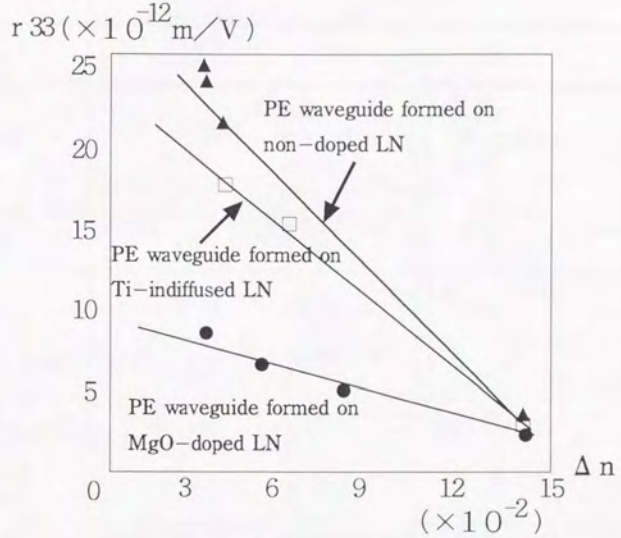

Fig. 3.5. The electrooptic constant r33 and the refractive -index of the annealed proton-exchanged waveguides

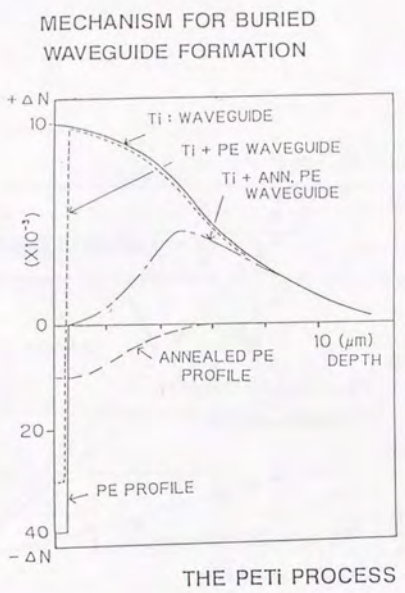

Fig. 3. 6. The annealed PETi waveguide formed on the Y-cut substrate [55]

Table 3.1. Parameters and electro-optic constants of proton-exchanged waveguides

Sample	A	B	C	D
Exchanging material	benzoic acid	pyro-phosphoric acid	pyro-phosphoric acid	pyro-phosphoric acid
Temperature (℃) Time (min)	205 40	230 12	230 12	200 76
Annealing	NO	200℃,2h	NO	200℃,2h
Equivalent Index	2.281	2.29	2.29	2.305
Thickness of guiding layer(μm)	0.52	0.50	0.50	0.61
Thickness of crystal(mm)	1.0	2.0	2.0	0.5
r'_{33} (10^{-12} m/V) (corrected)	1.52	1.49	1.41	1.38
r'_{33} (10^{-12} m/V) (uncorrected)	3.86	3.83	3.76	2.74
r'_{32} (10^{-12} m/V) (corrected)		0.58	0.59	

Table 3.2. The electro-optic constants in the $LiNbO_3$ substrates

	$LiNbO_3$	MgO-doped $LiNbO_3$
r_{33}	32.6	34.3
r_{13}	11.3	11.1
r_{22}	6.5	5.8

Table 3.3. Half-wave voltage of crystal A

Distance between electrodes (mm)	Voltage between crystal to induce π phaseshift Vs		
	1	2	3
d=1.5	349	377	339
d=1.35	320	324	349
d=1.3	376	359	381
d=1.1	322	318	327

Table 3.4. Values of electrooptic constant r_{33}

	Proton-exchanged condition	Annealing Time (350°C)	Δn	$r_{33} \times 10^{-12}$ (m/v)
Undoped LN	230°C 12min	0h	0.145	3.4(pure=1.0)
		2h	0.039	20.6
		2h+1h	0.034	23.2
		2h+2h	0.032	23.6
Titanium-Indiffused LN	230°C 15min	0h	0.145	2.7(pure=0.56)
		2h	0.063	14.8
		2h+2h	0.042	17.6
MgO-doped LN	230°C 23min	0h	0.145	2.7(pure=0.13)
		2h	0.079	4.7
		2h+2h	0.053	6.5

Table 3.5. Fabrication conditions and electro-optic constants of the TiPE waveguides

Sample	1	2	3	4	5
Titanium Thickness	250 Å	800 Å	800 Å	800 Å	800 Å
Diffusion Temperature	1000 ℃	1000 ℃	1000 ℃	1000 ℃	1000 ℃
Diffusion Time	8h	10h	10h	10h	10h
Diffusion Atmosphere	wetO_2	wetO_2	wetO_2	wetO_2	wetO_2
Proton-Exchange	NO	210 ℃ 4min	210 ℃ 8min	210 ℃ 4min	210 ℃ 8min
Annealing	NO	NO	NO	350 ℃ 2h wetO_2	350 ℃ 80min wetO_2
$r'_{22}(\times 10^{-12}$ m/V)	7.36	7.44	7.11	7.34	7.36

Chapter IV

Quantitative Measurements of Photorefractive Sensitivity of Optical Waveguides

Abstract

The photorefractive sensitivities of Ti-indiffused $LiNbO_3$ waveguides, proton-exchanged $LiNbO_3$ waveguides, and Rb ion-exchanged KTP waveguides are quantitatively measured. Although the photorefractive sensitivity is very small in proton-exchanged layer formed on the $LiNbO_3$ substrate, it increases by the annealing process.

The photorefractive sensitivity of the thin-film $LiNbO_3$ waveguides using the $Li_2O-V_2O_5$ flux and that of waveguides using $Li_2O-B_2O_3$ flux are also quantitatively measured and are compared. The waveguides grown using the $Li_2O-B_2O_3$ flux are proven to be much more resistant to optical damage than those grown using the $Li_2O-V_2O_5$ flux.

4.1 Introduction

The ion-exchanged waveguides formed on the $LiNbO_3$ (LN) and the potassium titanyl phosphate (KTP) are the very attractive materials for short-wavelength applications as well as the modulators and switches. The quantitative estimation of the photorefractive effect of the material becomes necessary when the material for the devices designed for the short wavelength is selected.

In the proton-exchanged waveguide and the Ti-indiffused waveguide, the optical properties of $LiNbO_3$ crystal are greatly changed because of the structural change [40] , [50] or the diffusion of the ions during the fabrication process [57] . Therefore, the degradation of the electrooptic constants [5] , [6] or the degradation of the resistance to optical damage is caused by the fabrication process of such waveguides [58] . The thin-film $LiNbO_3$ waveguide is very attractive because it has almost the same optical properties as those of $LiNbO_3$ crystal itself and the merits of $LiNbO_3$ crystal can be fully utilized. Moreover, it is much easier to design optical devices by using the thin-film waveguides than the Ti-indiffused waveguides and proton-exchanged waveguides because they have the step-index depth profile which can be controlled independent of the width of the waveguide.

In this chapter, we have measured the photorefractive sensitivities of various types of the proton-exchanged $LiNbO_3$ waveguides and Rb ion-exchanged KTP waveguides for the first time by using the diffraction-grating method. These values are compared

with the photorefractive sensitivity of the Ti-indiffused waveguides formed on the nondoped and MgO-doped $LiNbO_3$ crystals, and that of $LiNbO_3$ thin-film waveguide fabricated by the liquid-phase epitaxy.

4.2 Mechanism of Photorefractive Effect

The mechanism of the photorefractive effect is explained by Chen as follows [59] . The photoexcited electrons from donor levels drift along z-axis leaving behind the positive charges of ionized trap centers. These photoexcited electrons will be retrapped and reexcited out of the traps until they finally drift out of the illuminated region and are retrapped there. Thus the space charge field is created along the z-axis, which leads to the photorefractive index change through the electrooptic effect (Fig. 4.1).

Therefore, it seems that the photorefractive effect depends both on the electrooptic constant and the distribution of the traps of the electrons such as Fe^{2+} ions.

4.3 Photorefractive Diffraction-Grating Method

Among the various methods, the photorefractive-grating method [60] is the most sensitive to small refractive index-change induced by the photorefractive effect. Moreover, the photorefractive effect induced by the light with polarization extraordinary to $LiNbO_3$ and the light with polarization ordinary to $LiNbO_3$ can be separately measured by this method.

In our experiment, the photorefractive diffraction-grating method

[60] is used to measure the photorefractive effect (Fig. 4.2). The argon−ion laser beam (514.5 nm) is split into two parts and coupled into and out of the waveguides using two rutile prisms. The intersecting angle of the two beams is about 25mrad and the TM_0 mode is excited. The grating due to the photorefraction is formed by the interference fringes of the argon−ion laser on the waveguides. The width of this writing beam is 230 μm. The diffraction efficiency is probed by the He−Ne laser beam (632.8nm) which is also coupled into and out of the waveguides using the rutile prisms. The refractive index change due to the photorefraction is obtained by the measurement of the diffraction efficiency of the grating.

The refractive index change Δn caused by the photorefraction can be calculated by the following equation.

$$\eta=(\sin(\pi\Delta nL/(\lambda\cos\theta)))^2, \qquad (4-1)$$

where η is the diffraction efficiency of the grating, L is the length of the interference (4 mm), θ is the Bragg angle of the grating, and λ is the wavelength of the He−Ne laser (632.8 nm).

Before starting the next measurement, the sample is moved slightly so that the light is coupled to the part without photorefraction.

4.4 Photorefractive Sensitivity of Ti−Indiffused Lithium Niobate Waveguides

It is reported that the Ti−indiffused waveguides are very susceptible to optical damage and the photorefractive sensitivity as large as 10^{-7} (cm^2/J) [60] is reported for the Ti−indiffused waveguides. It is also reported that the MgO−doped $LiNbO_3$ crystals are more resistant to photorefractive effect than the non−doped crystals [54]. In this section, the photorefractive sensitivities of the Ti−indiffused waveguides formed on the MgO−doped crystals and non−doped crystals are compared and the effect of MgO−doping on the photorefraction in the Ti−indiffused waveguide is investigated for the first time.

4.4.1 Ti−indiffused $LiNbO_3$ waveguides

4.4.1.A Fabrication of Waveguides

Ti−diffused waveguide are fabricated by the thermal in−diffusion method [1].

Titanium metal film (410 ~ 755 Å) is evaporated on to the surface of the z−cut $LiNbO_3$ (z−cut MgO−doped $LiNbO_3$) crystal by the sputtering or the electron beam evaporation method. This sample is placed in the alumina tube and is heated up to 1000 ℃. The oxygen is bubbled into the water before flowing into the tube in order to suppress the out−diffusion of Li_2O [2]. Waveguiding layer is formed by diffusing the titanium film at 1000 ℃ for 8 ~ 14h in a wet oxygen atmosphere.

The diffusion rate of the titanium is very small in the MgO−doped crystal compared with that in the non−doped crystal.

4.4.1.B Measurement of Photorefractive Sensitivity

The photorefractive diffraction-grating method explained in section 4.3, is used to measure the photorefractive sensitivity. The photorefractive sensitivity is defined as,

$$S=\Delta n/E \qquad (4-2)$$

where E is the energy density in the waveguide.

4.4.1.C Results of Experiment

The measured photorefractive sensitivity of the Ti-indiffused waveguides is shown in table 4.1.

The photorefractive sensitivity of the Ti-indiffused waveguides formed on the MgO-doped $LiNbO_3$ crystal is smaller than that formed on the nondoped $LiNbO_3$ crystal by two orders of magnitude. The Ti-indiffused waveguiding layer becomes less resistant to optical damage as the titanium film evaporated on to the substrate becomes thicker.

4.4.2 Proton-Exchanged Lithium Niobate Waveguides and ion-exchanged KTP Waveguides

Various types of the proton-exchanged waveguides are formed on the nondoped $LiNbO_3$, MgO-doped $LiNbO_3$, and Ti-indiffused $LiNbO_3$ crystals, and their photorefractive sensitivities are

quantitatively measured. The photorefractive sensitivity of Rb ion-exchanged waveguides formed on KTP crystals is also quantitatively measured for the first time and is compared with the above results.

4.4.2.A Fabrication of Waveguides

The optical planar waveguides are fabricated on x-cut and z-cut nondoped $LiNbO_3$ substrates, z-cut MgO-doped $LiNbO_3$ substrates, and z-cut Ti-indiffused $LiNbO_3$ substrates by the proton-exchange method [7] . The temperature of proton-exchange ranges from 200 ℃ to 230 ℃ and the proton-exchange time ranges from 20 min ~ 5 h. After the proton-exchange process, the waveguides are annealed at 300 ~ 352 ℃ for several hours.

The samples A, B1, B2, and B3 shown in Table 4.2 are fabricated on the z-cut nondoped $LiNbO_3$ crystals, while the samples M0, M1, and M2 are fabricated on the z-cut MgO-doped crystals. The samples C1 and C2 are fabricated on the x-cut nondoped crystals. The samples T0 and T1 are fabricated on the z-cut Ti-indiffused (400 ~ 450 Å -thick films) $LiNbO_3$ substrates.

On sample A, M0 and T0, 2 μm deep proton-exchanged layer is formed and is not annealed, while on samples B1, B2, B3, C1, C2, M1, M2 and T1, thin proton-exchanged layer is formed and is annealed for two or four hours at 300 ~ 352 ℃ .

The optical planar waveguides were also fabricated on z-cut KTP crystals by the ion-exchange method [13] , [47] . The Rb

ions are diffused into the substrate for 10 ～ 45 minutes at 320 ℃. Ba^{2+} ions are added to the salt for the purpose of controlling the diffusion rate of the Rb^{+} ions and reducing the melting point of the salt [47]. The fabrication condition is shown in Table 4.3.

4.4.2.B Results of the experiment

The examples of the diffraction efficiency of the proton−exchanged $LiNbO_3$ waveguides as a function of the duration of the illumination of the argon laser are shown in the Figs. 4.3, 4.4, 4.5, 4.6 and 4.7.

As the annealing time increases, the waveguides becomes gradually susceptible to optical damage. As shown in Figs. 4.3 and 4.5, the annealed waveguides are more susceptible to the photorefraction than the waveguides which is not annealed. And in the case of the annealed waveguides, the diffraction efficiency of the He−Ne laser saturates for a short duration of the argon laser. The waveguides without annealing is not susceptible to photorefraction and the large power density is needed (Figs. 4.4 and 4.6). The photorefraction of these waveguides saturates after a long duration time. Both in the non−doped crystal and MgO−doped crystal, the effect of annealing the waveguides on the photorefraction is almost the same.

The diffraction efficiency of the KTP waveguides is shown in Fig. 4.7. The Rb ion−exchanged waveguide formed in the molten mixture of $RbNO_3$ (85% molar) and $Ba(NO_3)_2$ (15% molar) seems to be more

susceptible to the optical damage than the waveguide formed in the molten mixture of $RbNO_3$ (97% molar) and $Ba(NO_3)_2$ (3% molar).

The photorefractive sensitivity is calculated from the measured data of diffraction efficiency and is shown in table 4.4.

The photorefractive sensitivity S of the proton−exchanged layer which is 2 μm deep and is not annealed, is about 10^{-11} ～ 10^{-12} cm^2/J. The photorefractive sensitivity S of the annealed proton−exchanged waveguide is however, about 10^{-9} ～ 10^{-8} cm^2/J, which means the annealed proton− exchanged waveguide is 10^{-2} ～ 10^{-3} times weaker to the optical damage than those without annealing.

The photorefractive sensitivity S of proton−exchanged waveguides without annealing is about 10^{-4} times as small as that of Ti−indiffused ones. From the above results, we can conclude that the proton−exchanged waveguide becomes week to optical damage by annealing.

The photorefractive sensitivity S of the Rb ion−exchanged KTP waveguides is about 10^{-9} ～ 10^{-10} cm^2/J and is almost the same as or less than that in annealed proton−exchanged waveguides annealed at 350 ℃ for several hours.

4.4.2.C Discussions

According to the mechanism of optical damage (photorefractive effect) proposed by Chen [59], it is very likely that the photorefractive sensitivity depends on both the electrooptic constant and the photoconductivity of the material. And photorefraction seems

to be proportional to the electrooptic constant and inversely proportional to the photoconductivity [54] .

It is reported that the MgO doped $LiNbO_3$ bulk crystals are more resistant to optical damage than the nondoped $LiNbO_3$ crystals because photoconductivity of the crystal is greatly improved by doping MgO [54] . In the case of proton-exchanged $LiNbO_3$ waveguides, however, the effect of doping MgO is very small, and the protons seem to play more dominant role than the Mg^{2+} ions.

Several papers [52] , [53] including of our own [61] have already reported that the electrooptic constant of the $LiNbO_3$ crystal is reduced by the proton-exchange but recovered by annealing.

Minakata *et al.* reported that the degradation of the electrooptic effect is caused by the structural change of the $LiNbO_3$ crystal during the proton-exchange process [40] . As the $LiNbO_3$ crystal is changed into a symmetric structure by proton-exchange, it is likely that proton-exchanged waveguide is reversed into an asymmetric structure by annealing.

Therefore, the increased photorefractive sensitivity in annealed proton-exchanged waveguides can be explained by the recovery of electrooptic constant caused by the large structural change of the crystal.

4.4.3 Lithium Niobate Thin-film Waveguides Formed by Liquid-Phase Epitaxy

In this section, 5 mol% MgO-doped $LiNbO_3$ thin-film waveguides are grown on $LiTaO_3$ substrates by liquid-phase epitaxy (LPE).

The photorefractive sensitivity of the thin-film $LiNbO_3$ waveguides using the $Li_2O-V_2O_5$ flux [62] and that of waveguides using $Li_2O-B_2O_3$ flux are quantitatively measured and compared.

4.4.3.A Fabrication of Thin-Film Waveguide

Five kinds of powders: Li_2CO_3, Na_2CO_3, Nb_2O_5, V_2O_5 (or B_2O_3), and MgO are mixed so that the melt composition is 5 mol% $MgO-LiNbO_3:Li_{0.7}Na_{0.3}VO_3$ = 20:80 mol%. This ratio is chosen to achieve lattice matching between the $LiNbO_3$ thin-film and the $LiTaO_3$ substrate.

The mixed materials in the platinum crucible are placed in the furnace as shown in Fig. 4.8 and are heated at 1000 ~ 1100 ℃ to obtain uniform molten salt. The salt is cooled below the saturation temperature at 930-950 ℃ until the supercooling state.

The $LiTaO_3$ substrate is placed in the platinum holder so that the $-z$ surface of the crystal becomes the lower side (see Fig. 4.8). The size of the substrate is typically two inches in diameter. After the equilibrium state is achieved, the substrate is dipped into the melt rotating at 10-100 rpm.

Then the $LiNbO_3$ thin-film is grown on the substrate for a few minutes by the flat one-side dipping LPE method, in which only the lower side of the substrate is dipped into the melt. The growth rate

is approximately 1 μm/min. After cooling to room temperature, the residue of the flux adhering to the film is washed away with water.

Thus an as-grown $LiNbO_3$ thin-film with a mirror finish is obtained. The film is mechanochemically polished in order to adjust its thickness, and the optical waveguide is fabricated.

4.4.3.B Measurement of Photorefractive Effect

The photorefraction is measured by both the qualitative method and the quantitative method. Samples shown in Table 4.5 are used, and the $LiNbO_3$ thin-film grown by using the $Li_2O-V_2O_5$ flux (LVM1, LVM2) and that grown by using the $Li_2O-B_2O_3$ flux (LBM1, LBM2) are compared with each other.

The photorefractive effect is first qualitatively measured by the conventional prism-coupling method as shown in Fig. 4.9 (a). The He-Ne laser beam (632.8 nm, 2 mW) is coupled into the $LiNbO_3$ thin-film waveguide by a rutile prism and output mode from the rutile prism is observed by a camera. If the material suffers from optical damage, the output mode will change its shape and broaden along the transverse direction shown in Fig. 4.9 (b).

The broadened beam is cut by the pinhole placed in front of the power meter and the optical damage can be estimated by the reduction of the output power (Fig. 4.9 (a)).

When the TM modes are excited, no reduction of the output power can be observed in the case of the $LiNbO_3$ thin-film waveguides using the $Li_2O-B_2O_3$ flux, while a considerable reduction

of the output power can be observed in the case of those using the $Li_2O-V_2O_5$ flux.

When TE modes are excited, no reduction of the output power can be observed in both cases. The photorefraction of the TM mode of the $LiNbO_3$ thin-film was further investigated by the following quantitative measurement.

In order to estimate the photorefraction quantitatively, the photorefractive diffraction-grating method (see section 4.3) is used and the argon-ion laser (514.5 nm) and He-Ne laser are used for the writing and probe beam, respectively . The photorefractive sensitivity S of the waveguides is measured.

4.4.3.C Results of Experiment

The photorefractive effect was first qualitatively measured by the experimental setup shown in Fig. 4.9.

In the case of samples LBM1 and LBM2, the output power of the TM mode is 100 μW and it does not change over 600 seconds of illumination of He-Ne laser. In the case of the thin-film waveguides using the $Li_2O-V_2O_5$ flux, however, the output power of the TM mode gradually changes from 110 to 55 μW over 600 seconds.

In order to estimate the photorefraction quantitatively, the photorefractive diffraction-grating method is used.

The diffraction efficiency of the $LiNbO_3$ thin-film waveguides as a function of the duration of the illumination of the argon laser is shown in Fig. 4.10.

Samples LVM1 and LVM2 are very susceptible to photorefraction and a power density of no more than 0.5 W/cm^2 is required for photorefraction.

Samples LBM1 and LBM2 are less susceptible to photorefraction than samples LVM1 and LVM2, and a power density as large as 17 W/cm^2 is required.

The photorefractive sensitivity of the $LiNbO_3$ thin-film waveguides shown in Table 4.6 is calculated from the diffraction efficiency of the He-Ne laser. The photorefractive sensitivity of samples LVM1 and LVM2 is about $10^{-6} \sim 10^{-7}$ cm^2/J and that of samples LBM1 and LBM2 is about 10^{-8} cm^2/J.

Although there are some differences in photorefractive sensitivity depending on the fabrication condition, the thin-film waveguides grown using the $Li_2O-V_2O_5$ flux system are more susceptible to optical damage than those grown using the $Li_2O-B_2O_3$ flux.

4.4.3.D Discussion

The photorefractive sensitivity of the $LiNbO_3$ thin-film waveguides is quantitatively measured. As a result, MgO-doped $LiNbO_3$ thin-film waveguides grown by using the $Li_2O-B_2O_3$ flux are proven to be much more resistant to optical damage than those grown by using the $Li_2O-V_2O_5$ flux. This result is in good agreement with the result obtained by the qualitative measurement.

It is reported by Tamada et al. that high optical absorption caused by the V^{3+} ions can be observed in the visible wavelength, especially

in the blue region [63] . It is very likely that the cause of the large photorefraction in the $LiNbO_3$ thin-film waveguides using the $Li_2O-V_2O_5$ flux is the V^{3+} ions being incorporated into the film from the flux during the growth. Therefore, the thin-film waveguide with high optical damage resistance can be obtained by using the $Li_2O-B_2O_3$ flux because no V^{3+} ions are introduced during the fabrication process.

The $LiNbO_3$ thin-film optical waveguides grown by liquid-phase epitaxy are suitable for use in optical waveguide-type devices such as optical switches, modulators and SHG devices for the following reasons:

(1) The $LiNbO_3$ thin-film waveguides have almost the same optical properties as $LiNbO_3$ crystal itself. Contrary to proton-exchanged waveguides, they have no degradation of the electrooptic constant and nonlinear-optic coefficient.

(2) They have the step-index depth profile which can be independently controlled by the width.

(3) Mg^{2+} [54] or other ions such as Nd^{3+} and Er^{3+} can be doped into the film. It may be easier to obtain a uniform concentration of the dopant along the depth direction in the $LiNbO_3$ film than in the $LiNbO_3$ crystal because it is much thinner than the crystal.

In addition to these merits, it is proven by our experiment that the optical damage of the $LiNbO_3$ thin-film waveguide can be greatly reduced by choosing the proper flux such as $Li_2O-B_2O_3$. This merit becomes very important when the device is designed for

short-wavelength applications, such as SHG devices.

4.5 Conclusion

In this chapter, photorefractive sensitivities of the proton-exchanged $LiNbO_3$, proton-exchanged MgO-doped (Ti-indiffused) $LiNbO_3$ and Rb ion-exchanged KTP waveguides are measured. The photorefractive sensitivities of the Ti-diffused waveguides formed on $LiNbO_3$ (MgO-doped $LiNbO_3$) crystals, and the photorefractive sensitivity of $LiNbO_3$ thin-film waveguide formed on the $LiTaO_3$ substrate are also measured. These results are compared with each other.

The photorefractive sensitivities of the Ti-indiffused waveguides formed on the MgO-doped crystals and non-doped crystals are compared. The photorefractive sensitivity of the Ti-indiffused waveguide formed on the MgO-doped $LiNbO_3$ (10^{-9} cm^2/J) is smaller than that formed on the nondoped $LiNbO_3$ (10^{-7} cm^2/J). However,the Ti-indiffused waveguiding layer formed on the MgO-doped $LiNbO_3$ becomes less resistant to optical damage as titanium film evaporated on to the substrate becomes thicker.

A quantitative estimation of the photorefraction has been made for the proton-exchanged waveguides fabricated both on $LiNbO_3$ and MgO-doped $LiNbO_3$ and Rb ion-exchanged KTP waveguides. The proton-exchanged $LiNbO_3$ waveguide is very resistant to optical damage and its photorefractive sensitivity is $10^{-11} \sim 10^{-12}$ cm^2/J [65] . However, in the case of the proton-exchanged

waveguide, a postannealing process is necessary for its application to optical devices because both the electrooptic constant [52] , [53] and the nonlinear-optic coefficient [66] are reduced during the proton-exchange process.

The conclusion of this experiment is as follows.

(1) Though the photorefractive sensitivity increases as the annealing time increases, the photorefractive sensitivities of the annealed waveguides is still much smaller than that of Ti-indiffused waveguides formed on the non-doped crystal.

(2) The effect of doping MgO on the photorefractive sensitivity of the proton-exchanged layer is very small.

(3) The cause of the increased photorefractive sensitivity of annealed proton-exchanged waveguides can be explained mainly by the recovery of electrooptic constant by annealing.

(4) The KTP waveguide is proved to be a very attractive material for SHG devices such as balanced phase matching devices, because it is resistant to optical damage if fabrication condition is properly chosen.

The photorefractive sensitivities of the thin-film $LiNbO_3$ waveguides using the $Li_2O-V_2O_5$ flux [62] and that of waveguides using $Li_2O-B_2O_3$ flux are also quantitatively measured and compared. The thin-film waveguide grown by using the $Li_2O-B_2O_3$ flux is no less resistant to optical damage than most other $LiNbO_3$ waveguides [64] , [65] .

The thin-film $LiNbO_3$ waveguide is more resistant to optical damage than the Ti-indiffused $LiNbO_3$ waveguides by about one order of magnitude. Although the thin-film waveguide grown by using

the $Li_2O-B_2O_3$ flux is much less resistant to optical damage than proton-exchanged $LiNbO_3$ waveguides fabricated without an annealing process, it is almost as resistant as the annealed proton-exchanged $LiNbO_3$ waveguides [65] . Therefore, the $LiNbO_3$ thin-film waveguide can be applicable to the devices for the visible light such as voltage sensors, by choosing the proper flux such as $Li_2O-B_2O_3$.

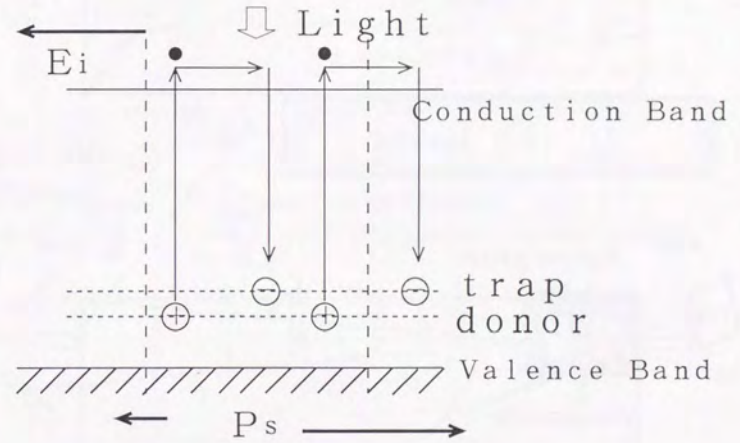

Fig. 4.1. Mechanism of the photorefractive effect

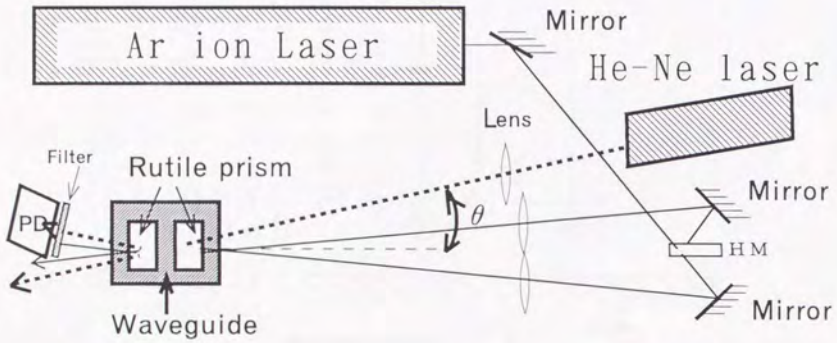

Fig. 4.2. Set up of the experiment

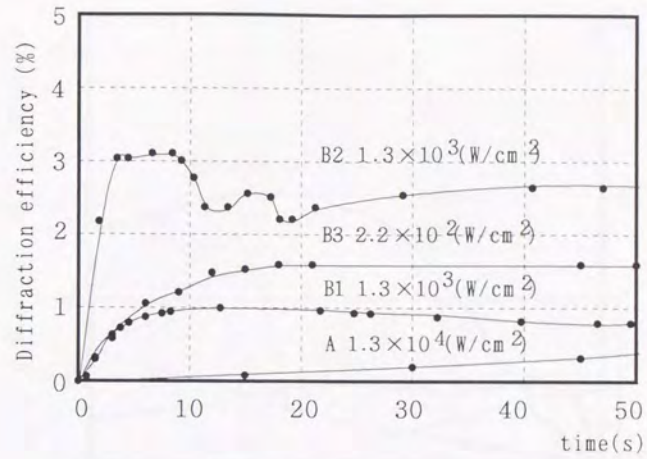

Fig.4.3. Diffraction efficiency of the proton-exchanged LN waveguides

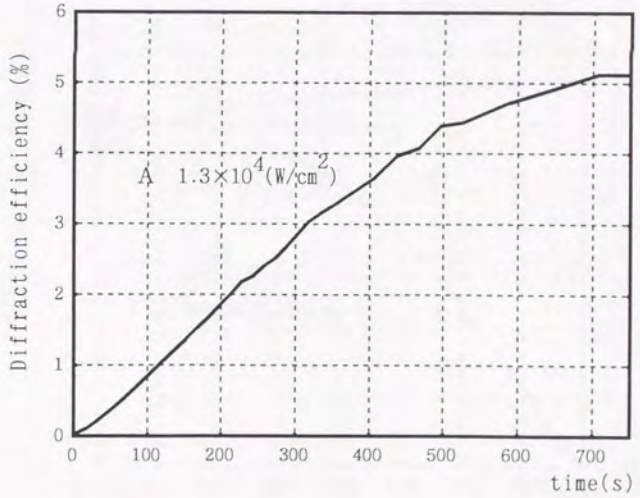

Fig. 4.4. Diffraction efficiency of the proton-exchanged LN waveguides (no annealing)

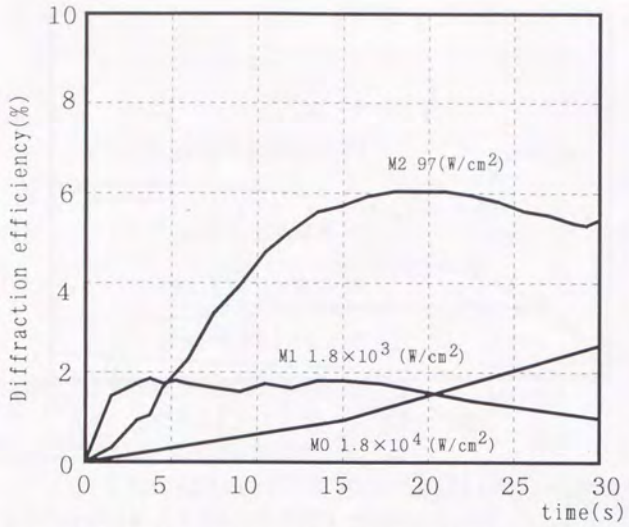

Fig. 4.5. Diffraction efficiency of the proton-exchanged MgO-doped LN waveguides

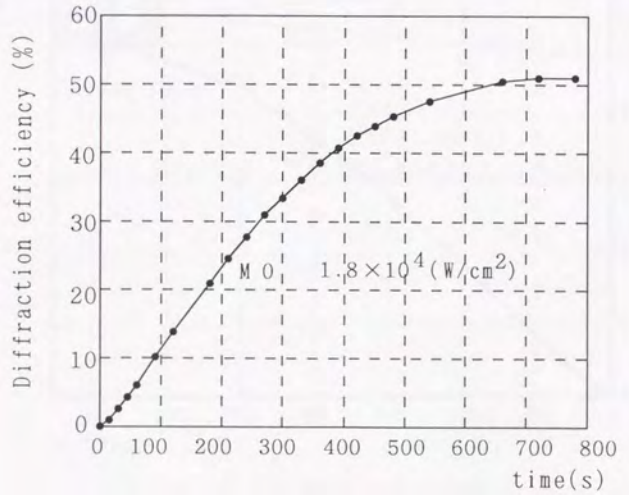

Fig. 4.6. Diffraction efficiency of the proton-exchanged MgO-doped LN waveguides (no annealing)

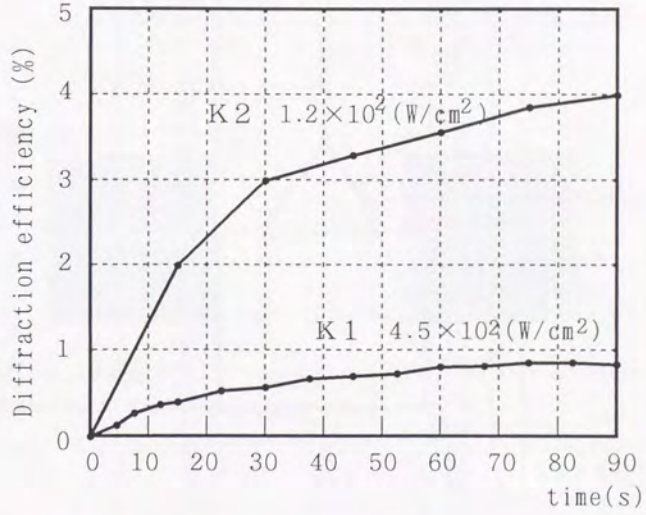

Fig. 4.7. Diffraction efficiency of the ion-exchanged KTP waveguides

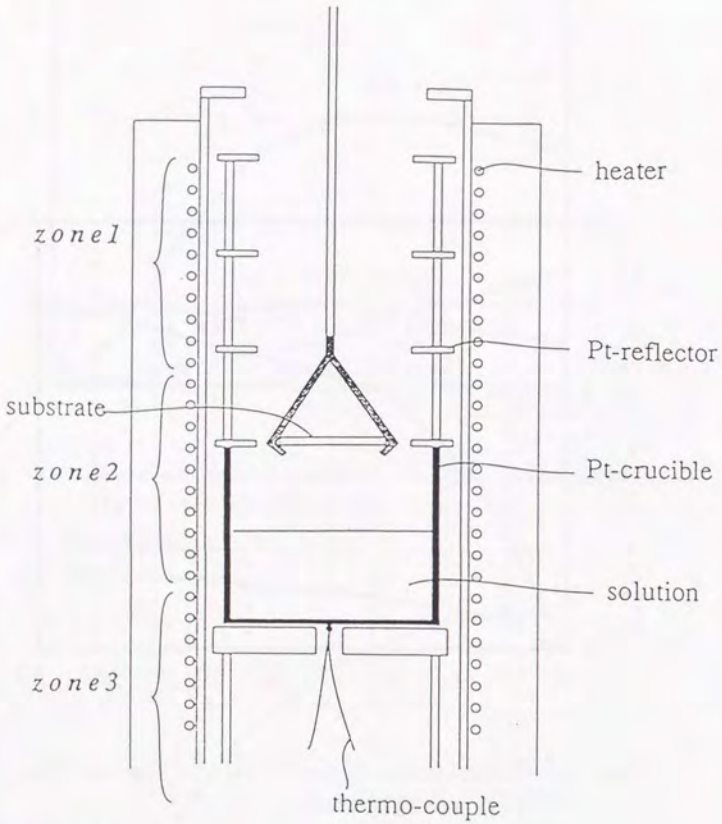

Fig. 4.8. Schematic illustration of LPE furnace.

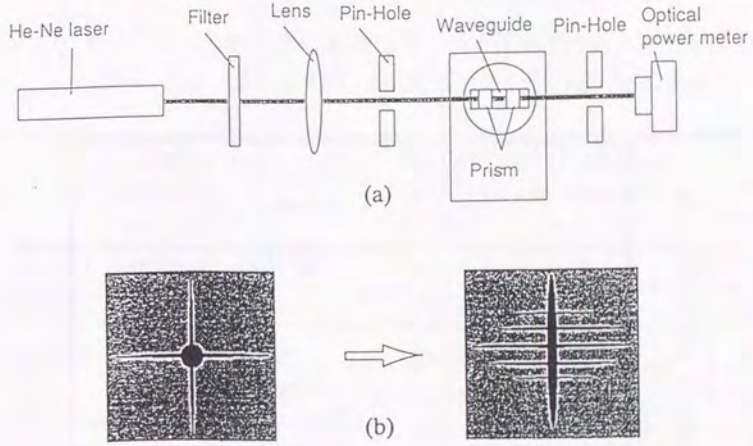

Fig. 4.9. (a) Experimental setup for qualitative measurement. (b) Output mode from the rutile prism.

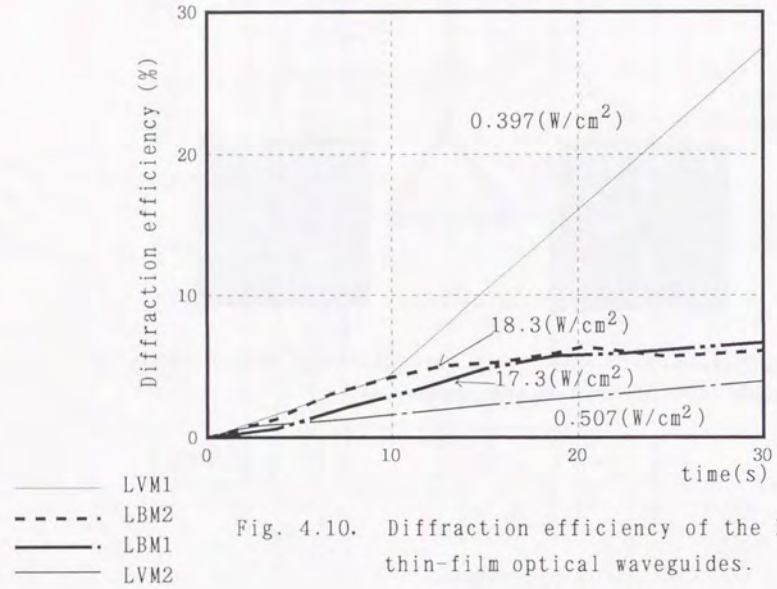

Fig. 4.10. Diffraction efficiency of the LiNbO3 thin-film optical waveguides.

Table 4.1. Parameters and photorefractive sensitivity of the Ti-indiffused optical waveguides

	Power density (W/cm^2)	Exposure time(sec)	Energy density (J/cm^2)	Diffraction efficiency η (%)	$\Delta n/E$ (cm^2/J)
LN	67.4	0.3	20.2	1.00	2.48×10^{-7}
(450Å)	106.4	0.3	31.9	1.18	1.71×10^{-7}
MgO doped	22.7	45	1.02×10^{3}	1.04	2.25×10^{-9}
LN(410Å)	33.7	45	1.52×10^{3}	2.29	2.25×10^{-9}
MgO doped	112	4.5	5.02×10^{2}	1.00	7.92×10^{-9}
LN(755Å)	382	4.5	1.72×10^{3}	10.4	7.57×10^{-9}

Table 4.2. Fabrication condition of the LN waveguides

	Sample	Initial depth of PE layer	Annealing conditions
LN (z-cut)	A	2.1 μm	no annealing
	B1	0.32 μm	350℃ 2h
	B2	0.31 μm	350℃ 4h
	B3	0.25 μm	350℃ 4h
LN (x-cut)	C1	0.53 μm	300℃ 2h
	C2	0.54 μm	350℃ 2h
MgO-doped LN(z-cut)	M0	1.9 μm	no annealing
	M1	0.47 μm	350℃ 2h
	M2	0.35 μm	352℃ 4h
Ti-indiffused LN(z-cut) (400～450Å Ti-film)	T0	2.1 μm	no annealing
	T1	0.39 μm	350℃ 4h

Table 4.3. Fabrication condition of the KTP waveguides

Sample	Diffusion Temperature	time	$Ba(NO_3)_2/RbNO_3$ mol%
K1	320℃	45min	3%
K2	320℃	10min	15%

Table 4.4. Parameters and photorefractive sensitivity of the waveguides

	Sample	Diffusion Depth	Energy density (J/cm^2)	Diffraction efficiency η (%)	$\Delta n/E$ (cm^2/J)
LN (z-cut)	A	2.1 μm	1.1×10^{6}	0.74	3.8×10^{-12}
	B1	2.1 μm	4.0×10^{3}	0.62	0.98×10^{-9}
	B2	1.8 μm	1.0×10^{3}	1.0	5.0×10^{-9}
	B3	3.7 μm	9.9×10^{2}	1.0	5.2×10^{-9}
LN (x-cut)	C1	0.9 μm	1.6×10^{6}	1.1	3.3×10^{-12}
	C2	3.1 μm	2.8×10^{2}	1.0	1.8×10^{-8}
MgO-doped LN(z-cut)	M0	1.9 μm	2.7×10^{5}	0.9	1.8×10^{-11}
	M1	1.9 μm	2.6×10^{3}	1.5	2.3×10^{-9}
	M2	4.7 μm	3.6×10^{2}	1.0	1.4×10^{-8}
Ti-indiffused LN(z-cut)	T0	2.1 μm	3.0×10^{5}	1.2	1.9×10^{-11}
	T1	2.5 μm	3.0×10^{2}	1.1	1.7×10^{-8}
KTP (z-cut)	K1	13 μm	6.7×10^{3}	0.5	5.2×10^{-10}
	K2	11 μm	7.4×10^{2}	1.0	6.8×10^{-9}

Table 4.5. Fabrication conditions for the LN thin-film waveguides

	Amount of doped MgO in the LN film	Flux	Film thickness
LVM1	5mol%	Li2O-V2O5	4 μm
LVM2	5mol%	Li2O-V2O5	4 μm
LBM1	5mol%	Li2O-B2O3	6.5 μm
LBM2	5mol%	Li2O-B2O3	tapered film (2～7 μm)

Table 4.6. Parameters and photorefractive sensitivity of the LN thin-film optical waveguides

sample	Power density (W/cm^2)	Energy density (J/cm^2)	Diffraction efficiency (%)	Photorefractive sensitivity (cm^2/J)
LVM1	1.1	2.1	5.0	5.3×10^{-6}
	0.4	3.9	4.3	2.7×10^{-6}
LVM2	4.3	1.3×10^{2}	5.4	1.1×10^{-7}
	0.51	23	5.4	5.2×10^{-7}
LBM1	26	5.9×10^{2}	5.4	2.0×10^{-8}
	17	2.6×10^{2}	4.9	4.3×10^{-8}
LBM2	25	1.3×10^{2}	5.0	8.8×10^{-8}
	18	2.3×10^{2}	5.1	4.9×10^{-8}

Chapter V

Optical Damage Resistance of the Ion-Exchanged Waveguides for Short-Wavelength Applications

Abstract

The photorefractive effect in the proton-exchanged $LiNbO_3$, proton-exchanged $LiTaO_3$, and Rb ion-exchanged KTP waveguides is investigated. The annealed proton-exchanged waveguide formed on the $LiTaO_3$ crystal is proven to be the most resistant to the photorefractive effect and is attractive material for short-wavelength applications.

The photorefractive sensitivity in the annealed proton-exchanged waveguide formed on the $LiTaO_3$ substrates with and without the periodically domain-inverted structure is compared. The photorefractive sensitivity seems to be smaller in the waveguide formed on the periodically domain inverted structure than that in the waveguide formed on the substrate without domain-inversion.

Temperature dependence of the photorefractive effect in the proton-exchanged $LiTaO_3$ waveguide is also investigated. Resistance to the photorefractive effect is greatly improved when the samples are heated at temperatures as high as 80 ℃.

5.1 Introduction

In chapter Ⅳ, the photorefractive sensitivities of Ti-indiffused waveguides, ion-exchanged waveguides, and thin-film waveguides are measured and compared. As a result, the photorefractive sensitivity in the proton-exchanged $LiNbO_3$ waveguide without annealing process is found to be very small.

In this chapter, the photorefractive effect in the ion-exchanged waveguides are investigated from the view point of practical application to the optical devices, especially to those designed for short-wavelength.

In 5.2, the photorefractive effect (optical damage) in the proton-exchanged $LiNbO_3$ and $LiTaO_3$ waveguides formed on the optical grade crystals is investigated and compared for the first time.

Although the structures of the $LiNbO_3$ and $LiTaO_3$ crystals are almost the same, the structural changes that they undergo during the proton-exchange process are slightly different. It is possible that this difference between the proton-exchanged $LiNbO_3$ and $LiTaO_3$ waveguides may affect their optical properties.

The effect of annealing on the ion-exchanged KTP waveguide is also investigated. As explained in chapter Ⅱ, the annealing process is also effective to change the refractive index profile in the Rb ion-exchanged KTP waveguide. The photorefractive effect in the Rb ion-exchanged waveguides with and without annealing process is compared.

The periodically domain-inverted structure is said to be resistant to photorefractive effect because the photorefraction in the domain-inverted parts and noninverted parts cancels with each other [69]. In 5.3, the effect of the periodically domain-inverted structure on the photorefractive effect is investigated.

In 5.4, temperature dependence of the photorefractive effect in the proton-exchanged $LiTaO_3$ waveguide is experimentally studied for the first time and the results are shown.

5.2 Optical Damage Resistance of Ion-Exchanged Waveguides

5.2.1 Proton-Exchanged Lithium Niobate and Lithium Tantalate Waveguides

5.2.1.A Fabrication of Waveguides

Slab waveguides are formed on the $LiNbO_3$ and $LiTaO_3$ crystals by the proton-exchange process using pyrophosphoric acid. After that, some of the waveguides are annealed in order to recover the reduced nonlinear coefficients [66] by the proton exchange. Both the $LiNbO_3$ and $LiTaO_3$ crystals used in this experiment are optical-grade crystals purchased from Yamaju Ceramics Co. Ltd.

The annealed proton-exchanged waveguides are formed under similar conditions to those in the proton-exchanged $LiNbO_3$ and $LiTaO_3$ waveguides used for SHG devices [20], [22]. The fabrication conditions of the waveguides are shown in Table 5.1.

5.2.1.B Measurement of Photorefractive Effect

The refractive index change Δn as a function of the duration of the illumination of the argon−ion laser can be written as follows [67] .

$$\Delta n = \Delta n_s(1 - \exp(-t/\tau)), \quad (5-1)$$

where Δn_s is the saturated index change, and τ is the build−up time constant. The build−up speed of the photorefraction can be estimated by τ. The photorefractive sensitivity, which can be expressed as follows, [67] is also estimated.

$$S = \Delta n_s/(\tau I_{ir}). \quad (5-2)$$

where I_{ir} is the irradiation intensity of the argon−ion laser in the waveguide.

5.2.1.C Results of Experiment

The photorefractive effects in the proton−exchanged $LiNbO_3$ and $LiTaO_3$ waveguides are measured and compared.

The irradiation intensity dependence of the saturated index change Δn_s of the samples NP1, NP2, TP1 and TP2 is shown in Fig. 5.1.

Δn_s increases almost proportionally to the irradiation intensity when the irradiation intensity is low. This result is in good agreement with the Glass model [68] when the photoconductivity is much smaller than the dark conductivity. The Δn_s is almost the same in $LiNbO_3$ samples and the proton−exchanged

$LiTaO_3$ without annealing process (NP1, NP2 and TP1). Δn_s is the smallest in the annealed proton−exchanged $LiTaO_3$ waveguide (TP2).

The irradiation intensity dependence of the inverse of the build−up time constant $1/\tau$ is shown in Fig. 5.2. The build−up time constant decreases as the irradiation intensity in the waveguiding layer increases. The $1/\tau$ values in samples NP1 and TP2 are very small compared to those in samples NP2 and TP1 and almost independent of the irradiation power, which indicates that the dark conductivity is dominant in samples NP1 and TP2 [67] .

The irradiation intensity dependence of the photorefractive sensitivity is shown in Fig. 5.3. The photorefractive sensitivity is extremely small in samples NP1 and TP2, while in samples NP2 and TP1, it is very large. The photorefractive sensitivity is increased by the annealing process in the case of the proton−exchanged $LiNbO_3$ waveguide. In the case of the $LiTaO_3$ waveguide however, it is decreased by the annealing process. Although the photorefractive sensitivity is much smaller in the proton−exchanged $LiNbO_3$ waveguide without annealing than in the annealed waveguide, the saturated index change in this waveguide is almost the same as that in the annealed waveguide. Both the saturated index change and photorefractive sensitivity are the smallest in the annealed proton−exchanged $LiTaO_3$ waveguides.

5.2.1.D Discussion

In this experiment, the photorefractive sensitivity is increased by

the annealing process in the $LiNbO_3$ waveguides, while it decreases in the $LiTaO_3$ waveguides. This result must be closely related to the profiles of the induced protons in the proton-exchanged layers because the resistance to photorefractive effect is greatly improved by the protons.

It is reported that oxidation of Fe^{2+} ions to Fe^{3+} takes place during the proton-exchange process, and Fe^{2+} ions are greatly reduced by this process [10] . The increased resistance to the photorefractive effect can be explained by this reduction of Fe^{2+} ions because the photorefractive effect is mostly based on the optical excitation of Fe^{2+} ions.

On the other hand, the increase in the surface extraordinary indices in the proton-exchanged $LiTaO_3$ waveguides due to the annealing process has been reported in several papers [44] [48] .

This phenomenon might be caused by the movement of the protons between the interstitial and substitutional sites. In the case of the proton-exchanged $LiNbO_3$ waveguides, however, such a phenomenon has not been reported.

It is very likely that the protons only in the substitutional sites contribute to the oxidation ($Fe^{2+} \rightarrow Fe^{3+}$) , and the Fe^{2+} ions which are responsible for the photorefraction are reduced only in these sites . Therefore the increased resistance to the photorefractive effect in the annealed proton-exchanged $LiTaO_3$ may be also caused by the movement of the protons from the interstitial sites to the substitutional sites. In the case of annealed proton-exchanged $LiTaO_3$ fabricated under the condition shown in Table 5.1, it seems

that this effect surpasses the increased electrooptic effect by annealing which causes the increase in photorefractive sensitivity.

The proton-exchanged $LiTaO_3$ waveguides reported by Yuhara *et al.* [42] , seem to be more susceptible to the photorefractive effect than our samples. This is partly because the substrates used for these experiments are purchased from the different company, and partly because the saw grade substrates are used in their experiment while the optical grade substrates are used in our experiment.

5.2.2 Rb Ion-Exchanged KTP Waveguides

5.2.2.A Fabrication of Waveguides

Slab waveguides are formed on the z-cut KTP substrates by the ion-exchange method using the $Ba(NO_3)_2/RbNO_3$ molten salt. Some of the waveguides are annealed after ion-exchange. Fabrication conditions are shown in Table 5.2.

5.2.2.B Results of Experiment

The effect of annealing on optical damage resistance of Rb-ion exchanged KTP waveguides is also investigated. The samples annealed at 325 ℃ and 350 ℃ are compared.

The intensity dependence of the saturated index change Δn_s, and the photorefractive sensitivity are shown in Figs. 5.4 and 5.5.

The effects of annealing at 325 ℃ and 350 ℃ on the optical damage resistance are shown in Figs.5.4 and 5.5 respectively. In

Fig.5.4, the refractive index change is the smallest in the annealed waveguide KTP3. In Fig.5.5, the refractive index change is the smallest in the annealed waveguide KTP5. In these waveguides, the ion-exchanged layers are formed by the ion-exchange process in the molten mixture of $RbNO_3$ (97% molar) and $Ba(NO_3)_2$ (3% molar) followed by the annealing process at 325 ℃ and 350 ℃ . In both samples (KTP3 and KTP5), the photorefractive sensitivity increases a little by the annealing process because the build-up time constant decreases by the annealing process.

In the Rb ion-exchanged waveguides, annealing the ion-exchanged layer is less effective in the resistance to the photorefractive effect than that in the proton-exchanged waveguides. The saturated index change in the KTP waveguide is almost the same as that in the annealed proton-exchanged waveguide. The photorefractive sensitivity of the KTP waveguide is $10^{-9} \sim 10^{-10}$ (cm^2/J) and is smaller than that in the annealed proton-exchanged waveguides.

In the case of the KTP crystals, the properties of some substrates are sometimes different from others even if these substrates are purchased from the same company. The photorefractive effect in the waveguides formed on the different substrates under the same fabrication condition (samples KTP5 and KTP7) is shown in Fig.5.6. Both samples are fabricated by the ion-exchange process in the molten mixture of $RbNO_3$ (97% molar) and $Ba(NO_3)_2$ (3% molar) followed by the annealing process at 350 ℃ for 50 minutes. Although the photorefractive sensitivity is almost the same in both

samples, the saturated index change in the sample KTP5 is smaller than that in the sample KTP7 by one order of magnitude. In the case of sample KTP7, the crystal seems to easily suffer damage by the ion-exchange process because the surface of the crystal becomes rough after the ion-exchange.

5.2.2.C Discussion

The ion-exchanged KTP waveguide is more resistant to photorefraction than the annealed proton-exchanged $LiNbO_3$ waveguide, while it is less resistant to photorefraction than the annealed proton-exchanged $LiTaO_3$ waveguides. In the ion-exchanged KTP waveguide, the photorefractive effect seems to be caused by the defects of the crystal in the waveguiding layer. The waveguide formed on the crystal which easily suffers damage by the ion-exchange process seems to be susceptible to photorefractive effect.

5.3 Effect of Periodically Domain-Inverted Structure on Photorefractive Effect

5.3.1 Preparation of Samples

The periodically domain-inverted structure is formed using a tantalum mask which is 5μm wide and 10.8 μm in period. The *z*-cut $LiTaO_3$ substrate is kept in the pyrophosphoric acid at 260 ℃ for 30 min, and the proton-exchanged layer is formed. Then, the

proton−exchanged layer is annealed at 525 ℃ for 2 min and the periodically domain−inverted slab structure, which is 4μm thick, is formed.

Slab waveguides are formed on both the $LiTaO_3$ substrate (sample A) and the substrate with the periodically domain−inverted structure (sample B) using the proton−exchange process in pyrophosphoric acid at 260 ℃ for 30min. After the proton−exchange process, the waveguides are annealed at 340 ℃ for 30 min. The thickness of the annealed proton−exchanged waveguide is about 2μm.

5.3.2 Quantitative measurement of photorefractive sensitivity

The photorefractive sensitivity of the two samples is determined by the photorefractive−grating method. In order to obtain the accurate diffusion depth, the diffusion depth of the waveguide is estimated by using the CCD camera, and compared with the value determined by the prism coupling methods. He−Ne laser is focused into the end of the waveguide and the output of the guided beam is observed by the CCD camera (Fig.5.7). As a result, the diffusion depth is 2.0 μm in sample A and 2.3μm in sample B.

5.3.3 Results of the experiment

The photorefractive sensitivity of the proton−exchanged $LiTaO_3$ waveguide formed on both the $LiTaO_3$ substrate (sample A) and the substrate with the periodically domain−inverted structure (sample B) are measured and compared. The photorefractive sensitivity of the

sample A and sample B is shown in Table 5.3. The photorefractive sensitivity of the sample B is smaller than that in sample A when the power density of the argon−ion laser in the waveguides is almost the same in both samples.

5.3.4 Discussion

The photorefractive sensitivity is very small in the annealed proton−exchanged $LiTaO_3$ waveguides. The photorefractive sensitivity in the annealed proton−exchanged waveguide formed on the periodically domain inverted structure seems to be even smaller than that formed on the substrate without domain−inversion.

Jundt *et al.* assumed that the periodically domain−inverted structure must be resistant to photorefractive effect [69] because the photorefraction in the domain−inverted parts and noninverted parts cancels with each other. Our experimental result seems to agree with their theory. It is very likely that the this effect should be the cause of the high resistance to optical damage.

5.4 Temperature Dependence on Photorefractive Effect

5.4.1 Preparation of Samples

It has been reported by Yuhara *et al.* [42] that the proton−exchanged $LiTaO_3$ waveguide becomes very resistant to optical damage with annealing under optimum conditions. In their report, the increased resistance to optical damage measured at room

temperature is larger in a sample with the Gaussian index profile than in a sample with the step index profile. In this section, the temperature dependences of a sample with the Gaussian index profile fabricated under optimum conditions and a sample with the step index profile, which is less affected by the annealing process, are compared.

The thin slab waveguiding layer is formed on a z-cut $LiTaO_3$ crystal by the proton-exchange process at 250 ℃ for 17min (sample LTB1), or 15min (sample LTB2) using benzoic acid. After the proton-exchange process the waveguides LTB1 and LTB2 are annealed at 325 ℃ for 30 min and 4 h, respectively.

The proton-exchanged layer of sample LTB1 has the step index depth profile and is 0.9 μm deep, while that of sample LTB2 has the Gaussian index profile and is 1.5 μm deep. Single-mode waveguides are formed on both sample LTB1 and sample LTB2.

5.4.2 Measurement of the Photorefractive Effect

The samples are uniformly heated by the ceramic heater embedded in the sample holder in order to measure the temperature dependence of the photorefraction.

The diffraction efficiency is measured after the temperature of the waveguide becomes stable.

The temperature dependence of both the saturated index change Δn_s induced by the photorefractive effect, and the build-up time constant τ is measured. The build-up speed of the photorefraction can be estimated by τ, which is related to the conductivity of the

waveguiding layer. The photorefractive sensitivity, which can be expressed as follows, is also estimated.

$$S = \Delta n_s/(\tau I_{ir}).$$

where I_{ir} is the irradiation intensity in the waveguide.

According to the Glass model, [68] the saturated index change Δn_s is proportional to the magnitude of the photovoltaic effect and inversely proportional to the conductivity, which can be expressed as follows [67] .

$$\Delta n_s(I_{ir}) = n_e^3 \frac{r_{33}}{2} \frac{\kappa \alpha I_{ir}}{\sigma_d + \sigma_{ph}} \qquad (5-3)$$

where κ is the Glass constant, α is the absorption coefficient, σ_d is the dark conductivity, and σ_{ph} is the photoconductivity which depends on the irradiation intensity I_{ir}.

5.4.3 Results of Experiment

The photorefractive effect is measured at 20 ℃ ~ 80 ℃ .

The intensity dependence of the saturated index change Δn_s of the samples LTB1 and LTB2 is shown in Fig. 5.8. The saturated index change Δn_s measured at 20 ℃ and 80 ℃ increases almost linearly with I_{ir} in the low-intensity region, while Δn_s measured at 40 ℃ and 60 ℃ does not vary linearly. In some cases, Δn_s measured at 40 ℃ and 60 ℃ is larger than that measured at 20 ℃ when the

irradiation intensity is low. This irregular behavior above room temperature may be caused by both the pyroelectric effect and the thermal diffusion effect of the electrons.

From eq. (5−3), the saturated index change is proportional to the irradiation intensity in the low−intensity region where the dark conductivity is dominant. When the samples are measured at 20 ℃ and 80 ℃ , the dark conductivity is supposed to be dominant because the saturated index change varies proportionally with the irradiation intensity.

The index change is larger in the sample LTB1 (with step index profile) than in the sample LTB2 (with Gaussian index profile) at both 20 ℃ and 80 ℃ . This difference may be due to the reduction of the traps of electrons by the annealing process [42] . The index change measured at 80 ℃ is much smaller than that measured at 20 ℃ in both samples. Therefore the samples hardly suffer photorefraction at 80 ℃ .

The inverse of the build−up time constant measured at 20 ℃ and 80 ℃ , where the dark conductivity seems to be dominant, is shown in Fig. 5.9. The build−up time constant decreases as the power density in the waveguiding layer increases. At very low irradiation power, $1/\tau$ cannot be obtained because the photorefractive effect is too small to be detected. In both samples LTB1 and LTB2, the intensity dependence of $1/\tau$ is smaller at 80 ℃ than at 20 ℃ . It seems that the dark conductivity is very large and thermal diffusion is dominant at 80 ℃ . At 20 ℃ , $1/\tau$ is larger in sample LTB1 than in sample LTB2, whereas at 80 ℃ , $1/\tau$ is smaller in sample LTB1

than in sample LTB2. This result indicates that thermal diffusion is less dominant in sample LTB1 than in sample LTB2.

$\Delta n_s/\tau$ of sample LTB1 and sample LTB2 is shown as a function of I_{ir} in Fig. 5.10. The photorefractive sensitivity is given by the slope, $\Delta n_s/(\tau I_{ir})$. $\Delta n_s/\tau$ increases almost proportionally to the irradiation intensity, which suggests that the photorefractive sensitivity is almost independent of the irradiation intensity. $\Delta n_s/\tau$, and thus the photorefractive sensitivity, is much larger in the sample LTB1 than in the sample LTB2 at 20 ℃ , whereas it is almost the same and is very small in both samples at 80 ℃ . This result also indicates that the effect of thermal diffusion on photorefraction is very large at 80 ℃ .

5.4.4 Discussion

The waveguiding layers with Gaussian index profile and with the step index profile are compared. The results obtained by our experiment are as follows.

(1) The dark conductivity is considered to be dominant at the low−intensity region when the sample is measured at 20 ℃ and 80 ℃ because the saturated index change varies proportionally with the irradiation intensity.

(2) The index change is smaller in the sample with the Gaussian index profile fabricated under optimum annealing conditions than in the sample with the step index profile when the samples are measured at both 20 ℃ and 80 ℃ . The samples hardly suffer photorefraction at 80 ℃ .

(3) The intensity dependence of $1/\tau$ is smaller at 80 ℃ than at 20 ℃ in both samples. Thermal diffusion seems to be less dominant in the sample with the step index profile than in the sample with the Gaussian index profile.

(4) The photorefractive sensitivity is much larger in the sample with the step index profile than in the sample with the Gaussian index profile at 20 ℃ , whereas it is almost the same and is very small in both samples at 80 ℃ .

In the low-intensity region, the dark conductivity seems to be dominant in the photorefractive effect, which is also the case with the proton-exchanged $LiNbO_3$ waveguides measured at room temperature [67] .

Resistance to the photorefractive effect is greatly improved when the samples are heated at temperatures as high as 80 ℃ , where the effect of the thermal diffusion on photorefraction is assumed to be very large.

It is reported by Yoshino and Inuishi [70] that in the case of iron-doped $LiNbO_3$ bulk crystal, the index change and build-up time constant greatly decrease when the sample is heated above 100 ℃ . In proton-exchanged $LiTaO_3$, however, both the index change and build-up time constant are reduced when the sample is heated at 80 ℃ . This difference can be explained by the increased conductivity in the waveguiding layer due to the proton-exchange process.

5.5 Conclusion

In this chapter, the photorefractive effect of proton-exchanged $LiNbO_3$, proton-exchanged $LiTaO_3$ and ion-exchanged KTP waveguides are investigated from the view point of the practical application.

The photorefractive effect in the proton-exchanged waveguides formed on the $LiNbO_3$ crystal and the $LiTaO_3$ crystal is closely investigated in detail and compared. The increased resistance to the photorefractive effect due to the annealing process is observed only in the proton-exchanged $LiTaO_3$ waveguide. This effect seems to be closely related to the increase of the surface refractive index in the proton-exchanged $LiTaO_3$ caused by the annealing process.

The effect of annealing on the ion-exchanged KTP waveguide is investigated. In the Rb ion-exchanged waveguides, annealing the ion-exchanged layer is less effective in the resistance to the photorefractive effect than that in the proton-exchanged waveguides. The saturated index change in the KTP waveguide is almost the same as that in the annealed proton-exchanged waveguide. The photorefractive sensitivity of the KTP waveguide is $10^{-9} \sim 10^{-10}$ (cm^2/J). The photorefractive sensitivity is smaller than that in the annealed proton-exchanged waveguides, while it is larger than that in the annealed proton-exchanged $LiTaO_3$ waveguide.

The photorefractive sensitivity of the proton-exchanged waveguide formed on the $LiTaO_3$ substrate with and without the periodically domain-inverted structure is compared. The

photorefractive sensitivity in the annealed proton−exchanged waveguide formed on the periodically domain inverted structure seems to be smaller than that formed on the substrate without domain−inversion. This may be because the photorefraction in the domain−inverted parts and noninverted parts cancels with each other.

Temperature dependence of the photorefractive effect in the proton−exchanged waveguides formed on $LiTaO_3$ substrates is investigated in detail. Resistance to the photorefractive effect is greatly improved above 80 ℃ , where the effect of the thermal diffusion on the photorefractive effect is assumed to be very large.

From our experimental results, it is proven that the photorefraction in the proton−exchanged $LiTaO_3$ waveguide is highly dependent on temperature. Therefore the waveguide must be handled with care when large temperature change in the atmosphere is expected.

The annealed proton−exchanged waveguide formed on the $LiTaO_3$ crystal is the most resistant to photorefractive effect because both the saturated index change and photorefractive sensitivity are the smallest of all the measured samples. From this point of view, the annealed proton−exchanged $LiTaO_3$ waveguide is the most attractive material for short−wavelength applications.

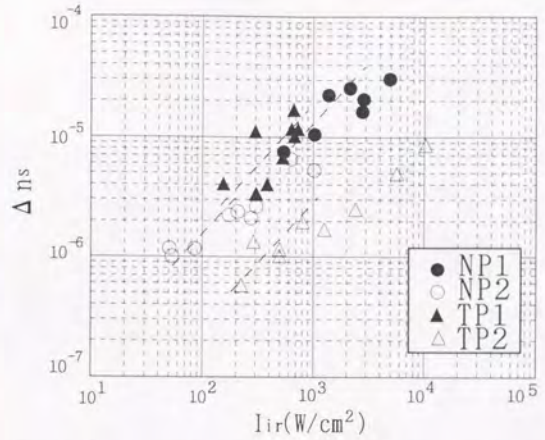

Fig. 5.1. Intensity dependence of the saturated index change Δn_s for the lithium niobate and lithium tantalate waveguides.

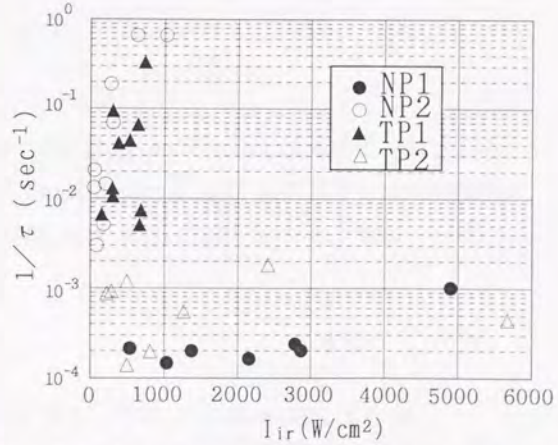

Fig. 5.2. Intensity dependence of the inverse of the build-up time constant $1/\tau$ for the proton-exchanegd lithium niobate and lithium tantalate waveguides.

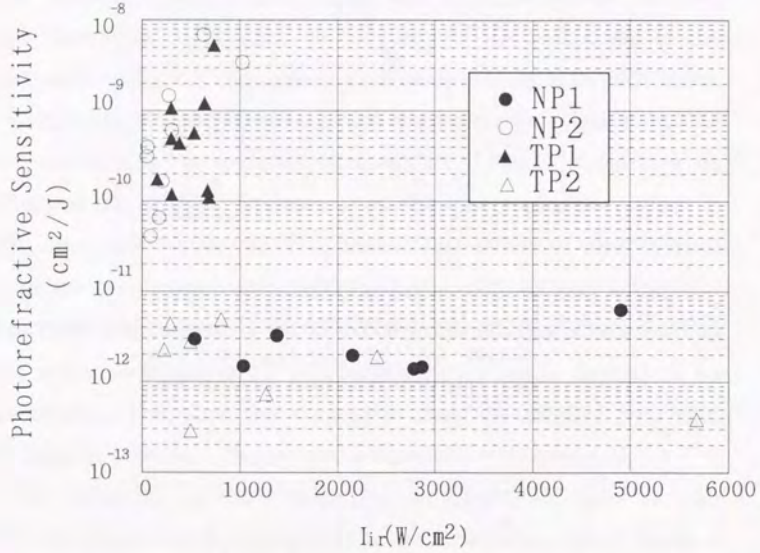

Fig. 5.3. Intensity dependence of the photorefractive sensitivity for the proton-exchanged lithium niobate and lithium tantalate waveguides.

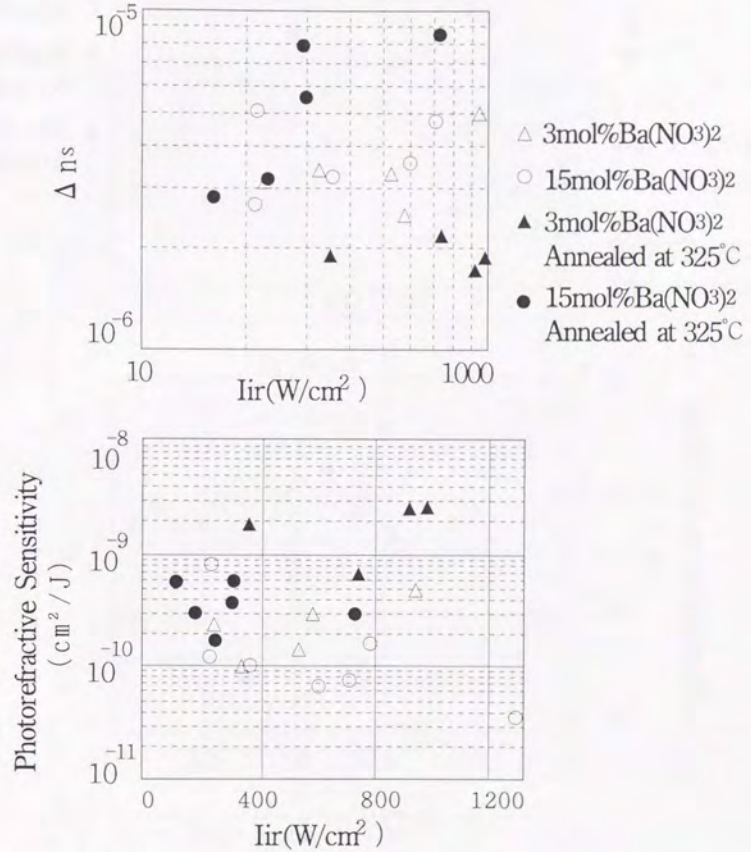

Fig. 5.4. Intensity dependence of the saturated index change Δ ns and the photorefractive sensitivity

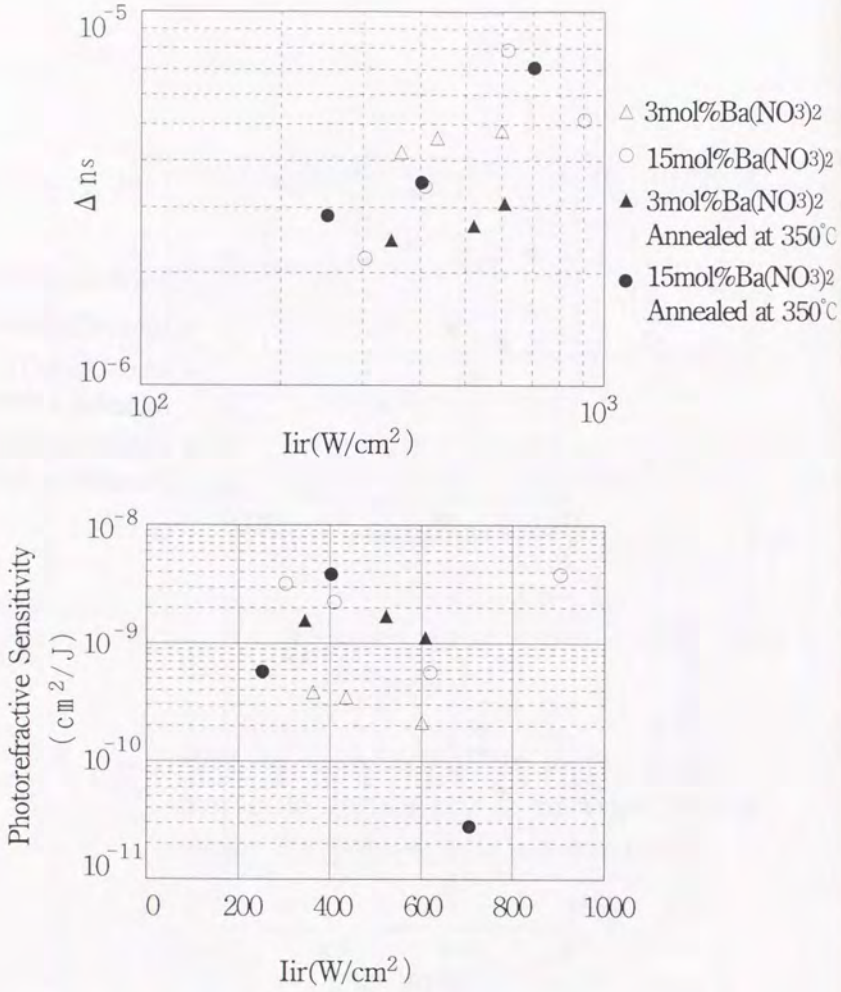

Fig. 5.5. Intensity dependence of the saturated index change Δ ns and the photorefractive sensitivity

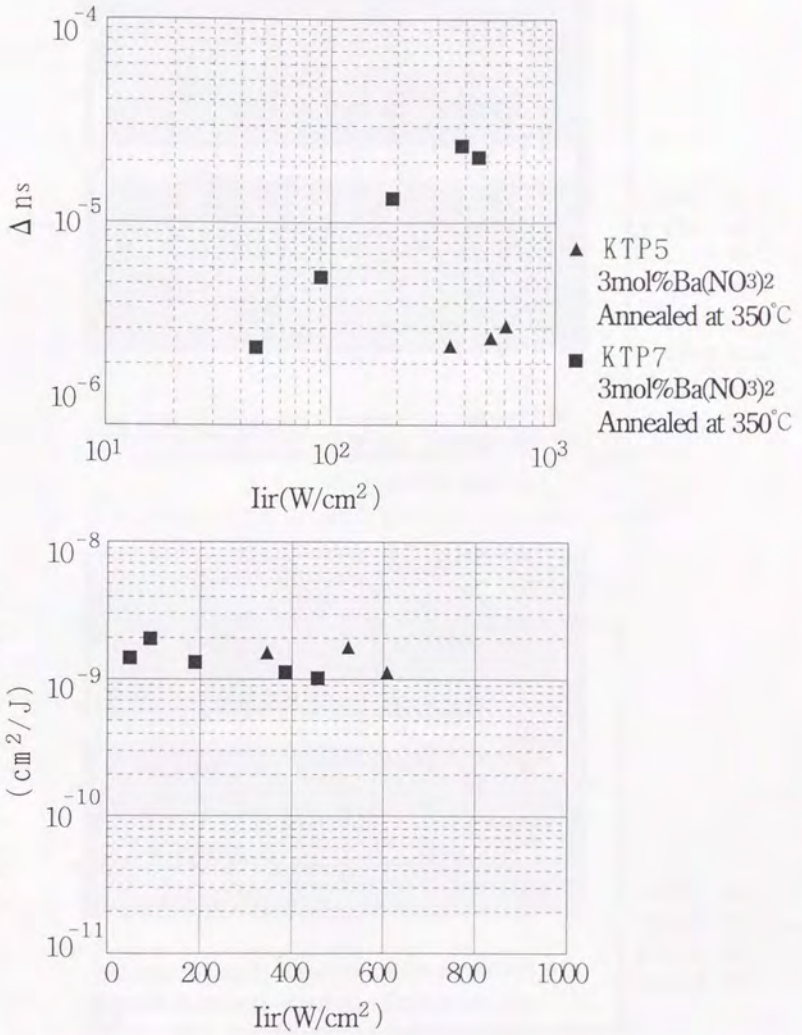

Fig. 5.6. Intensity dependence of the saturated index change Δ ns and the photorefractive sensitivity

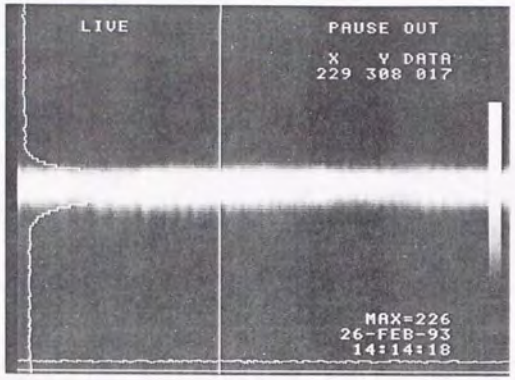

(a) Proton−exchanged waveguide formed on the lithium tantalate substrate (depth: 2.0μm)

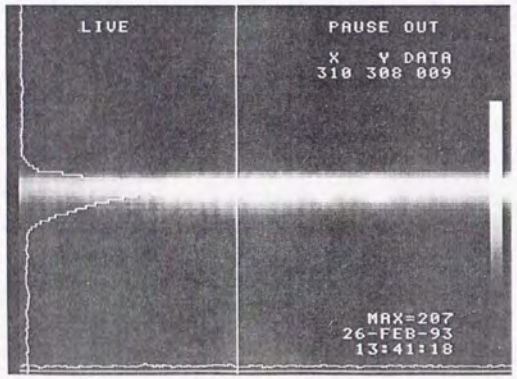

(b) Proton−exchanged waveguide formed on the periodically domain−inverted structure (depth: 2.3μm)

Fig. 5.7. Measurement of the depth of the waveguide formed on the periodically domain−inverted structure: The output of He−Ne laser from the end of the crystal

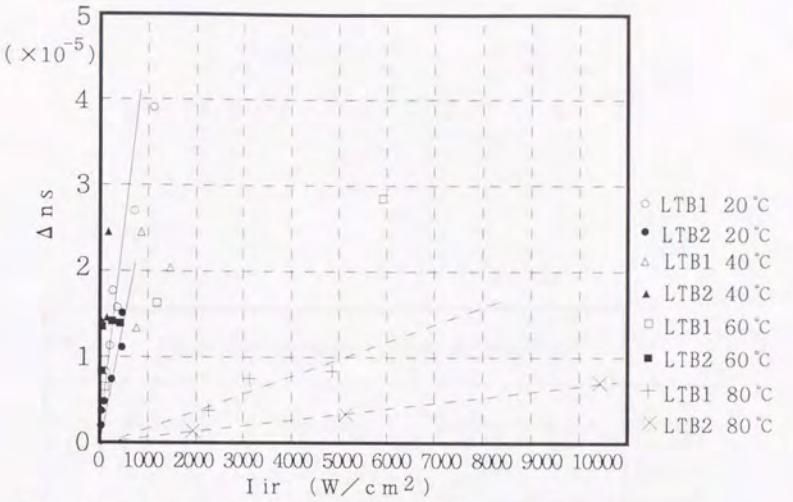

Fig. 5.8. Intensity dependence of the saturated index change Δns for the proton-exchanged lithium tantalate waveguides

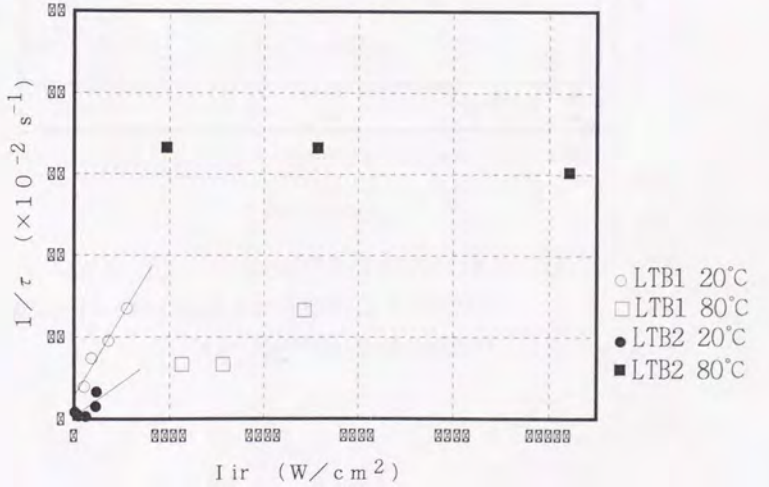

Fig. 5.9. Intensity dependence of the inverse of the build-up time constant $1/\tau$ for the proton-exchanged lithium tantalate waveguides

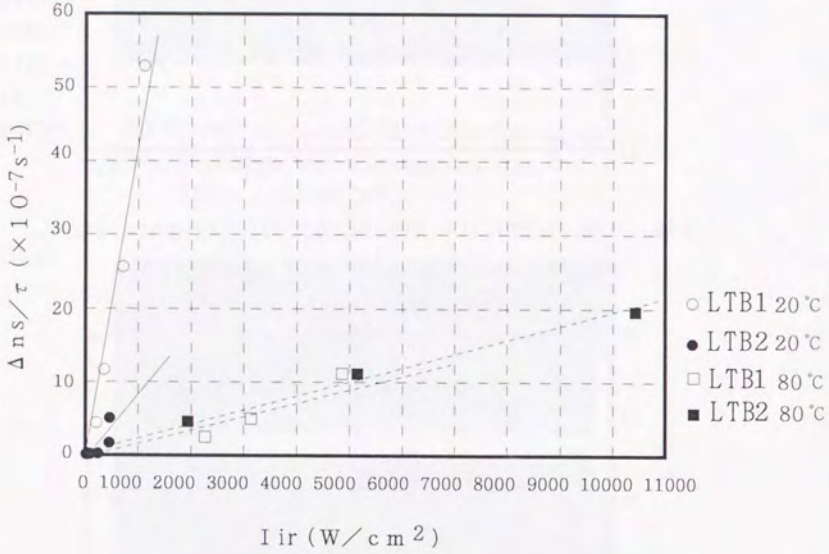

Fig. 5.10. Intensity dependence of $\Delta ns/\tau$ for the proton-exchanged lithium tantalate waveguides

Table 5.1. Fabrication conditions of the waveguides.

Sample	Proton-exchange conditions	Annealing conditions	Surface refractive index	Diffusion depth(μm)
NP1	230℃ 3h 14min		2.340	2.1
NP2	200℃ 30min	350℃ 4h	2.239	3.6
TP1	260℃ 4h		2.194	2.8
TP2	260℃ 30min	340℃ 30min	2.212	1.4

Table 5. 2. Fabrication Conditions of the ion-exchanged KTP waveguides

Sample	Ba(mol%)	Ion-exchange temperature (℃)	Ion-exchange time (min)	Annealing temperature (℃)	Annealing time (min)
KTP1	3	320	45		
KTP2	15	320	10		
KTP3	3	320	45	325	80
KTP4	15	320	10	325	80
KTP5	3	320	45	350	50
KTP6	15	320	10	350	50
KTP7	3	320	45	350	50

Table 5.3. Photorefractive sensitivity of the proton-exchanged layer formed on the lithium tantalate substrate with and without the domain-inverted structure

Sample	Domain-inverted structure	Power density (W/cm^2)	Energy density (J/cm^2)	Photorefractive Sensitivity (cm^2/J)
A	NO	5.73×10^{3}	1.29×10^{4}	3.8×10^{-10}
		6.93×10^{3}	1.56×10^{4}	3.5×10^{-10}
B	YES	5.56×10^{3}	5.42×10^{4}	9.4×10^{-11}
		6.37×10^{3}	6.69×10^{4}	7.7×10^{-11}

Chapter VI

Conclusion

Abstract

The present study on the ion-exchanged optical waveguides formed on ferroelectric crystals is briefly summarized. The relations between each chapters are clarified and the important points derived from the study are explained.

The optical properties of the ion-exchanged waveguides are investigated in detail for the fundamental understanding of the waveguide material and for their application to optical devices.

6.1 Formation of Optical Waveguides and Lattice Constants of Ion-exchanged Waveguides

In Chapter Ⅱ, the refractive index profiles of the ion-exchanged waveguides and the lattice constant changes due to the fabrication process are experimentally studied. The refractive index profiles are determined using the prism coupler method, and the lattice constants are determined by the x-ray diffraction using the double crystal method.

Proton-exchanged slab waveguides are formed on the three types of the lithium niobate substrates: nondoped, Ti-indiffused, and MgO-doped, and the refractive index profiles of these waveguides are measured.

The surface refractive index of the proton-exchanged layer decreases according as the annealing time increases, and the refractive index profile of the proton-exchanged layer is gradually changed into the Gaussian profile. The diffusion of the protons into the substrate by the annealing process seems to be disturbed by the Mg^{2+} or Ti^{4+} ions which are doped or diffused in the substrate.

Although the increase in the surface refractive index due to the annealing process is reported for the proton-exchanged $LiTaO_3$ waveguide, this phenomenon is not observed in the proton-exchanged $LiNbO_3$ waveguides.

It is confirmed by our experiment that annealing process is effective for controlling the refractive index profile in the Rb ion-exchanged KTP waveguide as well as in the proton-exchanged $LiNbO_3$ waveguides.

The lattice constant seems to be increased by the Rb ion-exchange process. In this case, the peak corresponds to the guiding layer is not so clear as in the proton-exchanged waveguide. The lattice constant is considerably reduced by the annealing process, and the strain caused by the ion-exchange process seems to be recovered by the annealing process.

The structural change of the $LiTaO_3$ crystal caused by the domain-inversion process is experimentally studied for the first time. Periodically domain-inverted structure is attractive for second-harmonic application. The lattice constants of the $LiTaO_3$ substrates without and with the domain-inverted slab structure and with the periodically domain-inverted structure are the same. The increase in lattice constant caused by the proton-exchange process ($\Delta c/c$) is 0.53 % in all the samples. The values $\Delta c/c$ measured in the annealed proton-exchanged waveguides with domain-inverted slab structure, with the periodically domain-inverted structure, and without the domain-inverted structure are 0.19 %, 0.21 % and 0.23 %, respectively. Our experimental results suggest that protons will diffuse more rapidly into the substrate by the annealing process in the domain-inverted structure than in the substrate without the domain-inverted structure.

6.2 Exact Estimation of Electrooptic Constants in Optical Waveguides

In Chapter Ⅲ, the electrooptic constants of the proton-exchanged $LiNbO_3$ waveguides are measured.

The pure electrooptic constant r'_{33} of the proton-exchanged layer formed on the $LiNbO_3$ crystal is measured with the correction considering the field distribution of the propagating mode. It is found that the value of the electrooptic constant is reduced to 1/20 of the electro-optic constant r_{33} of the bulk crystal by the proton-exchange process. The effect of annealing the proton-exchanged layers formed on the three kinds of $LiNbO_3$ substrates referred in Chapter Ⅱ, is investigated. After the annealing process, the values of electrooptic constant r_{33} increase in all the waveguides. The MgO-doped crystal is rather insensitive to the increase of the r_{33} caused by the annealing process.

As is shown in Chapter Ⅱ, the lattice constant is increased by the proton-exchange process and is decreased by the postannealing process. The degradation and the recovery of r_{33} should be caused by this structural change of the crystal, between the diamond structure of $LiNbO_3$ (trigonal system, 3m) and a Perovskite structure (cubic system, m3m) with electrooptic constant is zero.

The annealing method gives advantages for optical waveguides to be used as integrated optical devices such as modulators and switches.

The polarization independent switch can be designed using the annealed PETi waveguide formed on the y-cut $LiNbO_3$ substrate. In

this case, the electrooptic effect depends on the electrooptic constant r_{22} in the waveguide. It is proven by our experiment that the electrooptic constant r_{22} is not reduced by the proton-exchange process. Therefore, it is possible that the simple polarization independent switches are fabricated using this PETi process on the y-cut $LiNbO_3$ crystal.

6.3 Quantitative Measurement of Photorefractive Sensitivity of Optical Waveguides

In chapter Ⅳ, a quantitative estimation of the photorefractive sensitivity has been made for the ion-exchanged waveguides fabricated on $LiNbO_3$, MgO-doped $LiNbO_3$ and KTP crystals. The photorefractive sensitivity of the proton-exchanged $LiNbO_3$ waveguiding layer without annealing process is the smallest in these waveguides. However, a postannealing process is necessary for its application to optical devices because both the electrooptic constant and the nonlinear-optic coefficient are reduced during the proton-exchange process.

The conclusion of this experiment is as follows.

(1)Though the photorefractive sensitivity increases as the annealing time increases, the photorefractive sensitivity of the annealed waveguides is still much smaller than that of Ti-indiffused waveguides formed on the non-doped crystal.

(2)The effect of doping MgO in the photorefractive sensitivity of the proton-exchanged layer is very small.

(3)In Chapter Ⅲ, it is found that the electrooptic constant of the proton-exchanged layer is increased by the annealing process. The cause of the increased photorefractive sensitivity of the annealed proton-exchanged $LiNbO_3$ waveguides can be explained mainly by this increased electrooptic constant in the guiding layer.

(4)The KTP waveguide seems to be resistant to optical damage if fabrication condition is properly chosen.

The $LiNbO_3$ thin-film waveguides formed on the $LiTaO_3$ substrate are compared with the above results. The thin-film waveguide grown by using the $Li_2O-B_2O_3$ flux is no less resistant to optical damage than most other $LiNbO_3$ waveguides. It is almost as resistant as the annealed proton-exchanged $LiNbO_3$ waveguides.

6.4 Optical Damage Resistance of the Ion-Exchanged Waveguides for the Short-Wavelength Application

In chapter Ⅴ, the photorefractive effect of the proton-exchanged $LiNbO_3$, proton-exchanged $LiTaO_3$ and ion-exchanged KTP waveguides is investigated in detail from the view point of the practical application to the devices designed for short-wavelength.

The photorefractive effect in the proton-exchanged waveguides formed on the $LiNbO_3$ crystal and the $LiTaO_3$ crystal is compared. The increased resistance to the photorefractive effect due to the annealing process is observed only in the proton-exchanged $LiTaO_3$ waveguide, which seems to be closely related to the increase of the surface refractive index in the proton-exchanged layer. This

phenomenon is not observed in the $LiNbO_3$ samples because only the reduction of the surface refractive index due to the annealing process is observed in the proton-exchanged $LiNbO_3$, as shown in Chapter Ⅱ. It is obvious that the resistance to the photorefractive effect largely depends on the profile of the proton-exchanged layer. In the case of the annealed proton-exchanged $LiTaO_3$ waveguide, the effect of above mentioned phenomenon seems to surpass the increased electrooptic effect due to the annealing process.

In the case of the Rb ion-exchanged waveguide, the influence of annealing the ion-exchanged layer is proven to be very small.

The photorefractive sensitivity in the annealed proton-exchanged $LiTaO_3$ waveguide formed on the periodically domain-inverted structure is also investigated. Photorefractive sensitivity seems to be smaller in the proton-exchanged layer formed on the domain-inverted structure than in the proton-exchanged layer without the domain-inverted structure. This may be due to the fact that the photorefraction in the domain-inverted parts and noninverted parts cancels with each other.

Temperature dependence of the photorefractive effect in the proton-exchanged waveguides formed on $LiTaO_3$ substrates is investigated in detail.

Resistance to the photorefractive effect is greatly improved above 80 ℃. From our experimental results, it is proven that the photorefraction in the proton-exchanged $LiTaO_3$ waveguide is highly dependent on temperature. Therefore the waveguide must be handled with care when large temperature change in the atmosphere is

expected.

The electrooptic constants and the photorefractive sensitivity of the above mentioned dielectric waveguides are compared in Fig. 6.1. From this figure, it is obvious that the annealed proton−exchanged waveguide formed on the $LiTaO_3$ crystal is the most resistant to photorefractive effect and therefore the most attractive material for short−wavelength applications. The Ion−exchanged KTP waveguide, $LiNbO_3$ thin−film waveguide and annealed proton−exchanged waveguide seem to be attractive for the electrooptic device applications, especially, for those used at visible wavelength.

6.5 Concluding remarks

The author has studied optical properties of the ion−exchanged waveguides. The study has been focused on the following three points.

1)Exact estimation of the electrooptic effects.
2)Quantitative measurement of the photorefractive effect.
3)The influence of the photorefractive effect on the device application.

The author hopes that the present study contributes to the fundamental understanding of the properties of the optical waveguides, and the device application in the fields of the optical memory, optical sensors and the optical communication.

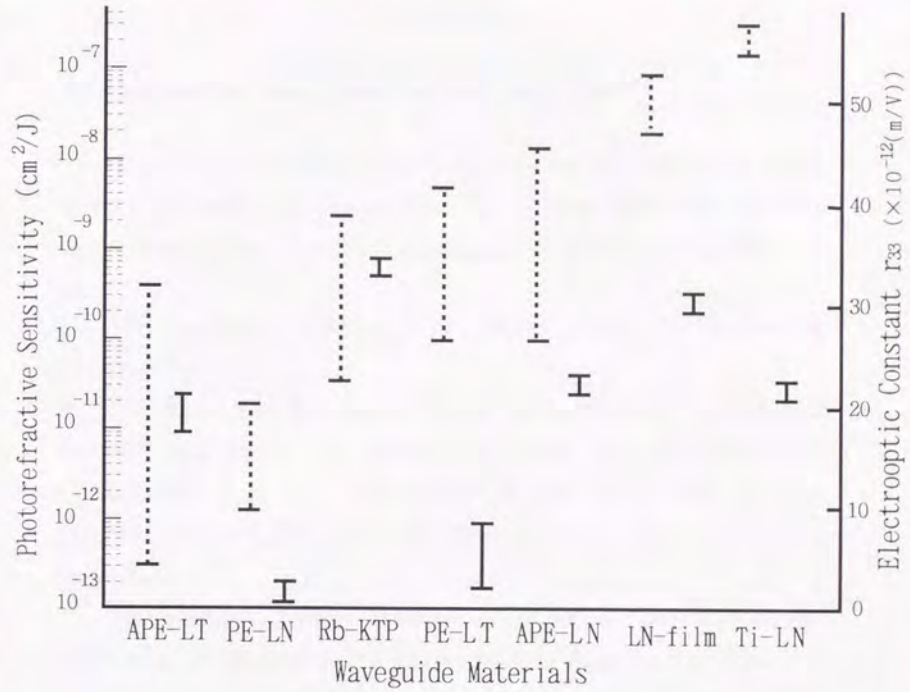

Fig. 6.1. The electrooptic constants and the photorefractive sensitivity of the dielectric waveguides

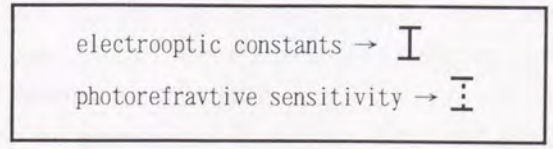

APPENDIX

A.1 Experimental Methods for Photorefractive Effect

There are other techniques to measure the photorefractive effect besides photorefractive grating methods. Among them, the following two techniques are often used to measure the photorefractive effect.

(1) The Senarmont Method (The Method using the Senarmont Compensator)

The photorefractive effect in the lithium niobate and lithium tantalate bulk crystal was measured by Chen using the Senarmont Compensator [59] . The spatial distribution of the optically induced change of the indices of refraction can be measured by this method.

The sample is positioned between the pair of crossed polarizers along with the Babinet−Soleil compensator as shown in Fig. A.1.1. A He−Ne laser (λ =632.8nm, output power $\fallingdotseq$ 20mW) focused approximately 0.2−mm diameter is used to induce an index change in the crystal. In order to measure the spatial distribution, the laser power is reduced to 1mW and the beam diameter to 0.03mm by reducing the diameter of an aperture inside the laser cavity.

The laser intensity is further reduced by the neutral density filter. This light with reduced intensity is used to probe the index change caused by the photorefractive effect.

Before the intense laser illumination, the birefringence ($n_e - n_o$), where n_e and n_o are the extraordinary and ordinary indices of

refraction, respectively, is probed with the low−intensity beam and the compensator by translating the sample orthogonal to the light propagation. Then the high power laser is used to induce the index changes for a specified period of time and ($n_e - n_o$) is probed again. The refractive index change $\Delta(n_e - n_o)$ induced by the intense laser illumination is observed by this method.

(2) The Waveguide Mach−Zehnder Interferometer

The photorefractive effect in the lithium niobate waveguide was measured by Fujiwara *et al.* using a waveguide Mach−Zehnder Interferometer [64] , [80] .

The waveguide pattern is a Mach−Zehnder interferometer for 1.3μm wavelength shown in Fig. A.1.2. The irradiation beam of wavelength λ_{ir} is fed into the upper arm of this Mach−Zehnder interferometer. Light input from port A brings about a photoinduced index change and consequently an asymmetry of optical path between the two interferometer arms. The phase retardation of the upper arm relative to that of the lower arm is expressed as follows.

$$\Gamma = \frac{2\pi}{\lambda} \int_0^L \Delta n(z) dz \qquad \text{(A.1.1)}$$

This retardation causes the probe output to be modulated as,

$$I_p(t) = I_p(0) \cos^2 \frac{\pi L \overline{\Delta n(t)}}{\lambda_p} \qquad \text{(A.1.2)}$$

where L is the length of the interferometer arms, λ_p the probe wavelength, and $\overline{\Delta n(t)}$ the average index change,

$$\overline{\Delta n}(t) = (1/L) \int_0^L \Delta n(z) dz$$

The probe light of 1.3μm is input from port B. Optical waves of two wavelengths are mixed at port C. The probe light is chopped at 270 Hz before entering port B and the probe output is measured by a lock−in amplifier placed after a photodetector. The probe light intensity is kept below 5μW to ensure that no photorefractive effect is caused by the probe. Port D monitors any temporal variation of the 1.3 μm probe light due to input fiber/waveguiding coupling.

Both the irradiation and probe beams are fed through optical fibers butt−coupled to input ports A and B. Δn_e and Δn_o are separately determined by adjusting the input probe polarization to the TM or TE mode, respectively. The irradiation beam polarization is adjusted to be 45° from the optical axis of the substrate.

The observed temporal change of the output can be converted to the time evolution of $\overline{\Delta n(t)}$, which is proven to be a good fit to an expression, $\overline{\Delta n(t)} = \overline{\Delta n_s}(1 - \exp(-t/\tau))$, where $n(t)$ denotes spatial averaging along the path I → II → III .

The photorefractive sensitivity in the initial stage, which is expressed as follows, is also determined by this method.

$$S(t \to 0) = \Delta n_s / I_{ir} \tau,$$

where t is the time duration of the irradiation.

A.2 Photorefractive Diffraction–Grating Method

In the waveguide with step index profile, the hologram (photorefractive diffraction–grating) along the depth direction is almost uniform. In the waveguide with Gaussian or other index profiles, however, it might be slightly changed along the depth direction.

To simplify the measurement, the hologram grating is assumed to be uniform along the depth direction in all the measured waveguides and the diffusion depth of the ions is regarded as the depth of these waveguides.

The eq.(4–1) is deduced from the coupled wave theory [79] .

This theory assumes monochromatic light incident on the hologram grating at or near the Bragg angle and polarized perpendicular to the plane of incidence. Only two significant light waves are assumed to be present in the grating: the incoming "reference" wave R, and the outcoming "signal" wave S.

The y–axis is chosen perpendicular to the surfaces of the medium, x–axis in the plane of incidence and parallel to the medium boundaries and the z–axis perpendicular to the paper. The grating vector $\vec{K}$ is oriented perpendicular to the fringe planes and is of length $K=2\pi/\Lambda$, where Λ is the period of the grating (Fig.A.2.1).

Wave propagation in the grating is described by the scalar wave equation,

$$\nabla^2 E + k^2 E = 0 \qquad \text{(A.2.1)}$$

where $E(x,y)$ is the complex amplitude of the z–component of the electric field, which is assumed to be independent of z, and to oscillate with an angular frequency ω. The propagation constant $k(x,y)$ is spatially modulated and related to the relative dielectric constant $\varepsilon(x,y)$ and the conductivity $\sigma(x,y)$ of the medium by,

$$k^2 = \frac{\omega^2}{c^2}\varepsilon - j\omega\mu\sigma \qquad \text{(A.2.2)}$$

where c is the light velocity in free space, and μ is the permeability of the medium which is assumed to be equal to that of free space. The constants of the medium are assumed to be independent of z.

The fringes of the hologram grating are represented by a spatial modulation of ε or σ as follows.

$$\varepsilon = \varepsilon_0 + \varepsilon_1 \cos(\vec{K} \cdot \vec{x})$$

$$\sigma = \sigma_0 + \sigma_1 \cos(\vec{K} \cdot \vec{x}) \qquad \text{(A.2.3)}$$

where ε_1 and σ_1 are the amplitudes of the spatial modulation, ε_0 is the averaged dielectric constant and σ_0 the average conductivity. ε and σ are assumed to be modulated in phase.

The radius vector $\vec{x}$ and the grating vector $\vec{K}$ is written as,

$$\vec{x}=\begin{bmatrix} x \\ y \\ z \end{bmatrix} \qquad \vec{K}=\begin{bmatrix} \sin\phi \\ \cos\phi \\ 0 \end{bmatrix} \qquad ; \qquad K=2\pi/\Lambda \tag{A.2.4}$$

Equation (A.2.2) and (A.2.3) can be combined in the form,

$$k^2=\beta^2-2j\alpha\beta+2\kappa\beta(\exp(j\vec{K}\cdot\vec{x})+\exp(-j\vec{K}\cdot\vec{x})) \tag{A.2.5}$$

where the average propagation constant β and the average absorption constant α are introduced:

$$\beta=2\pi(\varepsilon_0)^{1/2}/\lambda, \quad \alpha=\mu c\sigma_0/2(\varepsilon_0)^{1/2}, \tag{A.2.6}$$

and the coupling constant κ between the reference wave R and the signal wave S is defined as,

$$\kappa=\frac{1}{4}\left(\frac{2\pi}{\lambda}\varepsilon_1/(\varepsilon_0)^{\frac{1}{2}}-j\mu c\sigma_1/(\varepsilon_0)^{\frac{1}{2}}\right) \tag{A.2.7}$$

β, and κ can be written as

$$\beta=2\pi n/\lambda, \quad \kappa=\pi m/\lambda-j\alpha_1/2, \tag{A.2.8}$$

under the conditions,

$$2\pi n/\lambda \gg \alpha \; ; \quad 2\pi n/\lambda \gg \alpha_1, \quad n \gg m, \tag{A.2.9}$$

where n is the average refractive index, and m and α_1 are the

amplitudes of the spatial modulation of the refractive index and the absorption constant, respectively. λ is the wavelength in free space.

The total electric field in the grating is the superposition of the two waves,

$$E=R(y)\exp(-j\vec{\rho}\cdot\vec{x})+S(y)\exp(-j\vec{\sigma}\cdot\vec{x}). \tag{A.2.10}$$

$\vec{\rho}$ is assumed to be equal to the propagation vector of the free reference wave in the absence of coupling. $\vec{\sigma}$ is forced by the grating and related to $\vec{\rho}$ and the grating vector by

$$\vec{\sigma}=\vec{\rho}-\vec{K}. \tag{A.2.11}$$

The components of $\vec{\rho}$ and $\vec{\sigma}$ are given by,

$$\vec{\rho}=\begin{bmatrix} \rho_x \\ \rho_y \\ 0 \end{bmatrix}=\beta\begin{bmatrix} \sin\theta \\ \cos\theta \\ 0 \end{bmatrix}$$

$$\vec{\sigma}=\begin{bmatrix} \sigma_x \\ \sigma_y \\ 0 \end{bmatrix}=\beta\begin{bmatrix} \sin\theta-(K/\beta)\sin\phi \\ \cos\theta-(K/\beta)\cos\phi \\ 0 \end{bmatrix} \tag{A.2.12}$$

In case the incidence angle is equal to the Bragg angle θ_0, the lengths of both $\vec{\rho}$ and $\vec{\sigma}$ are equal to the free propagation

constant β, and the Bragg condition is obeyed.

$$\cos(\phi-\theta)=K/2\beta. \tag{A.2.13}$$

The coupled wave equations are derived as follows. Equations (A.2.1) and (A.2.5) are combined and the equations (A.2.10) and (A.2.11) are inserted. Then the terms with equal exponentials ($\exp(-j\vec{\rho}\cdot\vec{x})$ and $\exp(-j\vec{\sigma}\cdot\vec{x})$) are compared and the following equations are obtained.

$$R''-2jR'\rho_y-2j\alpha\beta R+2\kappa\beta S=0 \tag{A.2.14}$$

$$S''-2jS'\sigma_y-2j\alpha\beta S+(\beta^2-\sigma^2)S+2\kappa\beta R=0, \tag{A.2.15}$$

where the primes indicate differentiation with respect to y. The waves generated in the directions of $\vec{\rho}+\vec{K}$ and $\vec{\sigma}-\vec{K}$ are neglected, together with all other higher diffraction orders.

Assuming that the energy interchange between S and R are slow and that energy is absorbed slowly, R'' and S'' can be neglected. We can rewrite the above equations,

$$c_R R'+\alpha R = -j\kappa S \tag{A.2.16}$$

$$c_S S'+(\alpha+j\vartheta)S= -j\kappa R \tag{A.2.17}$$

The abbreviations c_R, c_S and ϑ stand for the expressions,

$$c_R=\rho_y/\beta=\cos\theta$$

$$c_S=\sigma_y/\beta=\cos\theta-(K/\beta)\cos\phi \tag{A.2.18}$$

$$\vartheta=(\beta^2-\sigma^2)/(2\beta).$$

It is straight forward to obtain the general solution of the coupled wave equations, which is

$$R(y)= r_1\exp(\gamma_1 y)+r_2\exp(\gamma_2 y) \tag{A.2.19}$$

$$S(y)= s_1\exp(\gamma_1 y)+s_2\exp(\gamma_2 y) \tag{A.2.20}$$

The equations (A.2.19) and (A.2.20) are inserted into the coupled wave equations, and the following equations are obtained.

$$(c_R\gamma_i+\alpha)r_i= -j\kappa s_i \tag{A.2.21}$$

$$i=1.2$$

$$(c_S\gamma_i+\alpha+j\vartheta)s_i=-j\kappa r_i \tag{A.2.22}$$

After multiplying the equations with each other, we get a quadratic equation for γi,

$$(c_R\gamma_i+\alpha)(c_S\gamma_i+\alpha+j\vartheta)=-\kappa^2 \tag{A.2.23}$$

with the solution,

$$\gamma_{12}=-\frac{1}{2}\left(\frac{\alpha}{c_R}+\frac{\alpha}{c_S}+j\frac{\delta}{c_S}\right)\pm\frac{1}{2}\left[\left(\frac{\alpha}{c_R}-\frac{\alpha}{c_S}-j\frac{\delta}{c_S}\right)^2-4\frac{\kappa^2}{c_Rc_S}\right]^{1/2}. \tag{A.2.24}$$

The boundary conditions are

$$R(0)=1,\quad S(0)=0 \tag{A.2.25}$$

If we insert these boundary conditions into the equations (A.2.19), (A.2.20), it follows immediately that

$$\begin{aligned} r_1+r_2&=1 \\ s_1+s_2&=0 \end{aligned} \tag{A.2.26}$$

Combining these relations with equation (A.2.22), we obtain

$$s_1=-s_2=-j\kappa/c_s(\gamma_1-\gamma_2) \tag{A.2.27}$$

Introducing these constants in equation (A.2.20), the amplitude of the signal wave at the output of the grating can be expressed as follows.

$$S(d)=j\frac{\kappa}{c_s(\gamma_1-\gamma_2)}(exp(\gamma_2 d)-exp(\gamma_1 d)) \tag{A.2.28}$$

The diffraction efficiency η is defined as,

$$\eta=\frac{|c_s SS^*|}{|c_R RR^*|}=\frac{|c_s|}{|c_R|}SS^* \tag{A.2.29}$$

where S is the amplitude of the output signal for a reference wave R

incident with unit amplitude.

From the equations (A.2.24) and (A.2.28),

$$\begin{aligned} S&=-j\left(\frac{c_R}{c_S}\right)^{1/2}\cdot exp(-\alpha d/c_R)\cdot e^{\xi}\cdot\frac{sin\,[v^2-\xi^2]^{1/2}}{[1-\xi^2/v^2]^{1/2}} \\ v&=\frac{\kappa d}{(c_R c_S)^{1/2}} \\ \xi&=\frac{1}{2}d\left(\frac{\alpha}{c_R}-\frac{\alpha}{c_S}-j\frac{\vartheta}{c_S}\right) \end{aligned} \tag{A.2.30}$$

For the lossless dielectric grating, we have $\kappa=\pi n_1/\lambda$ and $\alpha=\alpha_1=0$. Equation (A.2.30) can be rewritten in the form,

$$\begin{aligned} S&=-j\left(\frac{c_R}{c_S}\right)^{1/2}e^{-j\xi}\frac{sin\,[v^2+\xi^2]^{1/2}}{[1+\xi^2/v^2]^{1/2}}, \\ v&=\frac{\pi n_1 d}{\lambda(c_R c_S)^{1/2}}, \\ \xi&=\frac{\vartheta d}{2c_S}, \end{aligned} \tag{A.2.31}$$

where v and ξ are redefined and are real-valued. The associated formula for the diffraction efficiency is

$$\eta = sin^2(v^2+\xi^2)^{1/2}/(1+\xi^2/v^2)\,. \qquad \text{(A.2.32)}$$

If there is no slant ($\phi=\pi/2$) and if the Bragg obeyed, then $c_R = c_S = \cos\theta_0$ and the following equation is obtained from equation (A.2.32).

$$\eta = \sin^2(\pi n_1 d/\lambda\cos\theta_0).$$

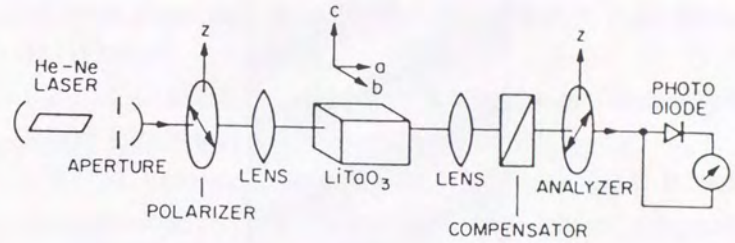

Fig. A.1.1. The Senarmont Method [59]

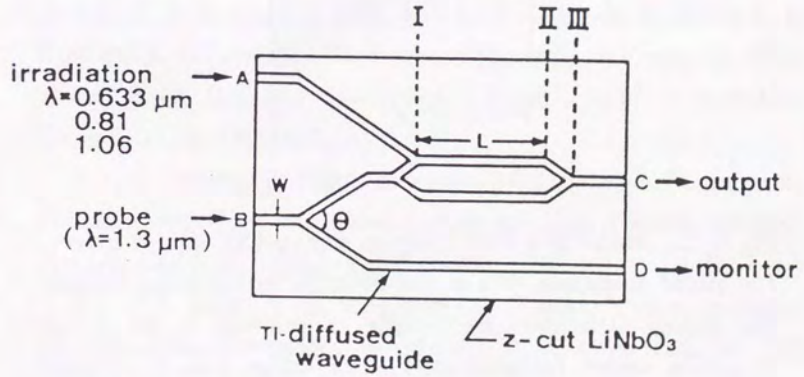

Fig. A.1.2. The Waveguide Mach–Zehnder Interferometer [64]

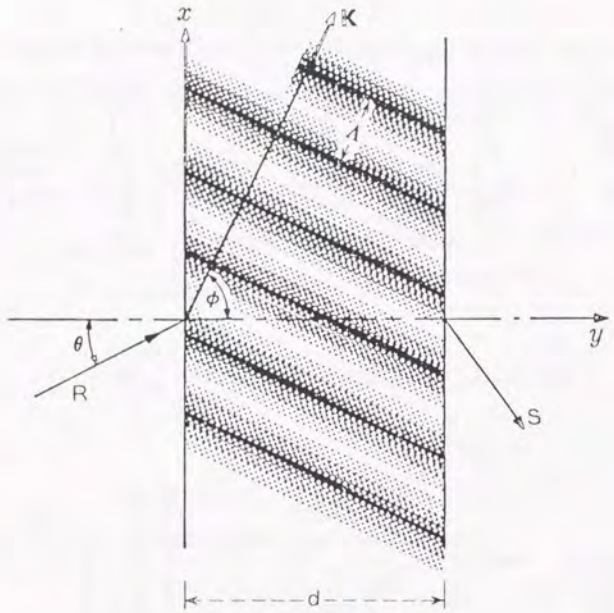

Fig. A.2.1. Model of a thick hologram grating with slanted fringes. The spatial modulation of n or α is indicated by the dotted pattern. The grating parameters are: θ–angle of incidence in the medium, K–grating vector (perpendicular to the fringe planes), Λ–grating period, ϕ–slant angle, and d–grating thickness [79] .

References

[1] W. K. Burns, P. H. Klein, and E. J. West, "Tidiffusion in Ti:LiNbO3 planar and channel optical waveguides", J. Appl. Phys., 50, 6175 (1979)

[2] J. L. Jackel, "Suppression of Outdiffusion in Titanium Diffused LiNbO3: A Review", J. Opt. Commun. 3, 82, (1982)

[3] O. Eknoyan, A. S. Greenblatt, W. K. Burns, and C. H. Bulmer, "Characterization of Ti:LiNbO3 deep waveguides diffused in dry and wet oxygen ambient", Appl. Opt., 25, 737, (1986).

[4] T. R. Ranganath, "Ti–diffused LiNbO3 Branched–Waveguide Modulators: Performance and Design", IEEE J. Quantum electron., QE–13, 290, (1977)

[5] R. E. Tench, J. M. Delavaux, L. D. Tzeng, R. W. Smith, L. L. Buhl, and A. C. Alferness, "Performance Evaluation of Waveguide Phase Modulator for Coherent Systems at 1.3 and 1.5μm", J. Lightwave Technol. LT–5, 492 (1987).

[6] C. Duchet, P. Fabre, S. samso, M. D. Maggio, "Electrooptic Modulator with Very Low Drive Voltage and High Thermal Stability", Tec. Dig. ECOC'89, ThB22–2, 421 (1989)

[7] J. L. Jackel, C. E. Rice, and J. J. Veselka, "Proton–exchange for high–index waveguides in LiNbO3", Appl. Phys. Lett. 41, 607 (1982).

[8] D. F. Clark, A. C. G. Nutt, K. K. Wong, P. J. R. Laybourn, and R. M. De La Lue, "Characterization of proton–exchange slab optical waveguides in z–cut LiNbO3", J. Appl. Phys. 54, 6218 (1983).

[9] M. M. Abouelleil and F. Leonberger, "Waveguides in Lithium Niobate", J. Am. Ceram. Soc., 72, 1311 (1989)

[10] W. K. Spillman Jr., N. A. Sanford, and R. A. Soref, "Optical waveguides in $LiTaO_3$ formed by proton exchange", Opt. Lett. 6 497 (1983)

[11] K. Tada, T. Murai, T.Nakabayashi, T. Iwashima, and Ishikawa, "Fabrication of $LiTaO_3$ optical waveguide by H^+ exchange method", Jpn. J. Appl. Phys., 43, 503, (1987).

[12] T. Yuhara, K. Tada, and Y. S. Li, "Anomalous refractive index change in proton−exchanged $LiTaO_3$ optical waveguides after annealing", Tech. Dig. of 2nd Topical Meeting on Integrated Photonics Research (1991) WC4.

[13] J. D. Bierlein and H. Vanherzeele, "Potassium titanyl phosphate; properties and new applications", J. Opt. Soc. Am. B, 6, 622 (1989)

[14] J. D. Bierlein, A. Ferretti, L. H. Brixner, and William Y. Hsu, "Fabrication and characterization of optical waveguides in $KTiOPO_4$", Appl. Phys. Lett. 50 1216 (1987).

[15] W. K. Risk, "Fabrication and characterization of planar ion−exchanged $KTiPOPO_4$ waveguides for frequency doubling", 58, 19 (1991)

[16] H. Iwakura, H. Yoshikawa, and Y. Ohno, "Application of Optical Waveguide Voltage Sensors", Technical Meeting of The Institute of Electronics, Information, and Communication (OQE90−60) 11 (1990)

[17] M. Haruna, H. Nakajima H. Nishihara, "Optical π−arc waveguide interferometer in proton−exchanged $LiNbO_3$ for temperature sensing", Appl. Opt., 24, 2483 (1985)

[18] H. Toda, M. Haruna and H. Nishihara, "Integrated−Optic Circuit for a Fiber−Laser−Doppler Velocimeter", Proc. OQE 85−160, 25 (1985).

[19] J. L. Jackel, D. H. Olson, and A. M. Glass, "Optical damage resistance of monovalent ion diffused $LiNbO_3$ and $LiTaO_3$ waveguides", J. Appl. Phys. 52, 4855, (1981).

[20] E. J. Lim, M. M. Fejer and R. L. Byer, "Second−Harmonic Generation of Green Light in Periodically Poled Planar Lithium Niobate Waveguide", Electron. Lett. 25 174 (1989).

[21] K. Yamamoto, K. Mizuuchi, K. Takeshige, Y. Sasai and T. Taniuchi, "Characteristics of periodically domain−inverted $LiNbO_3$ and $LiTaO_3$ waveguides for second harmonic generation", J. Appl. Phys. 70 1947 (1991).

[22] K. Mizuuchi, K. Yamamoto and T. Taniuchi, "Second−harmonic generation of blue light in a $LiTaO_3$ waveguide", Appl. Phys. Lett. 58, 2732 (1991).

[23] S. Itoh, N. Nakayama, T. Ohta, M. Ozawa, H. Okuyama, K. Nakano, A. Ishibashi, M. Ikeda and Y. Mori, "491−nm ZnCeSe/ZnSe/ZnMgSSe SCH Laser Diode with a Low Operating Voltage", Jpn. J. Appl. Phys. 32, L1530 (1993).

[24] S. Nakamura, M. Senoh and T. Mukai, "P−GaN /N−InGaN/N−GaN Double−Heterostructure Blue−Light−Emitting Diodes", Jpn. J. Appl. Phys. 32, L8 (1993).

[25] K. Shinozaki, Y. Miyamoto, H. Okayama, T. Kamijoh and T.

Nonaka, "Second-harmonic generation device with integrated periodically domain-inverted regions and distributed Bragg reflector in a $LiNbO_3$ channel waveguide", Appl. Phys. Lett. 58, 1934 (1991).

[26] P. A. Franken, A. E. Hill, C. W. Peters, and G. Weinreich, "Generation of optical harmonics," Phys. Rev. Lett., Vol. 7, pp.118-119, Aug. 1961.

[27] K. Yamamoto, K. Mizuuchi, Y. Kitaoka and M. Kato, "High power blue light generation by frequency doubling of a laser diode in a periodically domain-inverted $LiTaO_3$ waveguide", Appl. Phys. Lett. 62 2599 (1993).

[28] M. Yamada, N. Nada, M. Saito and K. Watanabe, "First-order quasi-phase matched $LiNbO_3$ waveguide periodically poled by applying an external field for efficient blue second-harmonic generation", Appl. Phys. Lett., 62 435 (1993).

[29] D. Eger, M. Oron, M.Katz, and Zussman, "Highly efficient blue light generation in $KTiOPO_4$ waveguides", Appl. Phys. Lett., 64, 3208 (1994).

[30] M. Seino, N. Mekada, T. Namiki, and H. Nakajima, "33-GHz·cm Broadband Ti: $LiNbO_3$ Mach-Zehnder Modulator", Tech Dig. ECOC'89, ThB 22-5, Gothenberg, Sweden, Sept. (1989).

[31] L. McCaughan, G. A. Bogert, "4 × 4 Ti: LiNbO3 integrated optical crossbar switch array", Appl. Phys. Lett., 47, 348 (1985)

[32] W. Warzanskyj, F. Heismann and R. C. Alferness, "Polarization-independent electro-optically tunable narrow-band wavelemgth filter", Appl. Phys. Lett. 53, 13 (1988)

[33] W. A. Stallard, A. R. Beaumont and R. C. Booth, "Integrated Optic Devices for Coherent Transmission", J. Lightwave Technol. LT-4, 852 (1986)

[34] R. Regner and W. Sohler, "Efficient second-harmonic generation in Ti:$LiNbO_3$ channel waveguide resonators", J. Opt. Soc. Am. B, 5, 267 (1988)

[35] T. Taniuchi and K. Yamamoto, "Second Harmonic Generation with GaAs Laser Diode in Proton-exchanged $LiNbO_3$ Waveguides", Tech. Dig. ECOC'86 171 (1986)

[36] A.L. Dawer, S. M. Al-Shukri, and R. M. De La Rue, " Guided wave acousto-optic interaction in proton-exchanged Y-cut $LiNbO_3$ " Appl. Phy. Lett., 48, 1597 (1986)

[37] M. Miyawaki and S. Ogura, "Efficient, damage resistant $LiNbO_3$ acousto-optic waveguide deflector" Appl. Phy. Lett., 47, 918 (1985)

[38] K. K. Wong, R. M. De La Rue, and S. Wright, "Electro-optic-waveguide frequency translator in $LiNbO_3$ fabricated by proton-exchange" Opt. Lett., 7, 5439 (1982)

[39] Retzon Chen and C. S. Tsai, "Thermally Annealed single-mode proton-exchanged channel-waveguide cuttoff modulator", Opt. Lett., 8, 546 (1986)

[40] M. Minakata, K. Kumagai, S. Kawakami, "Lattice constant changes and electro-optic effects in proton-exchanged lithium niobate optical waveguides", Appl. Phy. Lett., 49, 992 (1986)

[41] K. Nakamura and H. Shimizu, "Ferroelectric inversion layers formed by heat treatment of proton-exchanged $LiTaO_3$", Appl. Phys. Lett. 56, 1535 (1990).

[42] T. Yuhara, Y. Kondo, Y. Li, K. Tada and Y. Fujii, "Effects of annealing and the melt dilution on photorefractive sensitivity of proton−exchanged $LiTaO_3$ optical waveguides", Tech. Dig. Fourth Optoelectronics Conf., (OEC'92) 224 (1992).

[43] K. Yamamoto and T. Taniuchi, "Proton−exchanged $LiNbO_3$ waveguides by new protonic source", Post−Deadline Papers of 1st Optoelectronics Conference, B11−4 (1986).

[44] Y. S. Li, T. Yuhara, K. Tada, and Y. Sakaguchi, "Characteristics of low−propagation−loss $LiTaO_3$ optical waveguides proton exchanged in pyrophosphoric acid", Tech. Dig. of 1st Topical Meeting on Intedgated Photonics Research (IPR'90) 141 (1990)

[45] M. De Micheli, J. Botineau, S. Neveu, P. Sibillot, D. B. Ostrowsky, and M. Papuchon, "Independent control of index and profiles in proton−exchanged lithium nibate guides", Opt. Lett., 8, 114 (1983)

[46] N. Goto and G. L. Yip, "Characterization of proton−exchange and annealed $LiNbO_3$ waveguides with pyrophosphoric acid", Appl. Opt. 28, 60 (1989)

[47] H. Higuchi, M. Haruna and H Nishihara, "Evaluation of basic properties of ion−exchanged KTP waveguides," Proc. OQE 90−140, 67 (1990).

[48] S. Kakio and M. Minakata, "Measurement of Electro−Optic Constants in Proton−Exchanged $LiTaO_3$ Optical Waveguides", Trans. IEICE, J76−C−I 514 (1993).

[49] L. P. Shi, W. Karthe and A. Rasch, "Effects of annealing in Rb:$KTiOPO_4$ waveguides", Jpn. J. Appl. Phys. 33, L730 (1994).

[50] M. Minakata, K. Kumagai and S. Kawakami, "Lattice Constant Changes and Electro−Optic Effects in Proton−Exchanged $LiNbO_3$ Optical Waveguides", Optoelectronics−Devices Technologies−, 1, 163 (1986).

[51] R. A. Becker, "Comparison of guided−wave interferometric modulators fabricated on $LiNbO_3$ via Ti indiffusion and proton−exchange" Appl. Phys. Lett., 43, 131, (1983).

[52] M. Rottschalk, A. Rasch, W. Karthe, "Electrooptic Behavior of Proton Exchanged lithium niobate Optical Waveguides", J. Opt. Com., 9, 19 (1988).

[53] P. G. Suchoski, T. K. Findakly, F. J. Leonberger, "Stable low−loss proton−exchanged lithium niobate waveguide devices with no electro−optic degradation", Opt. Lett., 13, 1050 (1988)

[54] D. A. Bryan, R. Gerson, H. E.Tomaschke, "Increased optical damage resistance in lithium niobate", Appl. Phy. Lett., 44, 847 (1984)

[55] A. C. G. Nutt and E. Sudo, "Simple Control of Ti−Diffused $LiNbO_3$ Waveguide Profile and Propagation Characteristics", Electron. Lett., 24, 57 (1988).

[56] G. Tohmon, J. Ohya, K. Yamamoto and T. Taniuchi, "Generation of Ultraviolet Picosecond Pulses by Frequency−Doubling of Laser Diode in Proton−Exchanged MgO: $LiNbO_3$ Waveguide", IEEE Photon. Tech. Lett. PT−2, 629 (1990).

[57] M. De Sario, M. N. Armenise and C. Canali, "TiO_2, $LiNb_3O_8$, and $(Ti_xNb_{1-x})O_2$ compound kinetics during Ti:$LiNbO_3$ waveguide fabrication in the presence of water vapors", J. Appl. Phys. 57, 1482 (1985) .

[58] J. Olivares, E. Dieguez, F. J. Lopez and J. M. Cabrera, "Fe ions in proton−exchanged $LiNbO_3$ waveguides", Appl. Phys. Lett., 61, 624 (1992).

[59] F. S. Chen, "Optically induced change of refractive indices in $LiNbO_3$ and $LiTaO_3$," J. Appl. Phys. 40, 3389 (1969)

[60] A. M. Glass, I. P. Kaminow, A. A. Ballman and D. H. Olson, "Absorption loss and photorefractive−index changes in Ti:$LiNbO_3$ crystals and waveguides," Appl. Opt. 19, 276 (1980)

[61] T. T. Lay, Y. Kondo, and Y. Fujii, "Effect of Annealing on Electrooptic Constant of the Undoped and the MgO−doped Lithium Niobate Optical Waveguides", The Trans. IEICE, E74, 3870 (1991).

[62] S. Kondo, S. Miyazawa, S. Fushimi and K. Sugii, "Liquid−phase−epitaxial growth of single−crystal $LiNbO_3$ thin film", Appl. Phys. Lett., 26 489 (1975).

[63] H. Tamada, A. Yamada and M. Saito, "$LiNbO_3$ thin−film optical waveguide grown by liquid phase epitaxy and its application to second−harmonic generation", J. Appl. Phys., 70, 2536, (1991).

[64] T. Fujiwara, S. Sato and H. Mori, "Wavelength dependence of photorefractive effect in Ti−indiffused $LiNbO_3$ waveguides", Appl. Phys. Lett., 54, 975 (1989).

[65] Y. Kondo, Y. Fujii, J. Squire and S. Miyaguchi, "Quantitatively Measured Photorefractive Sensitivity of Proton−Exchanged LN, Proton−Exchanged MgO−Doped LN, and Ion−exchanged KTP Waveguides", Tech. Dig. of Tenth Topical Meeting Gradient−Index Optical Systems, T.5.5, 171 (1992).

[66] T. Suhara, H. Tazaki and H. Nishihara, "Measurement of reduction in SHG coefficient of $LiNbO_3$ by proton exchanging", Electron. Lett., 25, 20 (1989).

[67] T. Fujiwara, X. Cao, R. Srivastiva and R. V. Ramaswamy, "Photorefractive effect in annealed proton−exchanged $LiNbO_3$ waveguides", Appl. Phys. Lett., 61, 743 (1992).

[68] A. M. Glass, "The Photorefractive Effect", Opt. Eng., 17, 470 (1978) .

[69] D. H. Jundt, G. A. Magel, M. M. Fejer, and R. L. Byer, "Periodically poled $LiNbO_3$ for high efficiency conversion, " Proc. CLEO CPDP22−1, 614 (1991).

[70] K. Yoshino and Y. Inuishi, "Optical Damage in Ferroelectric Crystals", Solid State Physics, 13, 720 (1975).

[71] M. M. Abouelleil and F. J. Leonberger, "Waveguides in Lithium Niobate", J. Am. Ceram., Soc., 72, 1311 (1989)

[72] T. Mitsui et al: Ferro−and Antiferroelectric substances, Landort−Bornstein (Springer−Verlag, Berlin · Heidelberg · New York , 1969), Vol. 3, p.94.

[73] P. Pantellis, J. R. Hill, S. N. Oliver and J. Davis, "Organic polymer films for nonlinear optics", Br. Telecom. Technol. J., 6, 5 (1988).

[74] T. Doumuki, H. Tamada and M. Saitoh, "Phase−matched second−harmonic generation in a Ta_2O_5/$KTiPO_4$ waveguide", Appl. Phys. Lett., 65, 2519 (1994).

[75] Y. Yamamato and T. Taniuchi, "Proton−Exchanged $LiNbO_3$ Waveguides Formed by Phosphoric Acid", Proc. OQE 86−72, 77 (1986).

[76] N. Yamada and Y. Yamamoto, "Refractive Index Profiles of $KTiOPO_4$ Ion−Exchanged Waveguides and Effect of Barium Ion", Jpn. J. Appl. Phys., 33, 6572 (1994)

[77] J. M. White and P. F. Heidrich, "Optical waveguide refractive index profiles determinesd from measurement of mode indices: a simple analysis", Applied Optics, 15, 151 (1976)

[78] T. Yuhara, K. Tada, and Y. Li, "Anomalous refractive index change and recovery of electro−optic coefficient r_{33} in proton−exchanged $LiTaO_3$ optical waveguides after annealing", J. Appl. Phys., 71, 3966 (1992).

[79] H. Kogelnik, "Coupled Wave Theory for Thick Hologram Gratings", The Bell System Technical Journal, 48, 2909 (1969)

[80] T. Fujiwara, R. Srivastava, X. Cao and R. V. Ramaswamy, "Comparison of photorefractive index change in proton−exchanged and Ti−indiffused $LiNbO_3$ waveguides", Opt. Lett. 18, 346 (1993).

Publishing List

(Papers and Letters)

[1] Y. Kondo, L. Hu, and Y. Fujii, "Exact Determination of Electro−Optic Constants of Single−Mode Proton−Exchanged Guiding Layers", Trans. IEICE, Vol.E71, No.11, pp.1122−1126, 1988.

[2] T. Lay, Y. Kondo, and Y. Fujii, "Effect of Annealing on Electrooptic Constant of the Undoped and the MgO−doped Lithium Niobate Optical Waveguides", Trans. IEICE, Vol.E74, No.11, pp.3870−3872, 1991.

[3] Y. Kondo, K. Okada and Y. Fujii, "Photorefractive Sensitivity of the Proton−exchanged LN Optical Waveguides and the Ion−Exchanged KTP Optical Waveguides", Seisan−Kenkyu, Vol. 45, No.5, pp.14−17, 1993.

[4] Y. Kondo, A. Onoe, S. Miyaguchi and Y. Fujii, "Quantitatively Measured Photorefractive Sensitivity of Proton−Exchanged Lithium Niobate, Proton−Exchanged Magnesium Oxide−Doped Lithium Niobate, and Ion−Exchanged Potassium Titanyl Phosphate Waveguides", Appl. Opt., Vol.33, No.16, pp.3348−3352, 1994.

[5] Y. Kondo, T. Kouyama, K. Ohno, M. Tsuji, M. Nakamura and Y. Fujii, "Optical Damage Resistance of $LiNbO_3$ Thin−film Optical Waveguides Grown by Liquid−phase Epitaxy", Jpn. J. Appl. Phys., Vol.33, Part 2, No.3A, pp.L338−L341, 1994.

[6] Y. Kondo, Y. S. Li, A. Onoe, K. Tada and Y. Fujii, "Lattice Constants of the Proton−Exchanged Waveguides Formed on the Domain−Inverted $LiTaO_3$", Jpn. J. Appl. Phys., Vol.33, Part 2, No.12B pp.L1769−1771, 1994.

[7] Y. Kondo and Y. Fujii, "The Photorefractive Effect in the Proton−Exchanged Waveguiding Layers Formed on the Lithium Niobate and Lithium Tantalate Crystals", Jpn. J. Appl. Phy., Vol.34, Part2, No.3A, pp.L309−311, 1995.

[8] Y. Kondo and Y. Fujii, "Temperature Dependence of the Photorefractive Effect in the Proton−Exchanged Optical Waveguides Formed on the Lithium Tantalate Crystals", Jpn. J. Appl. Phys., Vol.34 No.3B pp. L365−L367, 1995.

(Technical Digests of the International Conferences)

[9] Y. Otsuka, L. Hu and Y. Fujii, "Electro−optic Constants of Single−Mode Proton−Exchanged $LiNbO_3$ Guiding Layer", Tech. Dig. of Microoptics Conference (MOC'87), pp.60−63, 1987.

[10] T. Yuhara, Y. Kondo, Y. S. Li, K. Tada and Y. Fujii, "Effect of

Annealing and Melt Dilution on Photorefractive Sensitivity of Proton−Exchanged $LiTaO_3$ Optical Waveguides", Tech. Dig. of Fourth Optoelectronics Conference (OEC'92), pp.224−225, 1992.

[11] Y. Kondo, Y. Fujii, J. Squire and S. Miyaguchi, "Quantitatively Measured Photorefractive Sensitivity of Proton−Exchanged LN, Proton−Exchanged MgO−Doped LN, and Ion−exchanged KTP Waveguides", Tech. Dig. of Tenth Topical Meeting Gradient−Index Optical Systems, T.5.5, pp.171−174, 1992.

[12] Y. Kondo and Y. Fujii, "Quantitative Estimation of Photorefractive Effect of Dielectric Optical Waveguide for SHG", Tech Dig. of 10th International Conference on Integrated Optics and Optical Fibre Communication (IOOC), WD2−5, Vol.2, pp.118−119, 1995.

[13] Y. Kondo and Y. Fujii, "Photorefractive Effect in Ion−Exchanged Optical Waveguides", Tech. Dig. of International Laser, Lightwave and Microwave Conference (ILLMC'95), pp.200−203, 1995.

Presentations (National)

[1] L. Hu, Y. Otuka and Y. Fujii, "Electrooptic Constants in Ion−Exchanged Optical Waveguides", Technical Meeting of The Institute of Electronics, Information, and Communication, Osaka, Nov. 1986.

[2] Y. Otuka, L. Hu and Y. Fujii, "Measurement of the Electrooptic Constants in proton−Exchanged Optical Waveguides" 23th Special Meeting; Japan Society of Applied Physics, Optics Division, Group of MICROOPTICS, Tokyo, Feb. 1987.

[3] L. Hu, Y. Otuka and Y. Fujii, "Electrooptic Constants in Proton−Exchanged Waveguides", General Conference 1987; The Institute of Electronics, Information, and Communication Engineers, Yokohama, Mar. 1987.

[4] Y. Otuka, L. Hu and Y. Fujii, "Electro−Optic Constants of Single−Mode Proton−Exchanged $LiNbO_3$ Waveguiding Layer", General Conference 1987; The Institute of Electronics, Information, and Communication Engineers, Kumamoto, Nov. 1987.

[5] Y. Kondo, L. Hu and Y. Fujii, "Fabrication and Estimation of the Proton−Exchanged $LiNbO_3$ Waveguide", Meeting on Optical Integrated Circuits, Tokyo, May, 1988.

[6] A. C. G. Nutt, Y. Kondo and Y. Fujii, " Measurements of r_{22} in Z−Propagating PETi $LiNbO_3$ Waveguides", 49th Autumn Meeting, 1988; The Japan Society of Applied Physics and Related Societies, Oct. 1988.

[7] Y. Kondo and Y. Fujii, "The Effects of Annealing on the TiPE Waveguides", 37th Spring Meeting, 1990; The Japan Society of Applied Physics and Related Societies, Asaka, Mar.1990.

[8] T. Lay, Y. Kondo and Y. Fujii, "Effect of Annealing on Electrooptic constants of the $LiNbO_3$ and MgO doped $LiNbO_3$", General Meeting, 1990; The Institute of Electronics, Information, and Commusication Engineers, Hiroshoma, Oct. 1990.

[9] Y. Kondo, T. Lay, Y. Fujii and E. Hombo, "Measurement of Photorefractive Sensitivity in the Titanium Indiffused Waveguides Fabricated on MgO Doped Lithium Niobate Crystals", 38th Spring Meeting 1991; The Japan Society of Applied Physics and Related Societies, Hiratsuka, Mar. 1991.

[10] T. Lay, Y. Kondo and Y. Fujii, "The Effect of Annealing on the Electro−Optic Constant of the Proton−Exchanged Waveguides in the Lithium Niobate Crystals",38th Spring Meeting 1991; The Japan Society of Applied Physics and Related Societies, Hiratsuka, Mar. 1991.

[11] Y. Kondo and Y. Fujii, "Photorefractive Sensitivity of The Annealed Proton−Exchanged $LiNbO_3$ Optical Waveguides", Technical Meeting of The Institute of Electronics, Information, and Communication, Okayama, Jan, 1991.

[12] Y. Kondo and Y. Fujii, "Photorefractive Effect of Proton−Exchanged LN and MgO−Doped LN Optical Waveguides", 39th Spring Meeting, 1992; The Japan Society of Applied Physics and Related Societies, Narashino, Mar. 1992.

[13] T. Yuhara, Y. Kondo, K. Tada and Y. Fujii, "Photorefractive Resistance of Proton−Exchanged $LiTaO_3$ Optical Waveguides", 39th Spring Meeting, 1992; The Japan Society of Applied Physics and Related Societies, Narashino, Mar. 1992.

[14] Y. Kondo, Y. Fujii, J. Squire and S. Miyaguchi, "Photorefractive Sensitivity of Proton−Exchanged LN Waveguides and Ion−Exchanged KTP Waveguides", Japan Optics'92, Kyoto, Sept. 1992.

[15] Y. Kondo, A. Onoe, S. Miyaguchi, T. Toma and Y. Fujii, "The Photorefractive Resistivity of Quasi−Phase−Matched SHG Devices", 40th Spring Meeting, 1993; The Japan Society of Applied Physics and Related Societies, Tokyo, Mar. 1993.

[16] Y. Kondo, T. Kohyama, K. Ohno, M. Tsuji, M. Nakamura and Y. Fujii, "The Photorefractive Sensitivity of the LN Thin Film Grown by LPE", 40th Spring Meeting, 1993; The Japan Society of Applied Physics and

Related Societies, Tokyo, Mar. 1993.
[17] Y. Kondo, T. Kohyama, K. Ohno, M. Tsuji, M. Nakamura and Yoichi Fujii, "The Photorefractive Effect of the LN Thin-Film Optical Waveguides Grown by Liquid Phase Epitaxy Using LV Flux and LB Flux", 18th Symposium on Optics, Tokyo, Jun. 1993.
[18] Y. S. Li, Y. Kondo, K. Tada and Y. Fujii, "Lattice constant in proton-exchanged $LiTaO_3$ optical waveguides for the quasi-phase-matched SHG devices", 54th Autumn Meeting, 1993; The Japan Society of Applied Physics and Related Societies, Sapporo, Sept. 1992.
[19] Y. Kondo and Y. Fujii, "Photorefractive Sensitivity of the Waveguides Formed on the Dielectric Materials", 14th Annual Meeting of the Laser Society of Japan, Chiba, Jan. 1994.
[20] Y. Kondo, K. Sugimoto and Y. Fujii, "Temperature Dependence of the Photorefractive Effect of the Proton-Exchanged Lithium Tantalate Waveguides", 19th Symposium on Optics, Tokyo, Jun. 1993.
[21] Yukiko Kondo and Yoich Fujii, "Temperature Dependence of the Photorefractive Effect in the Proton-exchanged Lithium Tantalate Optical Waveguides", Japan-China Symposium on Advanced Information Technology, Tokyo, 1994.
[22] Y. Kondo, M. Minakata and Yoichi Fujii, "The Influence of Annealing the Proton-Exchanged Lithium Niobate and Lithium Tantalate Waveguides on the Photorefractive Effect", Japan Optics'94, Hamamatsu, Sept. 1994.
[23] Y. S. Li, Y. Kondo, K. Tada and Y. Fujii, "Lattice Constant and Photorefractive Effect in the Rb Ion-Exchanged Waveguides Formed on the KTP Crystals", 42th Spring Meeting, 1995; The Japan Society of Applied Physics and Related Societies, Hiratsuka, Mar. 1995.
[24] Y. Kondo and Y. Fujii, "The Photorefractive Effect in the Rb Ion-Exchanged Waveguides Formed on the KTP Crystals", General Conference 1995; The Institute of Electronics, Information, and Commusication Engineers, Fukuoka, Mar. 1995.
[25] T. Kato, Y. Kondo and Y. Fujii, "Analysis of Optical Digital Switch by X Branch Waveguide on KTP", 42th Spring Meeting, 1995; The Japan Society of Applied Physics and Related Societies, Hiratsuka, Mar. 1995.

(Other Works)

[1] W. Kinase, H. Kato, Y. Otsuka and Masayuki Miyanaga, "Theory of Kerr Effect in Benzene C_6H_6 (Anisotropic Molecule), Nitrobenzene $C_6H_5NO_2$ and Water H_2O (Polar Molecules)", Journal of the Physical Society of Japan, Vol.55, No11, pp.4103-4112, 1986.
[2] T. Kato, H. Sotobayashi, Jung-Keun Lee, Yukiko Kondo and Yoichi Fujii, "Multipoint Temperature Sensor Using Fibre-Optic Ring Resonator by Pulse-Frequency Localization ", Tech. Dig. of International Symposium on Optical Tools for Manufacturing and Advanced Automation, Distributed and Multiplexed Fiber Optic Sensors 3, Vol.2071, pp.153-162, 1993.
[3] Y. Fujii and Y. Kondo, "Orthomorphic Conditions of Tilted Binocular Stereoscopic Image", 36th Spring Meeting, 1989; The Japan Society of Applied Physics and Related Societies, Chiba, Apr. 1989.
[4] Y. Fujii and Y. Kondo, "Orthomorphic Image Transmission and Display", The 23th Conference on Image Technology, Tokyo, Dec. 1992.
[5] Y. Fujii and Y. Kondo, "Orthomorphic Image Transmission and Display", 3D Forum, Vol.7, No.2, pp38-41, 1993.